Mata, J., Martins, S., Mattielli, N., Madeira, J., Faria, B., Ramalho, R. S., ... Martins, L. (2017). The 2014-15 eruption and the short-term geochemical evolution of the Fogo volcano (Cape Verde): Evidence for small-scale mantle heterogeneity. *Lithos*, *288-289*, 91-107. https://doi.org/10.1016/j.lithos.2017.07.001

# The 2014-15 eruption and the short-term geochemical evolution of the Fogo volcano (Cape Verde): evidence for small-scale mantle heterogeneity

J. Mata[1*]; S. Martins[1]; N. Mattielli[2]; J. Madeira[1]; B. Faria[3]; R.S. Ramalho[1,4,5]; P. Silva[6,1]; M. Moreira[7]; R. Caldeira[8]; M. Moreira[6,1]; J. Rodrigues[9]; L. Martins[1]

1- Instituto Dom Luiz, Faculdade de Ciências, Universidade de Lisboa, 1749-016 Lisboa, Portugal.
2- Laboratoire G-Time, DGES, Université Libre de Bruxelles, ULB, Av. Roosevelt, 50, CP 160/02, 1050 Brussels, Belgium
3- Instituto Nacional de Meteorologia e Geofísica, Mindelo, Cabo Verde
4- School of Earth Sciences, University of Bristol, Wills Memorial Building, Queen's Road, Bristol, BS8 1RJ, UK
5- Lamont-Doherty Earth Observatory at Columbia University, Comer Geochemistry Building, 61 Route 9W, P. O. Box 1000, Palisades, NY 10964–8000, USA
6- Instituto Politécnico de Lisboa, ISEL/ADF, Lisboa, Portugal
7- Institute de Physique du Globe de Paris (France)
8- Laboratório Nacional de Energia e Geologia, I.P., 2610-999 Amadora, Portugal.
9- Geologist, Cabo Verde

*- Corresponding author: jmata@fc.ul.p

**Keywords**

2014-15 Fogo Island (Cape Verde) eruption; Ocean island basalts; Mantle heterogeneity; Short-term magmatic variation; Volcano plumbing system

## 1- Introduction

The Earth's mantle is highly heterogeneous as depicted by the composition of oceanic basalts and particularly by those from oceanic islands (e.g. Hofmann, 2003; White, 2015). Such heterogeneity is considered the result of mixing in different proportions of the so-called mantle components (Zindler and Hart, 1986; Stracke et al., 2005). The length scale of mantle heterogeneities sampled by oceanic basalts is highly variable, sometimes encompassing large regional domains (e.g. DUPAL and SOPITA anomalies; Hart, 1984; Staudigel et al., 1991; White, 2015), but being also evident at the scale of a single magmatic province, as reported, for example, for the Azores (e.g. Beier et al., 2008), Cape Verde (Gerlach et al., 1988; Doucelance et al., 2003) and Galápagos (Gibson et al., 2012) archipelagos. The same is true at the scale of a single island edifice (e.g. Barker et al., 2010; Mourão et al., 2012a; Nobre Silva et al., 2013), even when considering quasi-coeval magmatic products (e.g. Madureira et al., 2011).

In this work we evaluate the small-scale heterogeneity of the mantle source feeding a plume-related intraplate volcano, as well as the short-term geochemical evolution of the magmas it generated. To this purpose we use as a case study the island of Fogo (Cape Verde Archipelago), one of the most active oceanic volcanoes in our planet. Indeed, since the mid-15$^{th}$ Century Fogo experienced about 27 eruptions mostly from vents located within a restricted area (≈50 km$^2$) of the island's summit depression (Fig. 1). The latest eruption occurred in 2014-2015 and constitutes the main object of this study. Their vents are practically coincident or localized less than 2 km away from those of the two previous eruptions (1995 and 1951, respectively). For this reason, Fogo constitutes a prime locality to test the existence of small-scale heterogeneities of mantle sources, as well as to investigate the recent short-term evolution of magmas issued from those sources. Here we characterize and discuss the geochemistry of the lava flows and pyroclasts extruded during the initial stages of the eruption (up to December 7, 2014). Even though we are only considering lavas formed during the first 15 out of 60 days of

eruption, the extracted information allows the demonstration of chemical differences relative to the products erupted in 1951 and 1995.

The preservation of such heterogeneities by magmas is also here discussed emphasizing the role of lithosphere thickness. The mineralogical, geochemical and physical characteristics of a volcano are partially constrained by what happens during magma transit from its source to the surface, i.e. by the nature and dynamics of the associated magma plumbing system (e.g. Longpré et al., 2008; Klügel et al., 2015; Cooper, 2017; Cashman et al., 2017). The Fogo's plumbing system is here assessed using barometric data, which indicates a location of the main magma chamber(s) into the mantle.

Our observations show that magmas erupted in 2014 mark a reversal from the tendency depicted by previous eruptions (Escrig et al., 2005), which exhibited an increasing contribution of a local end-member with relatively radiogenic Sr.

## 2- Cape Verde Geological Setting

The Cape Verde Archipelago (Eastern Central Atlantic; Fig. 1) lies on top of the largest bathymetric anomaly in the Earth's oceans – the Cape Verde Rise – that coincides with important geoid, heat flow, gravity, and seismic anomalies (e.g. Dash et al., 1976; Courtney and White, 1986; Wilson et al., 2013; Liu and Zhao, 2014). The archipelago, which stand on 120–140 Ma-old seafloor (Williams et al., 1990) is regarded as a hotspot resulting from the impingement of a mantle plume on the quasi-stationary (<1 $cm.a^{-1}$ in the region; Pollitz, 1991; Holm et al., 2008) Nubian plate. These would explain the long-lasting volcanic activity and, at least partially, the age distribution of volcanism and the geometry of both the archipelago and the Cape Verde Rise (Lodge and Helffrich, 2006; Holm et al., 2008; Madeira et al., 2008; Ramalho et al. 2010, Ramalho, 2011). The presence of a mantle plume deeply anchored in the lower mantle is suggested by seismic data (Montelli et al., 2006; Forte et al., 2010; Vinnik et al, 2012; Saki et al., 2015; French and Romanowicz, 2015) and of noble gas studies performed on

146 carbonatites and alkaline silicate rocks (Christensen et al., 2001; Doucelance et al.,
147 2003; Mata et al., 2010; Mourão et al., 2012b). The oldest exposed hotspot-related
148 volcanism is ~26 Ma (Torres et al., 2010) and at least three islands are considered
149 volcanically active (Santo Antão, Brava and Fogo; see e.g. Madeira et al., 2010; Eisele
150 et al., 2015; Faria and Fonseca, 2014) but only Fogo had post-settlement eruptions.
151 Magmatism in Cape Verde is strongly alkaline, as testified by the occurrence of
152 nephelinitic, melanephelinitic, and melilititic rocks on several islands. It also is well
153 known by its striking geochemical heterogeneity, allowing the isotopic separation of the
154 islands into two groups (Northern and Southern). Lavas from the Southern group have
155 more radiogenic Sr, but unradiogenic Nd and Pb ratios than those from the Northern
156 group, which are also exhibit more unradiogenic He signatures. In addition, magmatic
157 rocks from the Southern group are positioned, on the $^{208}Pb/^{204}Pb$ vs. $^{206}Pb/^{204}Pb$
158 diagram, above the Northern Hemisphere Reference Line (NHRL; Hart, 1984) whilst
159 lavas from the Northern group tend to plot along the NHRL (e.g. Gerlach et al., 1988;
160 Doucelance et al., 2003; Holm et al., 2006; Kogarko and Asavin, 2007; Martins et al.,
161 2010; Mourão et al. 2012a and references therein). Notable exceptions to this scenario
162 include Brava (the southwesternmost island), which depicts both typical Northern (older
163 sequences) and Southern (younger volcanism) isotope signatures (Mourão et al., 2012a),
164 and the neighbouring Cadamosto seamount, which also presents typical Northern
165 signatures (Barker et al., 2012).
166
167 **2.1 Fogo Volcano**
168 Fogo is one of the youngest of the Cape Verde Islands and a very prominent oceanic
169 volcano, standing ~7 km above the surrounding seafloor. The island exhibits a slightly
170 asymmetric conical shape, being truncated atop by a summit depression open to the
171 east. This 8 km-wide depression - Chã das Caldeiras - is surrounded on three sides by a
172 almost vertical wall – the Bordeira – up to 1 km tall. Inside the summit depression and

on its eastern side, a 1100 m high strato-volcano – Pico do Fogo – grew up to an elevation of 2829 m (Fig. 1). Fogo volcano is therefore interpreted as a compound volcano, featuring a "somma-vesuvio" association of a younger strato-cone on top of an older, collapsed volcanic edifice (Ribeiro, 1954; Foeken et al., 2009). The opening to the east of the summit depression is interpreted as the result of a massive flank collapse (Day et al., 1999; Brum da Silveira et al., 2006), as attested by a landslide debris deposit extending offshore into the channel between Fogo and Santiago (e.g. Masson et al., 2008), and by field evidence documenting the impact of a megatsunami in the neighbouring island of Santiago (Paris et al., 2011; Ramalho et al., 2015). The present-day Pico do Fogo stands on, and partially fills, the collapse scar, and naturally post-dates the collapse event, which is interpreted to have occurred either at ~117 or at ~73 ka (cf. Eisele et al. 2015 and Ramalho et al. 2015). A older basement is, however, exposed in two shallow valleys near the city of São Filipe, where plutonic calciocarbonatites were dated from 2.5 Ma to 5.1 Ma (Hoernle et al., 2002; Madeira et al., 2005; Foeken et al., 2009). These suggest a > 2 Myr volcanic hiatus in the evolution of Fogo.

Fogo volcano is very active, with 27 eruptive events since 1500 AD (Ribeiro, 1954). The mean recurrence interval between eruptions is 19.8 years, but with individual intervals ranging from 1 to 94 years. Historical eruptions seem to have been confined to Chã das Caldeiras and the eastern slope of the volcano, as it was the case of the recent 1951, 1995 and 2014/2015 events (Fig. 1).

The latest eruption started on November 23, 2014 and continued until February 7, 2015. The eruption occurred on a NE-SW trending 700 m-long fissure located on the SE flank of the previous 1995 cinder cone, an adventitious vent developed on the SW flank of Pico do Fogo (Figs. 2A, 2B e 2D). This eruption started with vigorous "hawaiian" fire-fountain activity, followed by strombolian activity, and later by simultaneous or alternating Hawaiian (Fig. 2C), strombolian and vulcanian (Fig. 2D) eruptive activity

from different craters along a fissural vent, lasting for several days. The eruption also emitted, from the first day, thick a'a lava flows (Fig. 2E; Supplementary Material S1) forming two initial lava lobes. A shorter lobe, 1.7 km-long, progressed southwestwards down to the flank of Cova Tina cone, stalling short of the Bordeira wall in this area. The second, longer lobe advanced 3 km to the northeast in the initial hours of the eruption, crossing the topographic barrier formed by the 1995 lava flows by advancing through the existing road cut. It advanced intermittently towards the village of Portela, causing widespread destruction (Fig. 2F). During the later stages of the eruption, thinner, more fluid, a'a and especially pahoehoe breakouts expanded the flow field to the west and north, the latter descending to the village of Bangaeira, destroying almost completely both villages and reaching a total length of 5.2 km (Fig.1). Overall, the resulting lava flows, with an average thickness of about 9 m, covered an area of 4.8 $km^2$, with extruded volumes estimated to correspond to ~45 × $10^6$ $m^3$, at a mean eruption rate of 6.8 $m^3.s^{-1}$ (Bagnardi et al. 2016; Richter et al. 2016). Lava flow thicknesses as high as 35 m (close to the vent), or 25 m on the lava ponding west of Portela, were described by Richter et al. (2016). See also Cappello et al. (2016) for additional information about the eruption.

## 3- Analytical procedures

Whole-rock major and trace element concentrations were obtained at Activation Laboratories, Ltd (Ancaster, Ontario, Canada) using the geochemical analytical package 4Lithoresearch (lithium metaborate/tetraborate fusion - ICP and ICP/MS).

Several certified reference materials from USGS (United States Geological Survey), GSJ (Geological Survey of Japan) and CCRMP (Canadian Certificate Reference Material Project) were run to check for accuracy (Supplementary Material S2). Errors associated with the accuracy are ≤ 4% for major elements and better than 9% for the REE and the most widely used incompatible elements. Reproducibility was generally

better than 5% for both major and trace elements. For detailed information regarding analytical and control procedures consult the Actlabs website (www.actlabs.com).

Mineral analyses were performed on carbon-coated polished thin sections using a JEOL SUPERPROBE™, model JXA-8200, in wavelength dispersive mode at the Departamento de Geologia da Faculdade de Ciências da Universidade de Lisboa (Portugal). Minerals were analysed with an acceleration voltage of 15 kV and a current of 25 nA, using a 5 μm wide beam for most minerals. Plagioclase and apatite were analysed using a 7 and 9 μm wide beam, respectively. The analyses performed in each mineral phase/glass were calibrated using the composition of reference material, with precisions being better than 2% and ordinarily around 1% (see Supplementary Material S3-H for specific minerals standards used in each mineral analysis).

Isotopic analyses of Pb, Nd, Sr and Hf were performed at the Laboratoire G-Time of the Université Libre de Bruxelles (ULB, Belgium) on a Nu Plasma I Multi-Collector Inductively Coupled Plasma Mass Spectrometer (MC-ICP-MS) (@ Nu instruments).

Sr analyses were performed in wet mode. In routine, the raw data was normalized to $^{86}Sr/^{88}Sr=0.1194$, and corrected for mass bias by standard sample bracketing using the lab's in-house Sr standard solution. The in-house shelf Sr standard was calibrated and normalized to the certified value of NBS 987 Sr standard (0.710248) reported by Weis et al. (2006). During our analytical sessions, in-house standard solution was run every two samples and gave an average value of 0.710287 ± 50 (2σ) for raw $^{87}Sr/^{86}Sr$ data (21 runs).

Nd and Hf were run in dry mode with an Aridus II desolvating system. To monitor the instrumental mass bias during the analysis sessions, the standard sample bracketing method was also applied. Standards were systematically run between every two samples, giving an average value in $^{143}Nd/^{144}Nd$ of 0.511921 ± 41 (2σ, 8 runs) for the Rennes Nd standard, and $^{176}Hf/^{177}Hf=0.282172$ ± 30 (2σ, 10 runs) for the JMC 475 Hf standard. The Nd and Hf isotopic measurements were internally normalised to

$^{146}Nd/^{144}Nd$=0.7219 and $^{179}Hf/^{177}Hf$=0.7325, respectively. All Hf and Nd isotopic data (Table 1) are normalized to the reference values of 0.511961 and 0.282160 as published by Chauvel and Blichert-Toft (2001) and Chauvel et al. (2011).

For the Pb isotope analyses, a Tl dopant solution was added for every sample and standard, within a Pb-Tl concentration ratio of ±5:1 (for a minimum signal of 100 mV in the axial collector - $^{204}Pb$). $^{202}Hg$ is routinely monitored to correct for the potential isobaric interference of $^{204}Hg$ on $^{204}Pb$. Mass discrimination was monitored using ln – ln plots and corrected by the external normalization and the standard sample bracketing technique using the recommended values of Galer and Abouchami (1998) (i.e. $^{206}Pb/^{204}Pb$=16.9405±15; $^{207}Pb/^{204}Pb$=15.4963±16; $^{208}Pb/^{204}Pb$=36.7219±44). The repeated measurements of the NBS981 gave the following values: $^{206}Pb/^{204}Pb$=16.9403±8, $^{207}Pb/^{204}Pb$=15.4961±10, $^{208}Pb/^{204}Pb$=36.7217±31 (2σ) for the NBS981 Pb standard (5 runs).

## 4- Results

The samples used in this study were collected during a field survey undertaken during the course of the last Fogo eruption, between November 27 and December 7, 2014. From all collected samples a sub-set of 14 was selected for petrographic, mineralogical and whole-rock elemental geochemical study (TABLE I), on the basis of its geographical and temporal distribution. Sr, Nd, Hf and Pb isotopes were determined for 8 samples (TABLE II), while the He isotope analysis was performed for one sample. On the Supplementary Material the reader can also find mineral chemistry data (S3) and the whole-rock normative compositions (S4). The composition of interstitial glasses determined by electron microprobe is also presented on Supplementary Material S3-G.

281 **4.1. Petrography and mineral chemistry**

282 On a chemical basis, lava flows and pyroclasts erupted up to December 7 are, sensu
283 lato, tephrites and phonotephrites (see *section* 4.3 and Fig. 3). Some of the most
284 important petrographic characteristics of the studied samples are depicted on Fig. 4 and
285 their mineral chemistry data are displayed on the Supplementary Material S3.

286

287 **4.1.1 Tephrites**

288 The bulk (≈ 85%) of the eruptive products corresponds to tephrites. The lavas are
289 vesicular and porphyritic with a hypocrystalline groundmass and with phenocrysts
290 amounting up to 10%. Samples are highly vesicular (up to 60% of the rock volume) and
291 the vesicles are irregular in shape and size.

292 The most abundant phenocryst phase is clinopyroxene. Even though all the
293 clinopyroxene phenocrysts are classified as diopside ($Wo_{49}En_{38}Fs_{13}$ to $Wo_{52}En_{36}Fs_{12}$)
294 according to IMA recommendations (Supplementary Material S-3A), in most samples
295 two groups must be considered regarding size and composition. One group corresponds
296 to phenocrysts with dimensions up to 2 mm and euhedral shapes. They are characterized
297 by normal zoning patterns, with $Al_2O_3$, FeO and $TiO_2$ increasing and MgO, CaO and
298 Mg# decreasing from core to rim. Opaque mineral inclusions are frequent. The other
299 group of phenocrysts occurs in clusters along with kaersutite, both with dimensions up
300 to 4 mm in length. Clinopyroxee megacrysts in these aggregates usually show complex
301 zoning patterns presenting abnormal compositional variations with increments of $Al_2O_3$,
302 FeO and $TiO_2$ towards the intermediate zone/mantle and then decreasing towards the
303 rim; the opposite occurs with MgO and CaO, suggesting a more complex and multistage
304 crystallization history as compared with the first group. Indeed the increase in
305 MgO/FeO and decrease in $TiO_2$ towards the rim is suggestive of a replenishment of the
306 magma chamber where these particular crystals were formed, reflecting an influx of less
307 evolved magmas, thus pointing out to mixing of distinct magma batches. However, both

groups of clinopyroxenes show similar $Al^{VI}$ values (0.059 to 0) and Al/Ti ratios indicating that megacrysts are cognate, being genetically related with the host lava and with the clinopyroxene phenocrysts. This assertion is also considered valid for keaersutite megacrysts given the chemical evidence for amphibole fractionation (see 5.1).

These kaersutite crystals are Mg- and Ti-rich (MgO = 12.8 – 13.0 wt.%; $TiO_2$ up to 6.07 wt.%), usually occurring in association with apatite and showing reaction rims where clinopyroxene and rhönite crystals are present, sometimes completely replacing the amphibole (Fig. 4D). Olivine crystals are restricted to inclusions in clinopyroxene phenocrysts, with no signs of resorption, and to the groundmass. In all lava samples the opaque minerals can be considered microphenocryts, being characterized by euhedral shapes and dimensions up to 1 mm. Most of the occurring oxides can be considered as titanomagnetites, with ulvöspinel component ($X_{USP}$) up to 57, and Cr# ranging from 1.6 to 5.3.

The groundmass is made up of small crystals immersed in a glassy matrix. These comprise plagioclase laths (labradorite, $An_{56-66}$) sometimes with a fluidal arrangement, clinopyroxene elongated crystals ($Wo_{49}En_{37}Fs_{14}$ to $Wo_{53}En_{32}Fs_{15}$), finely disseminated opaque minerals (titanomagnetites, $58 < X_{USP} < 67$), rare olivine (Fo ≈ 72%), and fluorapatite (1.7 to 2.8 wt.% of F). The electron-microprobe analyses of interstitial glass revealed it to be very rich in alkalis (11.8 to 15.8 wt%, $K_2O+Na_2O$) and poor in MgO (down to 0.66 wt%) having tephriphonolitic and phonolitic ($SiO_2$ up to 54.15 wt%) compositions (see Fig. 3).

### 4.1.2 Phonotephrites

These lavas are vesicular hemicrystalline/hypocrystalline and sparsely porphyritic (phenocrysts up to 3% vol.). The vesicles are elongated reaching up to 10 mm in length and corresponding to 50 to 80% of rock volume. The clinopyroxene phenocrysts are

335 euhedral up to 3 mm in size, frequently showing complex oscillatory zoning patterns
336 and inclusions of opaque minerals. Despite the striking optical zoning patterns, all the
337 clinopyroxene phenocrysts are classified as diopside with a short compositional range
338 ($Wo_{49}En_{35}Fs_{10}$ to $Wo_{53}En_{40}Fs_{14}$), being very similar to that reported for the tephrites.
339 Olivine (Fo=80-84%) is scarce, being identified only as a core inclusion in a
340 clinopyroxene phenocryst. Microphenocrysts (up to 1mm) of equant opaque minerals
341 are classified as titanomagnetites ($X_{USP}$ = 44-46; Cr# = 1.15-5.4). Kaersutite
342 pseudomorphs are frequent. They consist of aggregates of rhönite and clinopyroxene
343 elongated crystals, displayed in inward radial arrangements totally or partially replacing
344 the amphibole. However, in either case, a border of small opaque minerals encloses the
345 altered/partially altered amphibole crystals. These kaersuites are similar (MgO = 11.9 –
346 12.7 wt.%: $TiO_2$ up to 6.04 wt.%) to those occurring as megacrysts/phenocrysts in
347 tephritic rocks, and the occurrence of apatite within or in close proximity to the
348 amphibole is frequent. The groundmass is composed of plagioclase microliths
349 (labradorite, $An_{54-66}$), elongated clinopyroxene crystals (average $Wo_{53}En_{31}Fs_{16}$), opaque
350 minerals ($38 < X_{USP} < 57$; Cr# = 0.67-1.49), scarce olivine and glass.
351 In one sample, a cluster of clinopyroxene, opaque crystals, and amphibole is interpreted
352 as a possible co-magmatic cumulate nodule. This interpretation is based on the large
353 dimension of the crystals, the sharp contrast between the mineral aggregate and the
354 surrounding rock matrix, and on its chemical similarity between its minerals and the
355 rock phenocrysts. The same interpretation is considered for an aggregate of small (0.5
356 mm in length) plagioclase crystals characterized by anorthite content up to 79 %.
357 Ultramafic nodules of cumulate origin, mainly composed of olivine, clinopyroxene, and
358 amphibole, were also reported for this eruption by Caldeira et al. (2015).
359
360
361

362 **4.2. Whole rock elemental composition**

363 Major and trace element analyses of the studied rocks are presented in Table I, while
364 normative compositions can be found in Supplementary Material S4.

365 As all other subaerial lavas in the Cape Verde Islands, Fogo's 2014 volcanic products
366 are alkaline. They plot dominantly in the $U_1$ field, but also in the $U_2$ (phonotephrites)
367 field of the TAS diagram (Fig. 3). Rocks plotting inside the $U_1$ field would be classified,
368 according their CIPW normative composition, either as nephelinites (normative *ne* >
369 20%) – the dominant type – or as melanephelinites (normative *ne* < 20%; normative *ab*
370 < 5%) according to the subdivision proposed by Le Bas ( 1989); (see S4). However, as
371 modal plagioclase can be identified in most of the rocks plotting in the U1 TAS field
372 and for all the samples normative *ol* < 10%, the classification as tephrites is here
373 preferred and used.

374 The rocks are representative of moderately evolved magmas characterized by Mg#
375 ranging from 55.32 to 45.98 and by $Na_2O/K_2O$ between 1.35 and 1.46. The less evolved
376 rocks (Mg# = 55.32 to 51.97) have $TiO_2$ contents varying from 3.65 to 3.75 wt%, $P_2O_5$
377 close to 1 (0.94 to 1.11 wt%), $CaO/Al_2O_3$ ratios ranging from 0.65 to 0.78 and
378 $K_2O/TiO_2$ ratios from 0.25 to 0.32.

379 The 2014 lavas are highly enriched in the most incompatible elements (Fig. 5), which is
380 depicted, for example, by $(La/Yb)_{cn}$ ratios > 20, with the most evolved rocks presenting
381 the highest values for this ratio (> 23). Primitive mantle normalized incompatible
382 elements patterns (Fig. 5c) show a significant enrichment of Nb and Ta relatively to the
383 light REE and the radiogenic heat producers K, Th and U. Small Hf negative anomalies
384 are also evident, which partially reflects the high Zr/Hf ratios (>49), well above the
385 value of 36 characterizing CI chondrites and the primitive mantle (e.g. Palme and
386 O'Neil, 2003).

387 The sampled pyroclasts and lava flows are similar in composition, the most significant
388 difference being the sulphur-enriched composition of pyroclasts (120 to 230 ppm;

389 $\overline{X} = 200$ ppm) as compared to lava flows (60 to 120 ppm; $\overline{X} = 84$ ppm ). This
390 indicates a more effective degassing of lava flows as a consequence of a slower cooling.
391 Most of the characteristics described above are similar to those of lavas erupted during
392 the two precedent eruptions (1995 and 1951), as Fig. 5 shows. Notwithstanding the fact
393 that the samples here studied are only representative of the lava emitted during the first
394 15 days of the eruption, some differences, however, were noticed: i) the 1995 lavas
395 present a slightly higher compositional range (MgO from 6,86 to 2.40 wt%; Hildner et
396 al., 2011) than the ones from 2014 (MgO from 6.23 to 2.93 wt%); ii) from the three
397 eruptions considered, the 1951 event produced the less evolved lavas (MgO up to 8.24
398 wt%; Hildner et al., 2012); iii) for the same $SiO_2$ content, the 1951 lavas tend to be less
399 alkali-rich than the 2014 and 1995 volcanics (Fig. 3); iv) the 2014 and 1995 erupted
400 materials are characterized by small compositional gaps ($\Delta SiO_2$ = 2.5% and 3.8%,
401 respectively) in opposition to the described for from the 1951 eruption for which no
402 phonotephrite compositions were reported (see Fig. 1 and references therein); v) for
403 these three eruptions, the most evolved products are the phonotephrites from the 1995
404 eruption, which also present the highest concentrations in incompatible elements like
405 Nb and Ta. However, the highest concentrations in light REE are found in
406 phonotephrites from the 2014 eruption, which show the highest La/Nb ratios. This
407 higher La/Nb are also observed for the less evolved rocks (MgO > 5 wt%), with 2014
408 lavas presenting $\overline{X}$ La/Nb = 0.69, whereas the 1995 and 1951 less evolved rocks show
409 $\overline{X}$ La/Nb=0.60 (cf. Table 1, Hildner et al., 2011 and Hildner et al., 2012).
410
411 **4.3. Whole rock isotope composition**
412 The results of Sr, Nd, Hf and Pb isotope analyses are shown on Table II. The lavas
413 erupted in 2014 at Fogo Island present isotope signatures akin to those typical of the
414 Southern islands in the Cape Verde Archipelago. Indeed, in opposition to what is
415 observed for the Northern capeverdean islands (Fig.6), they are characterized by

relatively unradiogenic $^{206}Pb/^{204}Pb$ ratios (up to 19.001) and plot above the Northern Hemisphere Reference Line (Δ7/4 from 0.99 to 1.57; Δ8/4 from 25.38 to 28.80; see Hart, 1984 for definitions of these parameters). Notwithstanding the fact that their $^{87}Sr/^{86}Sr$ (0.70361 to 0.70369) and $^{143}Nd/^{144}Nd$ (0.51276 to 0.51279) ratios are clearly more and less radiogenic, respectively, than those observed for the Northern islands, the 2014 lavas plot on the second quadrant of the $^{87}Sr/^{86}Sr$ vs. $^{143}Nd/^{144}Nd$ diagram (Fig. 7A). This indicates a provenance from a time-integrated depleted source(s), i.e. which evolved over time with lower Rb/Sr and higher Nd/Sm than those of the BSE (bulk silicate earth) and the CHUR (chonditic uniform reservoir), respectively. Compared to the lavas extruded during the 1951 and 1995 eruptions, the 2014 rocks present more unradiogenic Sr and radiogenic Nd signatures (Fig. 7). The 2014 lavas also exhibit slightly more radiogenic $^{206}Pb/^{204}Pb$ ratios than the most samples from the two previous eruptions, the same being true for $^{207}Pb/^{204}Pb$ ratios (Fig. 6A). Lavas from these 3 eruptions are amongst the Cape Verde rocks with lower $^{206}Pb/^{204}Pb$ ratios. As is typical of the Southern Cape Verde Islands, rocks from these 3 eruptions are characterized by positive Δ8/4, plotting above the NHRL (Fig. 6B).

The 2014 lavas' $^{176}Hf/^{177}Hf$ ratios range from 0.28294 to 0.28296 (Table II). A time-integrated evolution with high Lu/Hf ratios compared to CHUR is shown by positive εHf values (5.88 to 6.62; Fig. 7B), plotting between the mantle arrays proposed by Vervoort (1999) and Chauvel (2008). These are the first $^{176}Hf/^{177}Hf$ determinations available for Fogo Island, preventing any comparison with previous results. However, noteworthy that the lavas erupted in 2014 plot inside the large field defined in the εNd-εHf space by the lavas from the neighbouring island of Santiago, which is characterized by significantly higher and lower $^{176}Hf/^{177}Hf$ ratios (see Barker et al., 2009; Martins et al., 2010). Significant correlations between any of these isotope signatures and ratios

441 involving incompatible trace elements have not been found. This will be discussed later
442 (see 5.3).
443 The $^{3}He/^{4}He$ ratio of a glassy phonotephrite was determined at the Intitut de Physique
444 du Globe de Paris (IPGP) using crushing for gas extraction. The obtained value (1.11±
445 0.13 Ra, where Ra is the present atmospheric ratio of $1.4 \times 10^{-6}$) for a $^{4}He$ concentration
446 of $2.8 \times 10^{-9}$ cc/g is interpreted as the result of atmospheric contamination during the
447 eruption/consolidation of lava. Consequently, this result will not be considered in the
448 discussion.
449
450 **5. Discussion**
451 **5.1 Mantle source composition and magma evolution**
452 Previous studies, explained the chemical variability of Fogo's lavas by mixing in
453 different proportions of HIMU-like (ancient recycled ocean crust) and EM1-like mantle
454 end-members, diluted by the presence of depleted upper mantle (Gerlach et al., 1988) or
455 by lower mantle material (Doucelance et al., 2003; Escrig et al., 2005) entrained by the
456 upward moving plume.
457 Although 2014 lavas present low $^{206}Pb/^{204}Pb$ ratios (up to 19.001), clearly below those
458 typical of magmas originated from sources dominated by the HIMU mantle component
459 (e.g. Kawabata et al., 2011), the HIMU fingerprint is shown by trace element patterns
460 (Fig. 5) displaying enrichment in Nb and Ta relative to the LREE and the LILE (e.g.
461 Niu et al., 2012). Aditionally, all the analysed rocks are characterized by positive $\Delta 8/4$
462 and $\Delta 7/4$ and plot below the mixing lines between a HIMU type end-member and DMM
463 or lower mantle compositions (Fig. 10), strongly suggesting the contribution of an
464 EM1-type end-member to the 2014 Fogo mantle source(s). Interestingly, the products
465 erupted in 2014 mark a change on the evolutionary trend reported by previous authors
466 for Fogo eruptions (Gerlach et al., 1988; Escrig et al., 2005) which was characterized by
467 an increasing contribution of the enriched component. Indeed, the 2014 lavas have less

468 radiogenic Sr, but more radiogenic Nd signatures than those from the 1951 and 1995
469 eruptions.
470 Fogo's 2014 lavas (MgO ≤ 6.4 wt %, Mg# ≤ 53.2; Ni ≤ 42 ppm) cannot be considered
471 representative of primary magmas. This fact and its chemical variability (MgO down to
472 2.93 wt.%; Ni down to 6 ppm) emphasize the role of magma evolution processes to
473 explain the observed compositional range. This is reinforced by the phonolitic
474 composition of the glassy groundmass of some lavas (MgO down to 0.66 wt%; total
475 alkalis up to 15.76 wt%; see Supplementary Material S3-G).
476 The important role of clinopyroxene fractionation is suggested by its occurrence as
477 phenocryst in most samples and by the Sc decrease with increasing concentration of
478 strongly incompatible trace elements such as La (Fig 8A), here used as a proxy of
479 magma evolution index. Fractionation of clinopyroxene must have been preceded by
480 crystallization of olivine as indicated by the occurrence of olivine inclusions in
481 clinopyroxene phenocrysts. The Dy/Dy* ratio, as defined by Davidson et al. (2013),
482 tends to decrease from up to 0.81 in tephrites, down to 0.61 in phonotephrites, a
483 tendency that, according to those authors, can be attributed either to amphibole or to
484 clinopyroxene fractionation. If the importance of clinopyroxene fractionation was
485 already demonstrated, the positive correlation of Dy/Dy* and Nb/U ratios (Fig. 8B)
486 emphasizes the role of amphibole since, at odds with what happens with this mineral,
487 clinopyroxene does not have the capacity to fractionate Nb from U (e.g. Adam and
488 Green, 2006).
489 The calculated water content of the melt during kaersutite crystallization range from
490 3.81 to 4.14 wt% (± 0.78 wt%) while oxygen fugacity is estimated in the range of 0.92
491 to 2.3 log units above NNO (± 0.37 log units) using the methodology of Ridolfi and
492 Renzulli (2012). The obtained $fO_2$ values are comparable to those reported for some
493 other intraplate ocean islands (e.g. Madeira; Mata and Munhá, 2004). These relatively
494 high $fO_2$ values are reflected in the composition of pyroxenes for which high $Fe3^+$

contents were calculates based on the stoichiometry (Suplementary material S3-A), but not in the amphibole (Suplementary material S3-C). This suggests the incorporation of Ti ($TiO_2$ up to 6.13 wt%) into the octahedral position of kaersutite through the substitution $^{[VI]}R^{2+} + 2OH^- = {}^{[VI]}Ti^{4+} + 2O^{2-}$, which favours high $Fe^{2+}/Fe^{3+}$ (Satoh et al., 2004).

As also reported for the previous Fogo's eruption (e.g. Munhá et al., 1997; Hildner et al., 2012) plagioclase did not play a significant role in the evolution of 2014 magmas, as inferred from its rarity among phenocrysts and from the continuous Sr increase (1194 to 1408 ppm) throughout the erupted suite. Judging from the comparatively high $Al_2O_3$, $Na_2O$ and $K_2O$ concentrations determined in the glassy phonolitic matrix, plagioclase and alkali feldspar fractionation was also not important for the generation of such evolved compositions. On the other hand, the role of Fe-Ti oxides and apatite fractionation is made evident by the significant decrease on $P_2O_5$ (Fig. 8C) and $TiO_2$ (not shown) concentrations from the most evolved tephrites ($SiO_2$ < 45.2.%) to phonotephrites ($SiO_2$ > 47.7 wt. %) (see also Table I). The fractionation of these two non-silicate phases, with the consequent significant increase in silica content of magmatic liquids, was probably the cause for the small compositional gap ($\Delta SiO_2$ = 2.5%) separating those two lithotypes.

Even though the isotope differences precludes the studied rocks to be considered comagmatic with those erupted in 1951 and 1995 (see section 4.4), samples from these three eruptions plot along the same trends in most variation diagrams, suggesting that they share a common magma evolution history (e.g. Fig. 8 A and C). However, Fig. 8B emphasizes, despite similar trends, the lower Nb/U and Dy/Dy* ratios of the 2014 rocks relatively to the rocks of similar degree of evolution generated during the two previous eruptions.

Indeed, the less evolved 2014 rocks are characterized by lower Nb/U ratios (60 ± 3) than the basanitic/tephritic lavas from the 1995 and 1951 eruptions (95 ± 4; Hildner et

al., 2011; 2012). Given the similar degree of evolution, these differences cannot be explained by fractional crystallization. The 2014 Nb/U ratios fits the typical OIB value (EM lavas excluded) of 52 ± 15 obtained by Hofmann (2003). As shown by this author, either the EM-type mantle components or the continental crust have significantly lower Nb/U ratios. Consequently the higher contribution of an enriched end-member (EM type) for the 1995 and 1951(see above) lavas cannot be invoked as a cause for their higher Nb/U ratios.

Nb/U ratios significantly higher than the typical OIB lavas have also been reported for some Canary lavas by Lundstrom et al. (2003). These authors defended that this can be the reflex of mixing between ascending plume-derived magmas and lithospheric melts with a significant contribution from amphibole present in low-solidus mantle domains. These domains would have been generated by metasomatic (s.l.) processes during previous stages of islands building. We suggest that a similar process may have been responsible for the significantly higher Nb/U and Dy/Dy* ratios of the 1995 and 1951 lavas. Since their vents, and probably also the ascending magma paths, were almost coincident with those of 2014, we speculate that such low-solidus lithospheric domains were already exhausted and did not contribute significantly for the composition of the subsequent 2014 eruption products.

As observed for the precedent 1995 eruption (Munhá et al., 1997; Silva et al., 1997; Hildner et al., 2011), the initial products erupted in 2014 were more evolved (phono-tephrites; $SiO_2$ up to 47.99 wt.%) than those emitted subsequently (tephrites, s.l.), for which $SiO_2$ contents as low as 43.03 wt.% were obtained. Considering the composition of the erupted magmas, assuming a complete degassing during eruption (suggested by very low loss on ignition), and using the algorithm of Giordano et al. (2008), the viscosity of the phonotephrites would have been some 10 times higher than that of the less evolved tephrites. This partially explains the evolution of lava flow morphology during the course of the eruption, which exhibited *a'a* characteristics during the initial

549 eruptive stages, whilst *pāhoehoe* type lavas became more frequent during the
550 subsequent effusion of the less viscous tephritic lava flows.
551
552 **5.2 Thermobarometric evidence for magma reservoirs into the mantle**
553 Geothermobarometric estimates based on phenocrysts and cognate megacrysts have
554 been considered to be important to constrain the magmatic plumbing system of a
555 volcano, given they can be used to calculate the depths of magma stalling/stagnation at
556 mantle/crustal chambers. Indeed, silicates are characterized by very low intra-crystalline
557 diffusion rates, thus tending to preserve the composition acquired at the moment of
558 crystallization.
559 We used the clinopyroxene-liquid thermobarometer of Putirka et al. (2003) for which
560 lower uncertainties are foreseen than those reported for methods only using the
561 clinopyroxene composition (Putirka, 2008; see also Geiger et al., 2016 for a review on
562 clinopyroxene thermobarometry). The method is based on jadeite–
563 diopside/hedenbergite exchange equilibria in hydrous conditions, which are shown to
564 have existed at Fogo by the presence of amphibole (see also above for an estimate of
565 water content in magma). As we used phenocryst cores and whole rock compositions as
566 proxies of the crystal-liquid pairs, the P-T results obtained will be regarded as the
567 conditions prevailing during early stages of clinopyroxene phenocrysts crystallization,
568 assuming that no magma mixing occurred after pyroxene crystallization.
569 In order to use mineral/liquid thermobarometers it is mandatory to test if the
570 crystal/melt pairs used testify equilibrium conditions. On a first approach a visual
571 screening was made to identify textural evidence for disequilibrium, those showing
572 irregular or reabsorbed shapes were avoided. Furthermore, only core analyses of un-
573 zoned or normally zoned phenocrysts where used. No mineral correction was made to
574 the whole-rock composition due to the lack of evidence for significant accumulation (≤
575 10 % of phenocryst phases).

576 Considering the concerns regarding the efficacy of the Fe-Mg exchange in deciphering
577 situations of pyroxene-melt equilibrium (e.g. Mollo et al., 2013), we used instead the
578 comparison between predicted and measured components in clinopyroxene (diopside-
579 hedenbergite; enstatite-ferrosilite; Ca-Tschermak's) as proposed by Putirka (1999).
580 Following the recommendations of Putirka et al. (2003), only clinopyroxenes whose
581 compositions are within the ± 2σ level of the predicted ones were used in the
582 thermobarometric calculations. The standard errors of estimation (SEE) of the Putirka et
583 al. (2003) method are 1.7 kbar and 33 ºC, while analytical uncertainties, calculated
584 using the relative standard deviation of whole rock and microprobe analyses of
585 reference materials are significantly lower than the uncertainties of the method.
586 The temperatures obtained for pyroxene crystallization range from 1045 to 1063 ºC for
587 the phonotephrites and 1102 to 1143 ºC for the tephrites. Pyroxene phenocrysts
588 crystallized from phonotephritic magmas at pressures in the range between 560 and 778
589 MPa, whereas the tephrites yield variations between 690 and 890 MPa (Fig. 9).
590 For amphiboles we used the single-phase thermobarometric and chemometric equations
591 proposed by Ridolfi and Renzulli (2012), based on multivariate least-squares regression
592 analyses of a large database of amphibole compositions in alkaline magma systems. For
593 this method the authors claim low uncertainties: P ± 11.5%, T ± 23.5ºC. The application
594 of the thermobarometer shows that the values obtained for kaersutites occurring in
595 phonotephrites and tephrites are similar within error (1032 to 1050ºC and 568 to 620
596 MPa; see Fig. 9).
597 The kaersutite occurring in the 2014 Fogo lavas show ubiquitous signs for
598 disequilibrium, presenting evidence for partial (reaction rims) to total
599 (pseudomorphosis) substitution by polycrystalline aggregates of rhönite and
600 clinopyroxene. We interpret the occurrence of rhönite and of the associated
601 clinopyroxene as a consequence of the kaersutite destabilization resulting from magma
602 degassing upon ascent, given the decrease of $H_2O$ solubility in magmas as pressure

603 drops (e.g. De Angelis et al., 2015). The destabilization of amphibole most probably
604 occurs at pressures below 100-150 MPa (e.g., Rutherford, 2008) with reaction rims
605 developing, for hornblende compositions, at pressures from circa 100 MPa down to 40
606 MPa (Browne and Gardener, 2006).
607 Amphibole reaction rims are often used to estimate magma ascent rate since their
608 thickness, size and the shape of the replacing mineral phases are all dependent on it
609 (Chiaradia et al., 2011; Browne and Gardner, 2006). Since the reaction rims observed in
610 kaersutite crystals from the 2014 lavas are thick (> 500 microns) and complete
611 pseudomorphosis of mm-sized crystals (up to 4mm) is common, it is valid to assume on
612 a qualitative basis and based on Browne and Gardener's (2006) experimental data that
613 the time of exposure of kaersutite to low $PH_2O$ before quenching at the surface was
614 relatively long (> 1 month). Thus, the occurrence of rhönite and the degree of kaersutite
615 replacement by rhönite suggest a late and short stagnation/stalling at crustal levels (i.e.
616 at pressures below 100 MPa; < 4.3 km below the island summit or < 1.5 km below sea
617 level) after a longer storage at deeper magma chambers.
618 In order to convert the calculated pressures to depths several assumptions has to be
619 done, the depth of Moho being the one with more impact in the obtained results.
620 Vinnik et al. (2012), proposed that at the Cape Verde archipelago the crust would be
621 significantly thicker than the normal oceanic crust, extending down to 20-30 km depth.
622 This was not supported by a later study (Wilson et al., 2013), which placed the Moho at
623 significantly shallower depths, in agreement with the models of Lodge and Helffrich
624 (2006), Pim et al. (2008) and Wilson et al. (2010). In this study we adopt 13.5 km as the
625 depth of Moho beneath the Fogo Island (see Wilson et al., 2010; 2013).
626 Considering a height of 5800 m for the Fogo island edifice (≈ 3000 m below present sea
627 level), an average density of 2400 $kg.m^{-3}$ (Dash et al., 1976) for the island edifice, a
628 crustal density of 2800 $kg.m^{-3}$ inferred from seismic receiver functions (Lodge and
629 Helffrich, 2006), a mantle density of about 3200 $kg.m^{-3}$ at the Fogo region (Pim et al.,

630 2008), a Moho depth at 13.5 km below sea level (Wilson et al., 2010; 2013) and taking
631 into account the uncertainties of the barometric methods (see above) the crystallization
632 depth of clinopyroxene phenocrysts ranges approximately (± 5.5 km) from 17.8 to 28.4
633 km below Fogo's summit, or 15.0 to 25.6 km below sea level. For amphiboles the same
634 presupposes allow considering their crystallization at depths between 18.2 and 19.9 km
635 (± 3 km) below Fogo's summit, or 15.4 to 20.1km below sea level. Considering the
636 most common estimates for the crustal thickness at the Cape Verde region (≈ 12 to 13.5
637 km; Lodge and Helffrich, 2006; Pim et al., 2008; Wilson et al., 2010; 2013) the
638 obtained results suggest that the major fractionation events occurred in magma
639 chambers located into the mantle.
640 Geobarometric studies of the previous two eruptions also revealed pre-eruptive magma
641 storage at shallow mantle depths, followed by a short-period of magma stalling at
642 crustal levels (Munhá et al., 1997; Hildner et al., 2011, 2012). The depths of
643 clinopyroxene equilibration obtained in this study for the 2014 eruption (890 to 560
644 MPa; see above), although partially overlapping those presented for the historical
645 eruptions by Hildner et al. (2011, 2012) (680 to 460 MPa), extends to higher pressures.
646 However it must be noted that the pressure estimates by those authors refer to the final
647 crystallization level, while our data represents the first crystallization stages of
648 clinopyroxene phenocrysts.
649 The causes for the development of magma reservoirs within the mantle are still not
650 understood. Changes in buoyancy have been considered as an explanation for magma
651 stagnation during ascent (e.g. Ryan, 1994). However, Jagoutz (2014) emphasized that,
652 ascending magmas can stagnate even when they are less dense than the surrounding
653 rocks. A similar point of view was defended by Menand (2008) who considered that
654 buoyancy is unlikely to be a major control in the emplacement of sills, which can be
655 viewed as precursors of magma reservoirs (Gudmundsson, 2012). Moreover, as shown
656 by Putirka (2017), hydrated magmas with MgO contents similar to those erupted in the

2014 Fogo eruption are less dense than the mantle, or even than the lower crustal rocks, indicating that buoyancy cannot be the explanation for the stagnation of Fogo magmas in the mantle. As proposed by Menand (2008), the presence of rheological anisotropies could be the primary factor determining the depth of magma stalling or stagnation. This can lead to the inference that the thickness of the elastic lithosphere exerts a major control on the depth of magma reservoirs. However, for the Cape Verde Archipelago the elastic thickness is estimated at 30 km (Pim et al., 2008) and our barometric data suggest magma emplacement at shallower depths, invalidating, in this case, such a proposal. Regional flexural stresses produced by the volcanic edifice loading are also thought to strongly influence the plumbing systems by generating a vertical contrast between tensile and compressive stress zones, capable of influencing the depth of magma stalling (see Putirka, 1997 and references therein). We do not have data to evaluate this hypothesis.

Whatever the cause for the development of mantle magma reservoirs, they seem to be common on ocean islands during periods of low magma supply rates (e.g. Longpré et al., 2008; Stroncik et al., 2009; Klügel et al., 2015) as was the case during the latest (this study) and the previous eruptions of Fogo volcano (Munhá et al., 1997; Hildner et al., 2011; 2012).

The scenario here proposed for the ascent of the 2014 Fogo magmas and of its plumbing system receives support from independent data. Indeed, a seismic event on October 4, 2014 (i.e. 50 days before the eruption) with a hypocentre 17 km below sea level (19.8 km below the Fogo summit), was interpreted by Instituto Nacional de Meteorologia e Geofísica (INMG, Cabo Verde) as resulting from the rupture of the roof of a mantle reservoir allowing magma transfer to shallower levels. Also, geodetic modelling of Sentinel-TOPS interferometry by Gonzalez et al. (2015) revealed the lack of deformation at the island-scale during and pre-eruption times, further suggesting the deep location of the main magma reservoirs.

684 **5.3 Evidence for small-scale mantle heterogeneity and short-term compositional**
685 **evolution of Fogo volcano.**

686 As mentioned above, the Cape Verde Archipelago is known by its remarkable
687 geochemical intra-island heterogeneity (e.g. Gerlach et al., 1988; Doucelance et al.,
688 2003). Significant intra-island time-dependent geochemical variations are also common
689 as shown for most Cape Verde Islands (e.g. Barker et al., 2010; Mourão et al., 2012 a).
690 Intra-island heterogeneities have also been described for presumably coeval rocks, such
691 is the case of the Recent Volcanics of São Vicente Island (Trindade et al., 2003), and
692 also of the Fogo Island where, as shown by Escrig et al. (2005), lavas erupted since
693 1785 present measurable variability on isotope signatures.

694 In opposition to incompatible trace-element ratios, which can be fractionated during
695 partial melting and crystal fractionation processes, radiogenic isotope ratios are not
696 changed during such events. They are thus a reliable indicator of source heterogeneity,
697 even though the isotope variability of lavas tends to be smaller than that of the mantle
698 source due to eventual mixing/homogenization processes (e.g. Stracke and Bourdon,
699 2009).

700 The 2014 volcanic products have clearly more unradiogenic Pb and Sr ($^{206}Pb/^{204}Pb$
701 down to 18.972; $^{87}Sr/^{86}Sr$ down to 0.703613) but more radiogenic Nd ($^{143}Nd/^{144}Nd$ up to
702 0.512789) signatures than the previous two eruptions ($^{206}Pb/^{204}Pb$ up to 19.273; $^{87}Sr/^{86}Sr$
703 up to 0.70379; $^{143}Nd/^{144}Nd$ down to 0.51272; see also Figs 6 and 7). Considering that
704 the 2014 lavas erupted from vents localized less than 200 and 2000 m of those from the
705 two previous eruptions (1951 and 1995) and that these 3 eruptions occurred within a
706 time lapse of only 63 years, such differences emphasize the presence of small-scale
707 heterogeneities in the mantle sources feeding the volcanism of Fogo Island and the
708 absence of significant magma mingling/homogenization before eruption.

709 The ability of magmas erupted from a volcano to show the source heterogeneity
710 depends on the degree of partial melting, on the size of magma chambers and on the

711 time of residence in such reservoirs. The higher the degree of partial melting, the higher
712 is the capability of the extracted magmas to average the composition of a heterogeneous
713 source. As a consequence low degree partial melts reflect better the compositional
714 variability of the source (e.g. Stracke and Bourdon, 2009; Martins et al., 2010). It is
715 accepted that the lithosphere exerts a major control in the final depth and extent of sub-
716 lithospheric mantle melting (e.g. Watson and Mckenzie, 1991; Humphrey and Niu,
717 2009; Niu et al., 2011), even though the thickness of mature (> 70Ma) oceanic
718 lithosphere does not surpass ≈90 km (Niu et al., 2011). The Cape Verde islands stand on
719 a 120-140 My old oceanic crust characterized by significantly high values of admittance
720 (geoid to depth ratio) (Monnerau and Cazennave, 1990). These suggests that lithosphere
721 may extend to depths below the spinel-garnet transition (≈3 GPa; Klemme and O'Neil,
722 2000) in agreement with previous studies for Cape Verde islands (e.g. Gerlach et al.,
723 1998; Barker et al., 2010; Mourão et al., 2012a). Even taking into account that the less
724 evolved 2014 magmas (tephrites) are not characterized by primary or primitive
725 compositions, this percept is endorsed by (Tb/Yb)n ratios higher than 2.3, which is
726 significantly above the threshold value of 1.8 proposed by Wang et al. (2002) as a proxy
727 for spinel-garnet facies transition. Indeed it would be necessary to consider a (Tb/Yb)n
728 increase higher than 27% during magma evolution – which is not expectable from the
729 commonly accepted D values (e.g. Adam and Green, 2006) – to place the mean melting
730 depths outside the garnet zone. Moreover, 2014 magmas show a Tb/Yb decrease from
731 tephrites for the more evolved phonotephrites.
732 The thickness of the lithosphere exerts a first-order control on the extent of partial
733 melting (e.g. Humphreys and Niu, 2009). For the present case, a lithosphere some 90
734 km thick (see above) would have constrained the melting to small extent. Despite the
735 exact extent of melting is difficult to assess given the significantly evolved character of
736 lavas (MgO < 6.4 wt%) and the uncertainty derived from the lack of knowledge about
737 the relative proportion of peridotite and eclogite in the mantle source, the highly $SiO_2$ -

738 undersaturated character of the Fogo lavas (2014: normative *ne* up to 23.04 %) and the
739 high TiO2 contents clearly suggest low percentages of partial melting, with the
740 consequent deficient averaging of the isotopic variability of the source. The above
741 referred lack of correlation between elemental and isotope ratios (see 4.3) also points to
742 low degrees of melting during which a significant elemental fractionation occurs erasing
743 any correlation between incompatible element ratios and isotope ratios (see Stracke and
744 Bourdon, 2009).
745 After extraction, the degree of melt homogenization will depend on the occurrence of a
746 plumbing system with large magmatic chamber(s), and of long magma residence times
747 within the system, allowing mixing of different batches of melt. Data gathered from
748 several islands suggest that for voluminous magma chambers to form, high magma
749 supply rates are needed; conversely, during evolutionary stages characterized by low
750 magma supply rates a plethora of small and ephemeral magma reservoirs tend to form,
751 many of them within the mantle (see Klügel et al., 2000; 2005; Stroncik et al., 2009 and
752 references therein), and this is also the case for the recent magmatism of Fogo. The
753 evidence for small and ephemeral magma reservoirs beneath Fogo was already
754 proposed for the previous eruptions (Munhá et al., 1997; Hildner et al., 2012). This may
755 be also the case for the 2014 eruption as suggested by the compositional change during
756 the latest two eruptions (from phonotephrites to basanites/tephrites) and, despite the
757 associated methodological errors, by distinct depths of magma chambers where
758 clinopyroxene and kaersutite crystalized, both evidences precluding a large
759 homogenizing reservoir.
760
761 **6. Concluding remarks**
762 • Magmas erupted from November 23 to December 7, 2014 at Fogo Island (Cape
763 Verde Archipelago) are alkaline, exhibit significantly evolved compositions (Ni
764 < 42 ppm) and are classified as tephrites and phonotephrites. The compositional

765 range is slightly smaller than that reported for the 1995 eruption, but larger than
766 the displayed by the 1951 eruption, for which no phonotephrites were erupted.

767 • Similarly to 1995 (Munhá et al., 1997; Silva et al., 1997; Hildner et al., 2011),
768 the eruption of phonotephritic lavas preceded the effusion of the tephritic ones
769 suggesting the existence of a compositional/density zoning inside the pre-
770 eruptive magma chamber or of several magma reservoirs, in agreement with
771 barometric data.

772 • Geobarometric estimates using clinopyroxene and kaersutite compositions
773 indicate that fractional crystallization mainly occurred in magma chambers
774 located in the mantle (down to 25.6 ± 5.5 km below the sea level), followed by a
775 short residence time (< 60 days) at crustal levels.

776 • Erupted magmas are characterized by positive εNd, εHf, Δ8/4 and Δ7/4. Their
777 compositions reflect a mantle source where ancient recycled ocean crust and an
778 enriched component (EM1-type) are present. The 2014 lavas have less
779 radiogenic Sr, but more radiogenic Nd compositions, than those from the 1951
780 and 1995 eruptions, marking a change on the evolutionary trend reported by
781 previous authors for Fogo (Gerlach et al., 1988; Escrig et al., 2005) which was
782 characterized by an increasing contribution of the EM1-type component.

783 • Although the 2014 eruption vents are almost spatially coincident with those of
784 1995 and less than 2 km away from the 1951 vents, their lavas are isotopically
785 different from those generated in the previous two eruptions. These differences
786 in magmas erupted on a very limited area and short interval (63 years) reflect the
787 heterogeneity of the mantle source and the lack of averaging/mingling during
788 partial melting and ascent through the plumbing system. For these, the lid effect
789 of the old (120-140 Ma) and thick lithosphere is considered of utmost
790 importance.

- The lower Nb/U ratios of the 2014 rocks as compared with previous eruptions is considered to reflect the lack of significant mixing of ascending plume magmas with lithospheric melts, as opposed to what has been hypothesized for 1995 and 1951 magmas.

**Acknowledgements**

We dedicate this paper to the memory of Luís Celestino Silva (1936-2017), a pioneer in the geology of Cape Verde: his knowledge, enthusiasm and kindness marked most of the authors of this work.

This research received financial support from FCT (Fundação para a Ciência e Tecnologia) through projects REGENA (PTDC /GEO-FIQ/3648/2012) and FIRE (PTDC/GEO-GEO/1123/2014), as well as through project UID/GEO/50019/2013 to Instituto Dom Luiz (IDL). R. Ramalho was funded by a FP7-PEOPLE-2011-IOF Marie Curie International Outgoing Fellowship, which is acknowledged. The authors are grateful to Pedro Rodrigues for skilled assistance during electron microprobe analyses. Field work of J. Mata was partially funded by Bernardo Mata. Kayla Iacovino is acknowledged for the permission to use her Excel spreadsheet to calculate magma viscosity (see http://www.kaylaiacovino.com/tools-for-petrologists/). Cristina de Ignacio, an anonymous reviewer and the Editor (Nelson Eby) are acknowledged for their constructive comments, corrections and suggestions, which significantly contributed for the quality of this paper.

**References**

Adam, J., Green, T. 2006. Trace element partitioning between mica and amphibole-bearing garnet lherzolite and hydrous basanitic melt: 1. Experimental results and the investigation of controls on partitioning behavior. Contributions to Mineralogy and Petrology 152, 1-17.

Bagnardi, M., Gonzàlez, P.J., Hooper, A. 2016. High-resolution digital elevation model from tri-stereo Pleiades-1 satellite imagery for lava flow volume estimates at Fogo Volcano: Tri-stereo Pleiades DEM of Fogo Volcano. Geophys. Res. Lett.,43, doi:10.1002/2016GL06945

Barker, A.K., Holm, P.M., Peate, D.W., Baker, J.A. 2009. Geochemical stratigraphy of submarine lavas (3–5 Ma) from the Flamengos Valley, Santiago, southern Cape Verde islands. Journal of Petrology 50, 169-193.

Barker, A.K., Holm, P.M., Peate, D.W., Baker, J.A. 2010. A 5 million year record of compositional variations in mantle sources to magmatism on Santiago, southern Cape Verde archipelago. Contributions to Mineralogy and Petrology 160, 133-154.

Barker, A.K., Troll, V.R., Ellam, R.M., Hansteen, T.H., Harris, C., Stillman, C.J., Andersson, A. 2012. Magmatic evolution of the Cadamosto Seamount, Cape Verde: beyond the spatial extent of EM1. Contributions to Mineralogy and Petrology 163, 949 -965.

Beier, C., Haase, K. M., Abouchami, W., Krienitz, M.-S., Hauff, F. 2008. Magma genesis by rifting of oceanic lithosphere above anomalous mantle: Terceira Rift, Azores. Geochemistry, Geophysics, Geosystems 9, Q12013.

Browne, B.L., Gardner, J.E. 2006. The influence of magma ascent path on the texture, mineralogy, and formation of hornblende reaction rims. Earth and Planetary Science Letters 246, 161-176.

Brum da Silveira, A., Madeira, J., Munhá, J., Mata, J.; Martins, S., Mourão, C., Tassinari, C. 2006. The summit depression of Fogo Island (Cape Verde): caldera and/or flank collapse? Abstracts and Programme of the George P. L. Walker symposium on Advances in Volcanology, Reykolt, Islândia, 23.

Caldeira, R., Guimarães, F., Mata, J. Silva, P., Moreira, M., Ferreira, P. 2015. Mineral Chemistry of Ultramafic Nodules from Lavas of the Fogo Island 2014 Eruption (Cape Verde). Preliminary results. Livro de Resumos do X Congresso Ibérico de Geoquímica/XVIII Semana de Geoquímica, 51-53, LNEG, Lisboa.

Cappello, A., G. Ganci, S. Calvari, N. M. Pérez, P. A. Hernández, S. V. Silva, J. Cabral, and C. Del Negro. 2016. Lava flow hazard modeling during the 2014–2015 Fogo eruption, Cape Verde, Journal of Geophysical Research, Solid Earth 121, 1-14.

Chauvel, C., Blichert-Toft, J. 2001. A hafnium isotope and trace element perspective on melting of the depleted mantle. Earth Planetary Science Letters 190, 137–151.

Chauvel, C., Lewin, E., Carpentier, M., Arndt, N., Marini, J.-C. 2008. Role of recycled oceanic basalt and sediment in generating the Hf–Nd mantle array. Nature Geoscience 1, 64–67.

Chauvel, C., Bureau, S., Poggi, C. 2011. Comprehensive chemical and isotopic analyses of basalt and sediment reference materials. Geostandards and Geoanalytical Research 35, 125–143.

Chiaradia, M., Müntener, O., Beate, B. 2011. Enriched basaltic andesites from mid-crustal fractional crystallization, recharge, and assimilation (Pilavo Volcano, Western Cordillera of Ecuador). Journal of Petrology 52, 1107-1141.

Christensen, B., Holm, P., Jambon, A., Wilson, J. 2001. Helium, argon and lead isotopic composition of volcanics from Santo Antão and Fogo, Cape Verde Islands. Chemical Geology 178, 127–142.

Cooper, K.M. 2017. What does a magma reservoir look like? The “crystal’s eye” view. Elements 13, 23-28.

Courtney, R., White, R. 1986. Anomalous heat flow and geoid across the Cape Verde Rise: Evidence for dynamic support from a thermal plume in the mantle. Geophysical Journal of the Royal Astronomical Society 87, 815-868.

Cashman, K.V., Sparks, R.S.J., Blundy, J.D. 2017. Vertically extensive and unstable magmatic systems: A unified view of igneous processes. Science 355, eaag3055, 9 pages.

Dash, B.P., Ball, M.M., King, G.A., Butler, I.W., Rona, P.A. 1976. Geophysical investigation of the Cape Verde archipelago. Journal of Geophysical Research 81, 5249-5259.

Davidson, J., Turner, S., Plank, T. 2013. Dy/Dy*: Variations Arising from Mantle Sources and Petrogenetic Processes. Journal of Petrology 54, 525-537.

Day, S., Heleno da Silva, S., Fonseca, J. 1999. A past giant lateral collapse and present day instability of Fogo, Cape Verde Islands. Journal of Volcanology and Geothermal Research 94, 191-218.

De Angelis, S.H., Larsen, J., Coombs, Dunn, A., Hayden, L. 2015. Amphibole reaction rims as a record of pre-eruptive magmatic heating: An experimental approach. Earth and Planetary Science Letters 426, 235–245

Doucelance, R., Escrig, S., Moreira, M., Gariépy, C., Kurz, M.D. 2003. Pb-Sr-He isotope and trace element geochemistry of the Cape Verde Archipelago. Geochimica et. Cosmochimica Acta 67, 3717-3733.

Eisele, S., Reißig, S., Freundt, A., Kutterolf, S., Nürnberg, D., Wang, K.L, Kwasnitschka, T. 2015. Pleistocene to Holocene offshore tephrostratigraphy of highly explosive eruptions from the southwestern Cape Verde Archipelago. Marine Geology 369, 233-250.

Escrig, S., Doucelance, R., Moreira, M., Allègre, C.J. 2005. Os isotope systematics in Fogo Island: evidence for lower continental crust fragments under the Cape Verde Southern islands. Chemical Geology 219, 93-113.

Faria, B., Fonseca, J. F. B. D. 2014. Investigating volcanic hazard in Cape Verde Islands through geophysical monitoring: network description and first results. Natural Hazards and Earth System Sciences 14, 485–499.

Foeken, J.P.T., Day, S., Stuart, F.M. 2009. Cosmogenic $^{3}$He exposure dating of the Quaternary basalts from Fogo, Cape Verdes: Implications for rift zone and magmatic reorganisation. Quaternary Geochronology 4, 37-49.

Forte, A.M., Quere, S., Moucha, R., Simmons, N.A., Grand, S.P., Mitrovica, J.X., Rowley, D.B. 2010. Joint seismic-geodynamic-mineral physical modelling of African geodynamics: a reconciliation of deep-mantle convection with surface geophysical constraints. Earth Planetary Science Letters 295, 329–341.

French, S.W., Romanowicz, B. 2015. Broad plumes rooted at the base of the earth's mantle beneath major hotspots. Nature 525, 95-99.

Galer, S.J.G., Abouchami, W. 1998. Pratical application of lead triple spiking for correction of instrumental mass discrimination. Mineralogical Magazine 62 A, 491-492.

Geiger, H., Barker, A., Troll, V. 2016. Locating the depth of magma supply for volcanic eruptions, insights from Mt. Cameroon. Scientific Reports 6, 33629.

Gerlach, D., Cliff, R., Davies, G., Norry, M., Hodgson, N. 1988. Magma sources of the Cape Verde archipelago: Isotopic and trace element constraints. Geochimica et Cosmochimica Acta 52, 2979-2992.

Gibson, S.A., Geist, D.G., Day, J.A., Dale, C.W. 2012. Short wavelength heterogeneity in the Galápagos plume: Evidence from compositionally diverse basalts on Isla Santiago. Geochemistry, Geophysics, Geosystems 13, doi: 10.1029/2012GC004244.

Giordano, D., Russell, J. K., Dingwell, D. B. 2008. Viscosity of magmatic liquids: A model. Earth and Planetary Science Letters, 217, 123-134.

González, P. J., M. Bagnardi, A. J. Hooper, Y. Larsen, P. Marinkovic, S. V. Samsonov, Wright, T. J. 2015. The 2014–2015 eruption of Fogo volcano: Geodetic modeling of Sentinel-1 TOPS interferometry. Geophysical Research Letters 42, 9239–9246.

Gudmundsson, A., 2012. Magma chambers: Formation, local stresses, excess pressures, and compartments: Journal of Volcanology and Geothermal Research 237–238, 19–41.

Hart, S.R. 1984. A large-scale isotope anomaly in the Southern Hemisphere mantle. Nature 309, 753-757.

Hildner, H., Klügle, A., Hauff, F. 2011. Magma storage and ascent during the 1995 eruption of Fogo, Cape Verde Archipelago. Contributions to Mineralogy and Petrology 162, 751–772.

Hildner, H., Klügle, A., Hansteen, T.2012. Barometry of lavas from 1951 eruption of Fogo, Cape Verde Islands: Implications for historic and prehistoric magma plumbing system. Journal of Volcanology and Geothermal Research 217-218, 73-90.

Hoernle, K., Tilton, G., Le Bas, M.J., Duggen, S., Garbe-Schönberg, D. 2002. Geochemistry of oceanic carbonatites compared with continental carbonatites: mantle recycling of oceanic crustal carbonate. Contribution to Mineralogy and Petrology 142, 520-542.

Hofmann, A.W. 2003. Sampling mantle heterogeneity trough oceanic basalts: isotopes and trace elements, in: Carlson, R. (Ed.), Treatise on geochemistry, vol. 2 - The mantle and core. Elsevier-Pergamon, Oxford, pp. 61-101.

Holm, P.M., Wilson, J.R., Christensen, B.P., Hansen, L., Hansen S.L., Hein, K.M., Mortensen, A.K., Pedersen, R., Plesner, S., Runge, M.K. 2006. Sampling the Cape Verde mantle plume: evolution of the melt compositions on Santo Antão, Cape Verde Islands. Journal of Petrology 47, 145-189.

Holm, P.M., Grandvuinet, T., Friis, J., Wilson, J.R., Barker, A.K., Plesner, S. 2008. An $^{40}$Ar-$^{39}$Ar study of the Cape Verde hot spot: Temporal evolution in a semistationary plate environment. Journal of Geophysical Research 113, B08201.

Humphreys, E., Niu, Y. 2009. On the composition of ocean island basalts (OIB): the effects of lithospheric thickness variation and mantle metasomatism. Lithos 112, 118-136.

Iwamori, H., Nakamura, H. 2015. Isotopic heterogeneity of oceanic, arc and continental basalts and its implications for mantle dynamics. Gondwana Research 27, 1131-1152.

Jagoutz O. 2014. Arc crustal differentiation mechanisms. Earth Planetary Science Letters 396, 67–77.

Jørgensen, J.Ø., Holm, P.M. 2002. Temporal variation and carbonatite contamination in primitive ocean island volcanics from S. Vicente, Cape Verde Islands. Chemical Geology 192, 249-267.

Kawabata, H., Hanyu, T., Chang, Q., Kimura, J., Nichols, A.R.L., Tatsumi, Y. 2011. The Petrology and Geochemistry of St. Helena Alkali Basalts: Evaluation of the Oceanic Crust-recycling Model for HIMU OIB. Journal of Petrology 52, 791-838.

Klemme, S., O'Neill, H., 2000. The near solidus transition from garnet lherzolite to spinel lherzolite. Contributions to Mineralogy and Petrology 138, 237-248.

Klügel, A., Hoernle, K.A., Schmincke, H-U, White, J.D.L. 2000. The chemically zoned 1949 eruption on La Palma (Canary Islands): Petrologic evolution and magma supply dynamics of a rift-zone eruption. Journal of Geophysical Research 105, 5997-6016.

Klügel, A., Hansteen, T.H., Galipp, K. 2005. Magma storage and underplating beneath Cumbre Vieja volcano, La Palma (Canary Islands). Earth and Planetary Science Letters 236, 211-226.

Klügel, A., Longpré, M-A., Cañada, L. C., Stix, J. 2015. Deep intrusions, lateral magma transport and related uplift at ocean island volcanoes. Earth and Planetary Science Letters 431, 140-149.

Kogarko, L.N., Asavin, A.M. 2007. Regional Features of Primary Alkaline Magmas of the Atlantic Ocean. Geochemistry International 45, 841-856.

Le Bas, M. 1989. Nephelinitic and basanitic rocks. Journal of Petrology 30, 1299-1312.

Le Maitre, R.W., 2002. Igneous rocks. A classification and glossary of terms. Recommendations of the International Union of Geological Sciences Subcommission on the systematics of igneous rocks. Cambridge University Press, Cambridge. 236pp.

Liu, X., Zhao, D. 2014. Seismic evidence for a mantle plume beneath the Cape Verde hotspot. International Geology Review 56, 1213-1225.

Lodge, A., Helffrich, G. 2006. Depleted swell root beneath the Cape Verde Islands. Geology 34, 449-452.

Longpré, M., Troll, V.R., Hansteen, T.H. 2008. Upper mantle magma storage and transport under a Canarian shield-volcano, Teno, Tenerife (Spain). Journal of Geophysical Research 113, doi: 10.1029/2007JB005422.

Lundstrom, C.C., Hoernle, K., Gill, J. 2003. U-series disequilibria in volcanic rocks from the Canary Islands: Plume versus lithospheric melting: Geochimica et Cosmochimica Acta 67, 4153–4177.

MacDonlad, G.A. 1968. Composition and origin of Hawaiian lavas. Geological Society of America Memoir 116, 477-452.

Madeira, J., Munhá, J., Tassinari, C., Mata, J., Brum, A., Martins, S. 2005. K/Ar ages of carbonatites from the Island of Fogo (Cape Verde). VIII Congresso Ibérico de Geoquímica e XIV Semana de Geoquímica (Portugal).

Madeira, J., Brum da Silveira, A., Mata, J., Mourão, C., Martins, S. 2008. The role of mass movements on the geomorphologic evolution of ocean islands: examples from Fogo and Brava in the Cape Verde archipelago. Comunicações Geológicas 95, 99-112.

Madeira, J., Mata, J., Mourão, C., Brum da Silveira, A., Martins, S., Ramalho, R., Hoffmann, D.L. 2010. Volcano-stratigraphic and structural evolution of Brava Island (Cape Verde) based on $^{40}Ar/^{39}Ar$, U–Th and field constraints. Journal of Volcanology and Geothermal Research 196, 219-235.

Madureira, P., Mata, J., Mattielli, N., Queiroz, G., Silva, P. 2011. Mantle source heterogeneity, magma generation and magmatic evolution at Terceira Island (Azores archipelago): Constraints from elemental and isotopic (Sr, Nd, Hf, and Pb) data. Lithos 126, 402-418.

Martins, S., Mata, J., Munhá, J., Mendes, M.H., Maerschalk, C., Caldeira, R., Mattielli, N. 2010. Chemical and mineralogical evidence of the occurrence of mantle metasomatism by carbonate-rich melts in an oceanic environment (Santiago Island, Cape Verde). Mineralogy and Petrology 99, 43-65.

Masson, D.G., Le Bas, T.P., Grevemeyer, I., Weinrebe, W., 2008. Flank collapse and large-scale landsliding in the Cape Verde Islands, off West Africa. Geochemistry, Geophysics, Geosystems 9 (7).

Mata, J., Munhá, J. 2004. Madeira Island alkaline lava spinels: petrogenetic implications. Mineralogy and Petrology 81, 85-111.

Mata, J., Moreira, M., Doucelance, R., Ader, M., Silva, L.C. 2010. Noble gas and carbon isotopic signatures of Cape Verde oceanic carbonatites: Implications for carbon provenance. Earth Planetary Science Letters 291, 70-83.

McKenzie, D., O'Nions, R.K. 1991. Partial melt distributions from inversion of rare earth element concentrations. Journal of Petrology 32, 1021-1091.

Menand, T. 2008. The mechanics and dynamics of sills in elastic layered media and their implications for the growth of laccoliths. Earth Planetary Science Letters 267, 93–99.

Millet, M.A., Doucelance, R., Schiano, P., David, K., Bosq, C. 2008. Mantle plume heterogeneity versus shallow-level interactions: A case study, the São Nicolau Island, Cape Verde archipelago. Journal of Volcanology and Geothermal Research 176, 265-276.

Mollo, S., Putirka, K., Misiti, V., Soligo, M., Scarlato, P. 2013. A new test for equilibrium based on clinopyroxene-melt pairs: Clues on the solidification temperatures of Etnean alkaline melts at post-eruptive conditions. Chemical Geology 352, 92-100.

Monnereau, M., Cazenave, A. 1990. Depth and geoid anomalies over oceanic hotspot swells: A global survey. Journal of Geophysical Research (Solid Earth) 95, 15-429.

Montelli, R., Nolet, G., Dahlen, F.A., Masters, G. 2006. A catalogue of deep mantle plumes: new results from finite-frequency tomography. Geochemistry, Geophysics, Geosystems 7, doi:10.1029/2006GC001248.

Mourão, C., Mata, J., Doucelance, R., Madeira, J., Millet, M-A., Moreira, M. 2012a. Geochemical temporal evolution of Brava Island magmatism: constraints on the variability of Cape Verde mantle sources and on the carbonatite-silicate magma link. Chemical Geology 334, 44-61.

Mourão, C., Moreira, M., Mata, J., Raquin, A., Madeira, J. 2012b. Primary and secondary processes constraining the noble gas isotopic signatures of carbonatites and silicate rocks from Brava Island: evidence for a lower mantle origin of the Cape Verde plume. Contributions to Mineralogy and Petrology 163, 995-1009.

Munhá, J.M., Mendes, M.H., Palácios, T., Silva, L.C., Torres, P.C., 1997. Petrologia e geoquímica da erupção de 1995 e de outras lavas históricas da ilha do Fogo, Cabo Verde. In: Réffega A et al. (eds). A Erupção Vulcânica de 1995 na Ilha do Fogo, Cabo Verde. IICT, Lisboa, 171-186.

Niu, Y., Wilson, M., Humphreys, E.R., O'Hara, M.J. 2011. The Origin of Intra-plate Ocean Island Basalts (OIB): the Lid Effect and its Geodynamic Implications. Journal of Petrology 52, 1443-1468.

Niu, Y.L., Wilson, M., Humphreys, E.R., O'Hara, M.J. 2012. A trace element perspective on the source of ocean island basalts (OIB) and fate of subducted ocean crust (SOC) and mantle lithosphere (SML). Episodes 35, 310-327.

Nobre Silva, I., Weis, D., Scoates, J. 2013. Isotopic systematics of the early Mauna Kea shield phase and insight into the deep mantle beneath the Pacific Ocean. Geochemistry, Geophysics, Geosystems 11, Q 09011. doi:10.1029/2010gc003176.

Palme, H., O'Neill, H.S.C. 2003. Cosmochemical estimates of mantle compositions. In: Carlson, R. (Ed.). The mantle and core. Treatise on Geochemistry 2, 1-38.

Paris, R., Giachetti, T., Chevalier, J., Guillou, H., Frank, N. 2011. Tsunami deposits in Santiago Island (Cape Verde archipelago) as possible evidence of a massive flank failure of Fogo volcano. Sedimentary Geology 239, 129-145.

Pim, J., Peirce, C., Watts, A.B., Grevemeyer, I., Krabbenhoeft, A. 2008. Crustal structure and the origin of the Cape Verde Rise. Earth Planetary Science Letters 272, 422-428.

Pollitz, F. 1991. Two-stage model of African absolute motion during the last 30 million years. Tectonophysics 194, 91-106.

Putirka, K. 1997. Magma transport at Hawaii: Inferences based on igneous thermobarometry. Geology 25, 69–72.

Putirka, K. 1999. Clinopyroxene + liquid equilibria to 100 kbar and 2450 K. Contributions to Mineralogy and Petrology 135, 151-163.

Putirka, K.D. 2008. Thermometers and barometers for volcanic systems. Reviews in Mineralogy and Geochemistry 69, 61-120.

Putirka, K.D. 2017. Down the crater: where magmas are stored and why they erupt. Elements 13, 11-16.

Putirka, K., Mikaelian, H., Ryerson, F., Shaw, H., 2003. New clinopyroxene-liquid thermobarometers for mafic, evolved, and volatile-bearing lava compositions, with applications to lavas from Tibet and the Snake River Plain, Idaho. American Mineralogist 88, 1542-1554.

Ramalho, R. 2011. Building the Cape Verde Islands. Springer Theses, 207 pp.

Ramalho, R., Helffrich, G., Cosca, M., Vance, D., Hoffmann, D., Schmidt, D.N. 2010. Episodic swell growth inferred from variable uplift of the Cape Verde hotspot islands. Nature Geoscience 3, 774-777.

Ramalho, R., Winckler, G., Madeira, J., Helffrich, G., Hipólito, A., Quartau, R., Adena, K., Schaefer, J. 2015 Hazard potential of volcanic flank collapses raised by new megatsunami evidence. Science Advances 1, doi: 10.1126/sciadv.1500456.

Ribeiro, O. 1954. A ilha do Fogo e as suas erupções. Junta de Investigações do Ultramar, Memórias, Série Geográfica I, Lisboa.

Richter, N., Favalli, M., Dalfsen, E.Z., Fornaciai, A., Fernandes, R.M.S., Rodriguez, N.P., Levy, J., Victória, S.S., Walter, Th.R. 2016. Lava flow hazard at Fogo Volcano, Cape Verde, before and after the 2014-2015 eruption. Natural Hazards and Earth Systems 16, 1925-1951.

Ridolfi, F, Renzulli, A. 2012. Calcic amphiboles in calc-alkaline and alkaline magmas: thermobarometric and chemometric empirical equations valid up to 1130 ºC and 2.2 GPa. Contributions to Mineralogy and Petrology 163, 877–895.

Rutherford, M.J. 2008. Magma ascent rates. In: Putirka, K.D. and Tepley, F.J., III (eds) Minerals, Inclusions and Volcanic Processes. Mineralogical Society of America and Geochemical Society Reviews, in Mineralogy and Geochemistry 69, 241-271

Ryan, M. 1994. Neutral-buoyancy controlled magma transport and storage in mid-ocean ridge magma reservoirs and their sheeted-dike complex: A summary of basic relationships. In: Magmatic Systems. Eds: M. P. Ryan, Chap. 6, Academic, San Diego, Caliornia.

Saki, M., Thomas, C., Nippress, S.E.J., Lessing, S. 2015. Topography of upper mantle seismic discontinuities beneath the North Atlantic: the Azores, Canary and Cape Verde plumes. Earth and Planetary Science Letters 409, 193-202.

Satoh, H., Yamaguchi, Y., Makino, K. 2004. Ti-substitution mechanism in plutonic oxy-kaersutite from the Larvik alkaline complex, Oslo rift, Norway. Mineralogical Magazine, Vol. 68, 687–697.

Silva, L.C., Mendes, M.H., Torres, P.C., Palácios, T., Munhá, J.1997. Petrografia das Formações Vulcânicas da Erupção de 1995 na Ilha do Fogo, Cabo Verde. In: Réffega, A. et al. (eds.). A Erupção Vulcânica de 1995, na Ilha do Fogo, Cabo Verde. IICT, Lisboa, 164-170.

Staudigel, H., Park, K.H., Pringle, M., Rubenstone, J.L., Smith, W.H.F., Zindler, A., 1991. The longevity of the South-Pacific isotopic and thermal anomaly. Earth and Planetary Science Letters 102, 24–44.

Stracke, A., Hofmann, A.W., Hart, S.R. 2005. FOZO, HIMU, and the rest of the mantle zoo. Geochemistry, Geophysics, Geosystems 6, Q05007, doi:10.1029/2004GC000824.

Stracke, A., Bourdon, B. 2009. The importance of melt extraction for tracing mantle heterogeneity. Geochimica et Cosmochimica Acta 73, 218-238.

Stroncik, N.A, Klügel A., Hansteen, T. H. 2009. The magmatic plumbing system beneath El Hierro (Canary Islands): Constraints from phenocrysts and naturally quenched basaltic glasses in submarine rocks. Contributions to Mineralogy and Petrology 157, 593-607.

Torres, P.C., Madeira, J., Silva, L.C., Brum da Silveira, A., Serralheiro, A., Mota Gomes, A. 1998. Carta Geológica das Erupções Históricas da Ilha do Fogo (Cabo Verde): revisão e actualização. Comunicações do Instituto Geológico e Mineiro 84, A193-196.

Torres, P., Silva, L.C., Munhá, J., Caldeira, R., Mata, J., Tassinari, C. 2010. Petrology and Geochemistry of lavas from Sal Island: Implications for the variability of the Cape Verde magmatism. Comunicações Geológicas 97, 35-62.

Trindade, M.J., Mata, J., Munhá, J. 2003. Petrogenesis of the Quaternary magmatism from the S. Vicente Island (Cape Verde). Comunicações do Instituto Geológico e Mineiro 90, 169-188.

Vervoort, J., Patchett, P., Blichert-Toft, J., Albarède, F. 1999. Relationships between Lu-Hf and Sm-Nd isotopic systems in the global sedimentary system. Earth and Planetary Science Letters 168, 79-99.

Vinnik, L., Silveira, G., Kiselev, S., Farra, V., Weber, M., Stutzmann, E. 2012. Cape Verde hotspot from the upper crust to the top of the lower mantle. Earth Planetary Science Letters 319-320, 259-268.

Wang, K., Plank, T., Walker J.D., Smith, E.I. 2002. A mantle melting profile across the Basin and Range, SW USA. Journal of Geophysical Research 107, ECV 5, 1-21.

Watson, S., McKenzie, D. 1991. Melt generation by plumes: A study of Hawaiian volcanism. Journal of Petrology 32, 501-537.

Weis, D., Kieffer, B., Maerschalk, C., Barling, J., de Jong, J., Williams, G., Hanano, D., Pretorius, W., Mattielli, N., Scoates, J., Goolaerts, A., Friedman, R., Mahoney, J. 2006. High-precision isotopic characterization of USGS reference materials by TIMS and MC-ICP-MS. Geochemistry, Geophysics, Geosystems 7, doi:10.1029/2006GC001283.

White, W.M. 2015. Isotopes, DUPAL, LLSVPs, and Anekantavada. Chemical Geology 419, 10-28.

Williams, C., Hill, I., Young, R., White, R.S. 1990. Fracture zones across the Cape Verde Rise, NE Atlantic. Journal of the Geological Society of London 147, 851-857.

Wilson, D., Peirce, C., Watts, A., Grevemeyer, I., Krabbenhoeft, A. 2013. Uplift at lithospheric swells-I: Seismic and gravity constraints on the crust and uppermost mantle structure of the Cape Verde mid-plate swell. Geophysical Journal International 182, 531-550.

Wilson, D., Peirce, C., Watts, A., Grevemeyer, I. 2013. Uplift at lithospheric swells-II: is the Cape Verde mid-plate swell supported by a lithosphere of varying mechanical strength? Geophysical Journal International 193, 798-819.

Zindler, A., Hart, S.R. 1986. Chemical geodynamics. Annual Reviews of Earth Planetary Sciences 14, 493-571.

1277 **Captions**

1278 **Fig. 1** – Geological map of the identified historical eruptions in Fogo (modified from
1279 Torres et al., 1998) superimposed on the digital terrain model of the island. The upper
1280 inset shows the location of the Island of Fogo in the archipelago of Cape Verde. The
1281 lower insets correspond to the legend of the geological map and to a structural sketch
1282 showing the geometry and location of the eruptive fissures of the last three eruptions
1283 (1951, 1995 and 2014/15), the Bordeira wall (continuous line represents the top; dashed
1284 line represents the base), and the crater rim of Pico do Fogo.

1285

1286 **Fig 2** – Photos of the 2014/15 Fogo eruption: A- general view looking East of Pico do
1287 Fogo with the active vents at the base of the cone, the flat region of Chã das Caldeiras
1288 covered with the 1995 and 2014 lava flows and the south-eastern tip of the Bordeira
1289 wall; the eruptive column rises 3 km above the vents and is dispersed by south-eastward
1290 wind at an altitude of approximately 5 km (photo taken on November 29, 2014, at 15:44
1291 UTC); B- the alignment of active vents, viewed from the south, during a low activity
1292 phase; the new cone is growing against the southeast flank of the 1995 cone (to the left);
1293 the lava flow is being fed by the southernmost vent; the lava flow at the base of the cone
1294 presents a lava channel and several skylights with degassing white columns (photo
1295 taken on December 2, 2014, at 19:35 UTC); C- night aspect of the central crater
1296 projecting plastic spatter fragments from the explosion of lava bubbles during an
1297 hawaiian lava lake phase (photo taken on November 28, 2014, at 20:48 UTC); D- aspect
1298 of vulcanian activity at the northernmost vent producing ash-laden episodic eruptive
1299 columns with the wind blowing from the north; the white plume marks the position of
1300 the effusive south vent (photo taken on November 30, 2014, at 19:24 UTC); E- aspect
1301 of the surface of the active lava flow seen from the northwest presenting strong thermal
1302 emission and degassing (photo taken on November 29, 2014, at 15:48 UTC); F- the
1303 village of Portela invaded by the front of the lava flow 3.5 km away from the effusive

1304 vent (photo taken on December 2, 2014, at 14:39 UTC). For more photos see
1305 Supplementary Material S1.
1306
1307 **Fig. 3** - Total alkali-silica (TAS) diagram (Le Maître, 2002) for the 2014 magmatic
1308 rocks and interstitial glass occurring in the matrix of the lava samples. The thick line is
1309 a compositional divider between alkaline and subalkaline volcanic rocks (MacDonald,
1310 1968). The compositional fields of the 1951 and 1995 are also shown for comparison
1311 (data from Doucelance et al., 2003; Escrig et al., 2005; Hildner et al., 2011;). U1, U2,
1312 U3 and Ph correspond to the field designations of Le Maitre et al. (2002) (U1:
1313 Tephrite/Basanite; U2: Pnotephrite; U3: Tephriphonolite; Ph: Phonolite). See the main
1314 text (*Section* 4.3) for a details on the systematics.
1315
1316 **Fig. 4** – Petrographic aspects of the lava flow samples showing the presence of
1317 clinopyroxene and kaersutite phenocrysts (A and B) in a hypocrystalline matrix with
1318 plagioclase, clinopyroxene and Fe-Ti oxides (A, B, C and D). Note the partial (A and B)
1319 or total (D) replacement of kaersutite by rhönite (opaque inosilicate of the aenigmatite
1320 group) which is marked by an arrow. Backscattered electron images showing a detailed
1321 view of the kaersutite rim replacement (E and F).
1322
1323 **Fig. 5** – Trace element characteristics of the 2014 eruptive products compared with
1324 those of the 1951 and 1995 eruptions (see Hildner et al., 2012 and Hildner et al., 2011,
1325 respectively). Normalizing values of Palme and O'Neil (2003).
1326
1327 **Fig. 6** - Pb isotopic compositions (A: $^{206}Pb/^{204}Pb$ vs. $^{207}Pb/^{204}Pb$; B: $^{206}Pb/^{204}Pb$ vs.
1328 $^{208}Pb/^{204}Pb$). Data sources: Northern Islands (Santo Antão, São Vicente and São
1329 Nicolau: Jørgensen and Holm, 2002; Holm et al., 2006; Millet et al., 2008) and
1330 Southern Islands (Fogo and Santiago: Doucelance et al., 2003; Barker et al., 2010;

1331 Martins et al., 2010). The 1951 and 1995 eruptions data are from Escrig et al., 2005.
1332 The heavy line represents the Northern Hemisphere Reference Line (NHRL) defined by
1333 Hart (1984). Also plotted are the compositions of mantle components (see main text for
1334 references).
1335
1336 **Fig. 7** – Sr, Nd (A) and Hf (B) isotope compositions. Data sources: the Santiago Island
1337 field was defined using data from Barker et al. (2009) and Martins et al. (2010). See
1338 caption of Fig. 6 for further references. No Hf isotope data exist for the 1951 and 1995
1339 eruptions.
1340
1341 **Fig 8 -** The role of clinopyroxene, olivine, amphibole and apatite fractionation on the
1342 liquid lines of descent for the 2014, 1995 and 1951 eruptions. In 8A and 8B fractional
1343 crystallization was modelled using the Rayleigh equation. Partition coefficients used in
1344 calculations can be find in the Supplementary Material S5-1 and data relative to the
1345 fractional crystallization vectors in the S5-2. Circular ticks represent consecutive
1346 increments of 5% crystallization. Crystallization vectors corresponds to F=0.7.
1347
1348 **Fig. 9** – Temperature and pressure conditions for crystallization of clinopyroxene and
1349 amphibole from the 2014 tephritic and phonotephritic rocks.
1350
1351 **Fig.10 -** Mixing model between depleted mantle (DMM) and recycled oceanic crust
1352 (ROC; ≈ HIMU), and between ROC and EM1and the lower mantle (LM). Values for
1353 these end-members are from Doucelance et al. (2003) (lower mantle), Iwamoro (2015)
1354 (EM1, DMM) and Mourão et al. (2012a) (ROC). Given that the 2014 Fogo lavas are
1355 characterized by a diluted contribution of ROC (see main text), making difficult its
1356 constraint, we considered 1.3 Ga as the age of recycling for mixing calculations, as
1357 determined by Mourão et al. (2012a) for the neighbouring Brava Island. Additional line

1358 corresponds to a mixture between recycled oceanic crust and lower mantle material in a
1359 60:40 proportion, with EM1. Circular marks represent 10% increments. See
1360 Supplementary Material S5-3 for mixing calculations.
1361

# The 2014-15 eruption and the short-term geochemical evolution of the Fogo volcano (Cape Verde): evidence for small-scale mantle heterogeneity

J. Mata[1*]; S. Martins[1]; N. Mattielli[2]; J. Madeira[1]; B. Faria[3]; R.S. Ramalho[1,4,5]; P. Silva[6,1]; M. Moreira[7]; R. Caldeira[8]; M. Moreira[6,1]; J. Rodrigues[9]; L. Martins[1]

1- Instituto Dom Luiz, Faculdade de Ciências, Universidade de Lisboa, 1749-016 Lisboa, Portugal.
2- Laboratoire G-Time, DGES, Université Libre de Bruxelles, ULB, Av. Roosevelt, 50, CP 160/02, 1050 Brussels, Belgium
3- Instituto Nacional de Meteorologia e Geofísica, Mindelo, Cabo Verde
4- School of Earth Sciences, University of Bristol, Wills Memorial Building, Queen's Road, Bristol, BS8 1RJ, UK
5- Lamont-Doherty Earth Observatory at Columbia University, Comer Geochemistry Building, 61 Route 9W, P. O. Box 1000, Palisades, NY 10964–8000, USA
6- Instituto Politécnico de Lisboa, ISEL/ADF, Lisboa, Portugal
7- Institute de Physique du Globe de Paris (France)
8- Laboratório Nacional de Energia e Geologia, I.P., 2610-999 Amadora, Portugal.
9- Geologist, Cabo Verde

*- Corresponding author: jmata@fc.ul.p

**Keywords**

2014-15 Fogo Island (Cape Verde) eruption; Ocean island basalts; Mantle heterogeneity; Short-term magmatic variation; Volcano plumbing system

## 1- Introduction

The Earth's mantle is highly heterogeneous as depicted by the composition of oceanic basalts and particularly by those from oceanic islands (e.g. Hofmann, 2003; White, 2015). Such heterogeneity is considered the result of mixing in different proportions of the so-called mantle components (Zindler and Hart, 1986; Stracke et al., 2005). The length scale of mantle heterogeneities sampled by oceanic basalts is highly variable, sometimes encompassing large regional domains (e.g. DUPAL and SOPITA anomalies; Hart, 1984; Staudigel et al., 1991; White, 2015), but being also evident at the scale of a single magmatic province, as reported, for example, for the Azores (e.g. Beier et al., 2008), Cape Verde (Gerlach et al., 1988; Doucelance et al., 2003) and Galápagos (Gibson et al., 2012) archipelagos. The same is true at the scale of a single island edifice (e.g. Barker et al., 2010; Mourão et al., 2012a; Nobre Silva et al., 2013), even when considering quasi-coeval magmatic products (e.g. Madureira et al., 2011).

In this work we evaluate the small-scale heterogeneity of the mantle source feeding a plume-related intraplate volcano, as well as the short-term geochemical evolution of the magmas it generated. To this purpose we use as a case study the island of Fogo (Cape Verde Archipelago), one of the most active oceanic volcanoes in our planet. Indeed, since the mid-15$^{th}$ Century Fogo experienced about 27 eruptions mostly from vents located within a ~~restrict~~restricted area (≈50 km$^2$) of the ~~edifice's~~island's summit depression (Fig. 1). The latest eruption occurred in 2014-2015 and constitutes the main object of this study. Their vents are practically coincident ~~(1995)~~ or localized less than 2 km away ~~(1951)~~ from those of the ~~2014-15 eruption.~~two previous eruptions (1995 and 1951, respectively). For this reason, Fogo constitutes a prime locality to test the existence of small-scale heterogeneities of mantle sources, as well as to investigate the recent short-term evolution of magmas issued from those sources. Here we characterize and discuss the geochemistry of the lava flows and pyroclasts extruded during the initial

stages of the eruption (up to December 7, 2014). Even though we are only considering lavas formed during the first 15 out of 60 days of eruption, the extracted information allows the demonstration of chemical differences relative to the products erupted in 1951 and 1995.

The preservation of such heterogeneities by magmas is also here discussed emphasizing the role of lithosphere thickness. The mineralogical, geochemical and physical characteristics of a volcano are partially constrained by what happens during magma transit from its source to the surface, i.e. by the nature and dynamics of the associated magma plumbing system (e.g. Longpré et al., 2008; Klügel et al., 2015; Cooper, 2017; Cashman et al., 2017). The Fogo's plumbing system is here assessed using barometric data, which indicates a location of the main magma chamber(s) into the mantle.

Our observations show that magmas erupted in 2014 ~~erupted~~ mark a reversal from the tendency depicted by previous eruptions (Escrig et al., 2005), which exhibited an increasing contribution of a ~~radiogenic Sr~~ local end-member with relatively radiogenic Sr.

## 2- Cape Verde Geological Setting

The Cape Verde Archipelago (Eastern Central Atlantic; Fig. 1) lies on top of the largest bathymetric anomaly in the Earth's oceans – the Cape Verde Rise – that coincides with important geoid, heat flow, gravity, and seismic anomalies (e.g. Dash et al., 1976; Courtney and White, 1986; Wilson et al., 2013; Liu and Zhao, 2014). The ~~islands~~archipelago, which stand on 120–140 Ma-old seafloor (Williams et al., 1990) ~~are~~is regarded as ~~the result of~~a hotspot ~~volcanism~~ resulting from the impingement of a mantle plume on the quasi-stationary (<1 cm.a$^{-1}$ in the region; Pollitz, 1991; Holm et al., 2008) Nubian plate. These would explain the long-lasting volcanic activity and, at least partially, the age distribution of volcanism and the geometry of both the archipelago and the Cape Verde Rise (Lodge and Helffrich, 2006; Holm et al., 2008; Madeira et al.,

2008; Ramalho et al. 2010, Ramalho, 2011). The presence of a mantle plume deeply anchored in the lower mantle is ~~also~~ suggested by seismic data (Montelli et al., 2006; Forte et al., 2010; Vinnik et al, 2012; Saki et al., 2015; French and Romanowicz, 2015) and of noble gas studies performed on ~~carbonatitic~~carbonatites and alkaline silicate rocks (Christensen et al., 2001; Doucelance et al., 2003; Mata et al., 2010; Mourão et al., 2012b). The oldest exposed hotspot-related volcanism is ~26 Ma (Torres et al., 2010) and at least three islands are considered volcanically active (Santo Antão, Brava and Fogo; see e.g. Madeira et al., 2010; Eisele et al., 2015; Faria and Fonseca, 2014) but only Fogo had post-settlement eruptions.

Magmatism in Cape Verde is strongly alkaline, as testified by the occurrence of nephelinitic, melanephelinitic, and melilititic rocks on several islands. It also is well known by its striking geochemical heterogeneity, allowing the isotopic separation of the islands into two groups~~, a~~ (Northern and ~~a~~ Southern~~.~~). Lavas from the Southern group have more radiogenic Sr, but unradiogenic Nd and Pb ratios than those from the Northern group, which are also exhibit more unradiogenic He signatures. In addition, magmatic rocks from the Southern group are positioned, on the $^{208}Pb/^{204}Pb$ vs. $^{206}Pb/^{204}Pb$ diagram, above the Northern Hemisphere Reference Line (NHRL; Hart, 1984) whilst lavas from the Northern group tend to plot along the NHRL (e.g. Gerlach et al., 1988; Doucelance et al., 2003; Holm et al., 2006; Kogarko and Asavin, 2007; Martins et al., 2010; Mourão et al. 2012a and references therein). Notable exceptions to this scenario include Brava (the southwesternmost island), which depicts both typical Northern (older sequences) and Southern (younger volcanism) isotope signatures (Mourão et al., 2012a), and the neighbouring Cadamosto seamount, which also presents typical Northern signatures (Barker et al., 2012).

## 2.1 Fogo Volcano

Fogo is one of the youngest of the Cape Verde Islands and a very prominent oceanic volcano, standing ~7 km above the surrounding seafloor. The island exhibits a slightly asymmetric conical shape, being truncated atop by a summit depression open to the east. This 8 km-wide depression - Chã das Caldeiras - is surrounded on three sides by a almost vertical wall – the Bordeira – up to 1 km tall. Inside the summit depression and on its eastern side, a 1100 m high strato-volcano – Pico do Fogo – grew up to an elevation of 2829 m (Fig. 1). Fogo volcano is therefore interpreted as a compound volcano, featuring a "somma-vesuvio" association of a younger strato-cone on top of an older, collapsed volcanic edifice (Ribeiro, 1954; ~~Machado and Assunção, 1965;~~ Foeken et al., 2009). The opening to the east of the summit depression is interpreted as the result of a massive flank collapse (Day et al., 1999; Brum da Silveira et al., 2006), as attested by a landslide debris deposit extending offshore into the channel between Fogo and Santiago (e.g. Masson et al., 2008), and by field evidence documenting the impact of a megatsunami in the neighbouring island of Santiago (Paris et al., 2011; Ramalho et al., 2015). The present-day Pico do Fogo stands on, and partially fills, the collapse scar, and naturally post-dates the collapse event, which is interpreted to have occurred either at ~117 or at ~73 ka (cf. Eisele et al. 2015 and Ramalho et al. 2015). A older basement is, however, exposed in two shallow valleys near the city of São Filipe, where plutonic calciocarbonatites were dated from 2.5 Ma to 5.1 Ma (Hoernle et al., 2002; Madeira et al., 2005; Foeken et al., 2009). These suggest a > 2 Myr volcanic hiatus in the evolution of Fogo.

Fogo volcano is very active, with 27 eruptive events since 1500 AD (Ribeiro, 1954). The mean recurrence interval between eruptions is 19.8 years, but with individual intervals ranging from 1 to 94 years. Historical eruptions seem to have been confined to Chã das Caldeiras and the eastern slope of the volcano, as it was the case of the recent 1951, 1995 and 2014/2015 events (Fig. 1).

198 The latest eruption started on November 23, 2014 and continued until February 7, 2015.
199 The eruption occurred on a NE-SW trending 700 m-long fissure located on the SE flank
200 of the previous 1995 cinder cone, an adventitious vent developed on the SW flank of
201 Pico do Fogo (Figs. ~~2C~~2A, 2B e 2D). This eruption started with vigorous "hawaiian"
202 fire-fountain activity, followed by strombolian activity, and later by simultaneous or
203 alternating ~~hawaiian,~~Hawaiian (Fig. 2C), strombolian and vulcanian (Fig. 2D) eruptive
204 activity from different craters along a fissural vent, lasting for several days. The
205 eruption also emitted, from the first day, thick a'a lava flows (Fig. 2E; Supplementary
206 Material S1) forming two initial lava lobes. A shorter lobe, 1.7 km-long, progressed
207 southwestwards down to the flank of Cova Tina cone, stalling short of the Bordeira wall
208 in this area. The second, longer lobe advanced 3 km to the northeast in the initial hours
209 of the eruption, crossing the topographic barrier formed by the 1995 lava flows by
210 advancing through the existing road cut. It advanced intermittently towards the village
211 of Portela, causing widespread destruction (Fig. 2F). During the later stages of the
212 eruption, thinner, more fluid, a'a and especially pahoehoe breakouts expanded the flow
213 field to the west and north, the latter descending to the village of Bangaeira, destroying
214 almost completely both villages and reaching a total length of 5.2 km (Fig.1). Overall,
215 the resulting lava flows, with an average thickness of about 9 m, covered an area of 4.8
216 $km^2$, with extruded volumes estimated to correspond to ~45 × $10^6$ $m^3$ ~~(Richter et al.~~
217 ~~2016;~~, at a mean eruption rate of 6.8 $m^3.s^{-1}$ (Bagnardi et al. 2016; Richter et al. 2016).
218 Lava flow thicknesses as high as 35 m (close to the vent), or 25 m on the lava ponding
219 west of Portela, were described by Richter et al. (2016). See also Cappello et al. (2016)
220 for additional information about the eruption.
221
222 **3- Analytical procedures**

Whole-rock major and trace element concentrations were obtained at Activation Laboratories, Ltd (Ancaster, Ontario, Canada) using the geochemical analytical package 4Lithoresearch (lithium metaborate/tetraborate fusion - ICP and ICP/MS).

Several certified reference materials from USGS (United States Geological Survey), GSJ (Geological Survey of Japan) and CCRMP (Canadian Certificate Reference Material Project) were run to check for accuracy (Supplementary Material S2). Errors associated with the accuracy are ≤ 4% for major elements and better than 9% for the REE and the most widely used incompatible elements. Reproducibility was generally better than 5% for both major and trace elements. ~~Four blanks were also analysed.~~ For detailed information regarding analytical and control procedures consult the Actlabs website (www.actlabs.com).

Mineral analyses were performed on carbon-coated polished thin sections using a JEOL SUPERPROBE™, model JXA-8200, in wavelength dispersive mode at the Departamento de Geologia da Faculdade de Ciências da Universidade de Lisboa (Portugal). Minerals were analysed with an acceleration voltage of 15 kV and a current of 25 nA, using a 5 μm wide beam for most minerals. Plagioclase and apatite were analysed using a 7 and 9 μm wide beam, respectively. The analyses performed in each mineral phase/glass were calibrated using the composition of reference material, with precisions being better than 2% and ordinarily around 1% (see Supplementary Material S3-H for specific minerals standards used in each mineral analysis).

Isotopic analyses of Pb, Nd, Sr and Hf were performed at the Laboratoire G-Time of the Université Libre de Bruxelles (ULB, Belgium) on a Nu Plasma I Multi-Collector Inductively Coupled Plasma Mass Spectrometer (MC-ICP-MS) (@ Nu instruments).

Sr analyses were performed in wet mode. In routine, the raw data was normalized to $^{86}Sr/^{88}Sr=0.1194$, and corrected for mass bias by standard sample bracketing using the lab's in-house Sr standard solution. The in-house shelf Sr standard was calibrated and normalized to the certified value of NBS 987 Sr standard (0.710248) reported by Weis

et al. (2006). During our analytical sessions, in-house standard solution was run every two samples and gave an average value of 0.710287 ± 50 (2σ) for raw $^{87}Sr/^{86}Sr$ data (21 runs).

Nd and Hf were run in dry mode with an Aridus II desolvating system. To monitor the instrumental mass bias during the analysis sessions, the standard sample bracketing method was also applied. Standards were systematically run between every two samples, giving an average value in $^{143}Nd/^{144}Nd$ of 0.511921 ± 41 (2σ, 8 runs) for the Rennes Nd standard, and $^{176}Hf/^{177}Hf$=0.282172 ± 30 (2σ, 10 runs) for the JMC 475 Hf standard. The Nd and Hf isotopic measurements were internally normalised to $^{146}Nd/^{144}Nd$=0.7219 and $^{179}Hf/^{177}Hf$=0.7325, respectively. All Hf and Nd isotopic data (Table 1) are normalized to the reference values of 0.511961 and 0.282160 as published by Chauvel and Blichert-Toft (2001) and Chauvel et al. (2011).

For the Pb isotope analyses, a Tl dopant solution was added for every sample and standard, within a Pb-Tl concentration ratio of ±5:1 (for a minimum signal of 100 mV in the axial collector - $^{204}Pb$). $^{202}Hg$ is routinely monitored to correct for the potential isobaric interference of $^{204}Hg$ on $^{204}Pb$. Mass discrimination was monitored using ln – ln plots and corrected by the external normalization and the standard sample bracketing technique using the recommended values of Galer and Abouchami (1998) (i.e. $^{206}Pb/^{204}Pb$=16.9405±15; $^{207}Pb/^{204}Pb$=15.4963±16; $^{208}Pb/^{204}Pb$=36.7219±44). The repeated measurements of the NBS981 gave the following values: $^{206}Pb/^{204}Pb$=16.9403±8, $^{207}Pb/^{204}Pb$=15.4961±10, $^{208}Pb/^{204}Pb$=36.7217±31 (2σ) for the NBS981 Pb standard (5 runs).

## 4- Results

The samples used in this study were collected during a field survey undertaken during the course of the last Fogo eruption, between November 27 and December 7, 2014. From all collected samples a sub-set of 14 was selected for petrographic, mineralogical

277 and whole-rock elemental geochemical study (TABLE I), on the basis of its
278 geographical and temporal distribution. Sr, Nd, Hf and Pb isotopes were determined for
279 8 samples (TABLE II), while the He isotope analysis was performed for one sample. On
280 the Supplementary Material the reader can also find mineral chemistry data (S3) and the
281 whole-rock normative compositions (S4). The composition of interstitial glasses
282 determined by electron microprobe is also presented on Supplementary Material S3-G.
283
284
285
286 **4.1. Petrography and mineral chemistry**

Formatted: List Paragraph

Formatted: Font: Not Bold

287 On a chemical basis, lava flows and pyroclasts erupted up to December 7 are, sensu
288 lato, tephrites and phonotephrites (see *section* 4.3 and Fig. 3). Some of the most
289 important petrographic characteristics of the studied samples are depicted on Fig. 4 and
290 their mineral chemistry data are displayed on the Supplementary Material S3.
291
292 **4.1.1 Tephrites**
293 The bulk ~~(~~(≈ 85%) of the eruptive products corresponds to tephrites. The lavas are
294 vesicular and porphyritic with a hypocrystalline groundmass and with phenocrysts
295 amounting up to 10%. Samples are highly vesicular (up to 60% of the rock volume) and
296 the vesicles are irregular in shape and size.
297 The most abundant phenocryst phase is clinopyroxene. Even though all the
298 clinopyroxene phenocrysts are classified as diopside ($Wo_{49}En_{38}Fs_{13}$ to $Wo_{52}En_{36}Fs_{12}$)
299 according to IMA recommendations (Supplementary Material S-3A), in most samples
300 two groups must be considered regarding size and composition. One group corresponds
301 to phenocrysts with dimensions up to 2 mm and euhedral shapes. They are characterized
302 by normal zoning patterns, with $Al_2O_3$, FeO and $TiO_2$ increasing and MgO, CaO and
303 Mg# decreasing from core to rim. Opaque mineral inclusions are frequent. The other

304 group of phenocrysts occurs in clusters along with kaersutite, both with dimensions up
305 to 4 mm in length. Clinopyroxee megacrysts in these aggregates usually show complex
306 zoning patterns presenting abnormal compositional variations with increments of $Al_2O_3$,
307 FeO and $TiO_2$ towards the intermediate zone/mantle and then decreasing towards the
308 rim; the opposite occurs with MgO and CaO, suggesting a more complex and multistage
309 crystallization history as compared with the first group. Indeed the increase in
310 MgO/FeO and decrease in $TiO_2$ towards the rim is suggestive of a replenishment of the
311 magma chamber where these particular crystals were formed, reflecting an influx of less
312 evolved magmas, thus pointing out to mixing of distinct magma batches. However, both
313 groups of clinopyroxenes show similar $Al^{VI}$ values (0.059 to 0) and Al/Ti ratios
314 indicating that megacrysts are cognate, being genetically related with the host lava and
315 with the clinopyroxene phenocrysts. This assertion is also considered valid for
316 keaersutite megacrysts given the chemical evidence for amphibole fractionation (see
317 5.1).
318 These kaersutite crystals are Mg- and Ti-rich (MgO = 12.8 – 13.0 wt.%; $TiO_2$ up to 6.07
319 wt.%), usually occurring in association with apatite and showing reaction rims where
320 clinopyroxene and rhönite crystals are present, sometimes completely replacing the
321 amphibole ~~and forming pseudomorphes~~ (Fig. 4D). Olivine crystals are restricted to
322 inclusions in clinopyroxene phenocrysts, with no signs of resorption, and to the
323 groundmass.
324 In all lava samples the opaque minerals can be considered microphenocryts, being
325 characterized by euhedral shapes and dimensions up to 1 mm. Most of the occurring
326 oxides can be considered as titanomagnetites, with ulvöspinel component ($X_{USP}$) up to
327 57, ~~but with low~~and Cr# ~~(~~ranging from 1.6 to 5.3~~).~~.
328 The groundmass is made up of small crystals immersed in a glassy matrix. These
329 comprise plagioclase laths (labradorite, $An_{56-66}$) sometimes with a fluidal arrangement,
330 clinopyroxene elongated crystals ($Wo_{49}En_{37}Fs_{14}$ to $Wo_{53}En_{32}Fs_{15}$), finely disseminated

opaque minerals (titanomagnetites, 58 < $X_{USP}$ < 67), rare olivine (Fo ≈ 72%), and fluorapatite (1.7 to 2.8 wt.% of F). The electron-microprobe analyses of interstitial glass revealed it to be very rich in alkalis (11.8 to 15.8 wt%, $K_2O$+$Na_2O$) and poor in MgO (down to 0.66 wt%) having tephriphonolitic and phonolitic ($SiO_2$ up to 54.15 wt%) compositions (see Fig. 3).

**4.1.2 Phonotephrites**

These lavas are vesicular hemicrystalline/hypocrystalline and sparsely porphyritic (phenocrysts up to 3% vol.). The vesicles are elongated reaching up to 10 mm in length and corresponding to 50 to 80% of rock volume. The clinopyroxene phenocrysts are euhedral up to 3 mm in size, frequently showing complex oscillatory zoning patterns and inclusions of opaque minerals. Despite the striking optical zoning patterns, all the clinopyroxene phenocrysts are classified as diopside with a short compositional range ($Wo_{49}En_{35}Fs_{10}$ to $Wo_{53}En_{40}Fs_{14}$), being very similar to that reported for the tephrites. Olivine (Fo=80-84%) is scarce, being identified only as a core inclusion in a clinopyroxene phenocryst. Microphenocrysts (up to 1mm) of equant opaque minerals are classified as titanomagnetites ($X_{USP}$ = 44-46; Cr# = 1.15-5.4).

Kaersutite pseudomorphs are frequent. They consist of aggregates of rhönite and clinopyroxene elongated crystals, displayed in inward radial arrangements totally or partially replacing the amphibole. However, in either case, a border of small opaque minerals encloses the altered/partially altered amphibole crystals. These kaersuites are similar (MgO = 11.9 – 12.7 wt.%: $TiO_2$ up to 6.04 wt.%) to those occurring as megacrysts/phenocrysts in tephritic rocks, and the occurrence of apatite within or in close proximity to the amphibole is frequent.

The groundmass is composed of plagioclase microliths (labradorite, $An_{54-66}$), elongated clinopyroxene crystals (average $Wo_{53}En_{31}Fs_{16}$), opaque minerals (38 < $X_{USP}$ < 57; Cr# = 0.67-1.49), scarce olivine and glass.

In one sample, a cluster of clinopyroxene, opaque crystals~~, an opaque mineral~~, and amphibole is interpreted as a possible co-magmatic cumulate nodule. This interpretation is based on the large dimension of the crystals, the sharp contrast between the mineral aggregate and the surrounding rock matrix, and on its chemical similarity between its minerals and the rock phenocrysts. The same interpretation is considered for an aggregate of small (0.5 mm in length) plagioclase crystals characterized by anorthite content up to 79 %. Ultramafic nodules of cumulate origin, mainly composed of olivine, clinopyroxene, and amphibole, were also reported for this eruption by Caldeira et al. (2015).

**4.2. Whole rock elemental composition**

Major and trace element analyses of the studied rocks are presented in Table I, while normative compositions can be found in Supplementary Material S4.

As all other subaerial lavas in the Cape Verde Islands, Fogo's 2014 volcanic products are alkaline. They plot dominantly in the $U_1$ field, but also in the $U_2$ (phonotephrites) field of the TAS diagram (Fig. 3). Rocks plotting inside the $U_1$ field would be classified, according their CIPW normative composition, either as nephelinites (normative *ne* > 20%) – the dominant type – or as melanephelinites (normative *ne* < 20~~%, but~~%; normative *ab* < 5%) according to the subdivision proposed by Le Bas ( 1989); (see ~~S-~~ ~~1~~S4). However, as modal plagioclase can be identified in most of the rocks plotting in the U1 TAS field and for all the samples normative *ol* < 10%, the classification as tephrites is here preferred and used.

The rocks are representative of moderately evolved magmas characterized by Mg# ranging from 55.32 ~~and~~to 45.98 and by $Na_2O/K_2O$ between 1.35 and 1.46. The less evolved rocks (Mg# = 55.32 to 51.97) have $TiO_2$ contents varying from 3.65 to 3.75

385 wt%, $P_2O_5$ close to 1 (0.94 to 1.11 wt%), $CaO/Al_2O_3$ ratios ranging from 0.65 to 0.78
386 and $K_2O/TiO_2$ ratios from 0.25 to 0.32.
387 The 2014 lavas are highly enriched in the most incompatible elements (Fig. 5), which is
388 depicted, for example, by $(La/Yb)_{cn}$ ratios > 20, with the most evolved rocks presenting
389 the highest values for this ratio (> 23). Primitive mantle normalized incompatible
390 elements patterns (Fig. 5c) show a significant enrichment of Nb and Ta relatively to the
391 light REE and the radiogenic heat producers K, Th and U. Small Hf negative anomalies
392 are also evident, which partially reflects the high Zr/Hf ratios (>49), well above the
393 value of 36 characterizing CI chondrites and the primitive mantle (e.g. Palme and
394 O'Neil, 2003).
395 The sampled pyroclasts and lava flows are similar in composition, the most significant
396 difference being the sulphur-enriched composition of pyroclasts (120 to 230 ppm;
397 $\bar{X} = 200$ ppm) as compared to lava flows (60 to 120 ppm; $\bar{X} = 84$ ppm ). This
398 indicates a more effective degassing of lava flows as a consequence of a slower cooling.
399 ~~Concerning elemental compositions, most~~Most of the characteristics described above
400 are similar to those of lavas erupted during the two precedent eruptions (1995 and
401 1951), as Fig. 5 shows. Notwithstanding the fact that the samples here studied are only
402 representative of the lava emitted during the first 15 days of the eruption, some
403 differences, however, were noticed: i) the 1995 lavas present a slightly higher
404 compositional range (MgO from 6,86 to 2.40 wt%; Hildner et al., 2011) than the ones
405 from 2014 (MgO from 6.23 to 2.93 wt%); ii) from the three eruptions considered, the
406 1951 event produced the less evolved lavas (MgO up to 8.24 wt%; Hildner et al., 2012);
407 iii) for the same $SiO_2$ content, the 1951 lavas tend to be less alkali-rich than the 2014
408 and 1995 volcanics (Fig. ~~3); iv~~3); iv) the 2014 and 1995 erupted materials are
409 characterized by small compositional gaps ($\Delta SiO_2$ = 2.5% and 3.8%, respectively) in
410 opposition to the described for from the 1951 eruption for which no phonotephrite
411 compositions were reported (see Fig. 1 and references therein); v) for these three

eruptions, the most evolved products are the phonotephrites from the 1995 eruption, which also present the highest concentrations in incompatible elements like Nb and Ta. However, the highest concentrations in light REE are found in phonotephrites from the 2014 eruption, which show the highest La/Nb ratios. This ~~is~~higher La/Nb are also observed for the less evolved rocks (MgO > 5 wt%), with 2014 lavas presenting $\bar{X}$ La/Nb = 0.69, whereas the 1995 and 1951 less evolved rocks show $\bar{X}$ La/Nb=0.60 (cf. Table 1, Hildner et al., 2011 and Hildner et al., 2012).

### 4.3. Whole rock isotope composition

The results of Sr, Nd, Hf and Pb isotope analyses are shown on Table II. The lavas erupted in 2014 at Fogo Island present isotope signatures akin to those typical of the Southern islands in the Cape Verde Archipelago. Indeed, in opposition to what is observed for the Northern capeverdean islands (Fig.6), they are characterized by relatively unradiogenic $^{206}Pb/^{204}Pb$ ratios (up to 19.001) and plot above the Northern Hemisphere Reference Line (Δ7/4 from 0.99 to 1.57; Δ8/4 from 25.38 to 28.80; see Hart, 1984 for definitions of these parameters). Notwithstanding the fact that their $^{87}Sr/^{86}Sr$ (0.70361 to 0.70369) and $^{143}Nd/^{144}Nd$ (0.51276 to 0.51279) ratios are clearly more and less radiogenic, respectively, than those observed for the Northern islands, the 2014 lavas plot on the second quadrant of the $^{87}Sr/^{86}Sr$ vs. $^{143}Nd/^{144}Nd$ diagram (Fig. 7A). This indicates a provenance from a time-integrated depleted source(s), i.e. ~~which evolved over time with lower Rb/Sr and higher Nd/Sm than those of the CHUR (chonditic uniform reservoir).~~

which evolved over time with lower Rb/Sr and higher Nd/Sm than those of the BSE (bulk silicate earth) and the CHUR (chonditic uniform reservoir), respectively. Compared to the lavas extruded during the 1951 and 1995 eruptions, the 2014 rocks present more unradiogenic Sr and radiogenic Nd signatures (Fig. 7). The 2014 lavas also exhibit slightly more radiogenic $^{206}Pb/^{204}Pb$ ratios than the most samples from the

two previous eruptions, the same being true for $^{207}Pb/^{204}Pb$ ratios (Fig. 6A). Lavas from these 3 eruptions are amongst the Cape Verde rocks with lower $^{206}Pb/^{204}Pb$ ratios. As is typical of the Southern Cape Verde Islands, rocks from these 3 eruptions are characterized by positive Δ8/4, plotting above the NHRL (Fig. 6B).

The 2014 lavas' $^{176}Hf/^{177}Hf$ ratios range from 0.28294 to 0.28296 (Table II). A time-integrated evolution with high Lu/Hf ratios compared to CHUR is shown by positive εHf values (5.88 to 6.62; Fig. 7B), plotting between the mantle arrays proposed by Vervoort (1999) and Chauvel (2008). These are the first $^{176}Hf/^{177}Hf$ determinations available for Fogo Island, preventing any comparison with previous results. However, noteworthy that the lavas erupted in 2014 plot inside the large field defined in the εNd-εHf space by the lavas from the neighbouring island of Santiago, which is characterized by significantly higher and lower $^{176}Hf/^{177}Hf$ ratios (see Barker et al., 2009; Martins et al., 2010). Significant correlations between any of these isotope signatures and ratios involving incompatible trace elements have not been found. This will be discussed later (see 5.3).

The $^{3}He/^{4}He$ ratio of a glassy phonotephrite was determined at the Intitut de Physique du Globe de Paris (IPGP) using crushing for gas extraction. The obtained value (1.11± 0.13 Ra, where Ra is the present atmospheric ratio of $1.4 \times 10^{-6}$) for a $^{4}He$ concentration of $2.8 \times 10^{-9}$ cc/g is interpreted as the result of atmospheric contamination during the eruption/consolidation of lava. Consequently, this result will not be considered in the discussion.

~~Compared to the lavas extruded during the 1951 and 1995 eruptions, the 2014 rocks present more unradiogenic Sr and radiogenic Nd signatures (Fig. 7). The 2014 lavas also exhibit slightly more radiogenic $^{206}Pb/^{204}Pb$ ratios than the most samples from the two previous eruptions, the same being true for $^{207}Pb/^{204}Pb$ ratios (Fig. 6A). Lavas from these 3 eruptions are amongst the Cape Verde rocks with lower $^{206}Pb/^{204}Pb$ ratios. As is~~

~~typical of the Southern Cape Verde Islands, rocks from these 3 eruptions are characterized by positive Δ8/4, plotting above the NHRL (Fig. 6B).~~

## 5. Discussion

### 5.1 ~~Magma~~Mantle source composition and magma evolution

Previous studies, explained the chemical variability of Fogo's lavas by mixing in different proportions of HIMU-like (ancient recycled ocean crust) and EM1-like mantle end-members, diluted by the presence of depleted upper mantle (Gerlach et al., 1988) or by lower mantle material (Doucelance et al., 2003; Escrig et al., 2005) entrained by the upward moving plume.

Although 2014 lavas present low $^{206}Pb/^{204}Pb$ ratios (up to 19.001), clearly below those typical of magmas originated from sources dominated by the HIMU mantle component (e.g. Kawabata et al., 2011), the HIMU fingerprint is shown by trace element patterns (Fig. 5) displaying enrichment in Nb and Ta relative to the LREE and the LILE (e.g. Niu et al., 2012). Aditionally, all the analysed rocks are characterized by positive Δ8/4 and Δ7/4 and plot below the mixing lines between a HIMU type end-member and DMM or lower mantle compositions (Fig. 10), strongly suggesting the contribution of an EM1-type end-member to the 2014 Fogo mantle source(s). Interestingly, the products erupted in 2014 mark a change on the evolutionary trend reported by previous authors for Fogo eruptions (Gerlach et al., 1988; Escrig et al., 2005) which was characterized by an increasing contribution of the enriched component. Indeed, the 2014 lavas have less radiogenic Sr, but more radiogenic Nd signatures than those from the 1951 and 1995 eruptions.

Fogo's 2014 lavas (MgO ≤ 6.4 wt %, Mg# ≤ 53.2; Ni ≤ 42 ppm) cannot be considered representative of primary magmas. This fact and its chemical variability (MgO down to 2.93 wt.%; Ni down to 6 ppm) emphasize the role of magma evolution processes to explain the observed compositional range. This is reinforced by the phonolitic

Formatted: English (United States)

Formatted: English (United States)

composition of the glassy groundmass of some lavas (MgO down to 0.66 wt%; total alkalis up to 15.76 wt%; see Supplementary Material S3-G).

The important role of clinopyroxene fractionation is suggested by its occurrence as phenocryst in most samples and by the Sc decrease with increasing concentration of strongly incompatible trace elements such as La (Fig 8A), here used as a proxy of magma evolution index. Fractionation of clinopyroxene must have been preceded by crystallization of olivine as indicated by the occurrence of olivine inclusions in clinopyroxene phenocrysts. ~~However, the smooth decrease of Ni during magma evolution (not shown), indicates that olivine role must have been restricted to previous stages of fractionation for which there were no magmas erupted.~~

~~With continuing magma evolution~~The Dy/Dy~~*~~,* ratio, as defined by Davidson et al. (2013), tends to decrease from up to 0.81 in tephrites, down to 0.61 in phonotephrites, a tendency that, according to those authors, can be attributed either to amphibole or to clinopyroxene fractionation. If the importance of clinopyroxene fractionation was already demonstrated, the positive correlation of Dy/Dy* and Nb/U ratios (Fig. 8B) emphasizes the role of amphibole since, at odds with what happens with this mineral, clinopyroxene does not have the capacity to fractionate Nb from U (e.g. Adam and Green, 2006~~; see also https://earthref.org/KDD/).~~).

The calculated water content of the melt during kaersutite crystallization range from 3.81 to 4.14 wt% (± 0.78 wt%) while oxygen fugacity is estimated in the range of 0.92 to 2.3 log units above NNO (± 0.37 log units) using the methodology of Ridolfi and Renzulli (2012). The obtained $fO_2$ values are comparable to those reported for some other intraplate ocean islands (e.g. Madeira; Mata and Munhá, 2004). These relatively high $fO_2$ values are reflected in the composition of pyroxenes for which high $Fe3^+$ contents were calculates based on the stoichiometry (Suplementary material S3-A), but not in the amphibole (Suplementary material S3-C). This suggests the incorporation of Ti ($TiO_2$ up to 6.13 wt%) into the octahedral position of kaersutite through the

519 substitution $^{[VI]}R^{2+} + 2OH^- = {}^{[VI]}Ti^{4+} + 2O^{2-}$, which favours high $Fe^{2+}/Fe^{3+}$ (Satoh et al.,
520 2004).
521 As also reported for the previous Fogo's eruption (e.g. Munhá et al., 1997; Hildner et
522 al., 2012) plagioclase did not play a significant role in the evolution of 2014 magmas, as
523 inferred from its rarity among phenocrysts and from the continuous Sr increase (1194 to
524 1408 ppm) throughout the erupted suite. ~~However, judging~~Judging from the
525 comparatively ~~low CaO~~high $Al_2O_3$, $Na_2O$ and ~~$Al_2O_3$~~$K_2O$ concentrations determined in
526 the glassy phonolitic matrix, plagioclase and alkali feldspar fractionation ~~must have~~
527 ~~been~~was also not important for the generation of such evolved compositions. On the
528 other hand, the role of Fe-Ti oxides and apatite fractionation is made evident by the
529 significant decrease on $P_2O_5$ (Fig. 8C) and $TiO_2$ (not shown) concentrations from the
530 most evolved tephrites ($SiO_2$ < 45.2.%) to phonotephrites ($SiO_2$ > 47.7 wt. %) (see also
531 Table I~~), which form two groups separated by a compositional gap ($\Delta SiO_2$ = 2.5%).~~).
532 The ~~generation of this gap is beyond the scope of this paper. However, we note that the~~
533 ~~gap is immediately preceded by the inflexion on the liquid line of descent of $P_2O_5$ (Fig.~~
534 ~~8C) and $TiO_2$ (not shown). Considering this, we interpret that small gap as the result of~~
535 ~~crystal~~ fractionation of these two non-silicate phases ~~(Fe-Ti oxides, apatite),~~ with the
536 consequent significant increase in silica content of magmatic liquids~~. Similar, but more~~
537 ~~important gap ($\Delta SiO_2$ = 3.8%) characterize the 1995 lavas (see Hildner et al., 2011), but~~
538 ~~not the rocks from the 1951 eruption~~, was probably the cause for ~~which no~~
539 ~~phonotephrite compositions were reported (see Fig. 1 and Fig. 8C and references~~
540 ~~therein).~~the small compositional gap ($\Delta SiO_2$ = 2.5%) separating those two lithotypes.
541 Even though the isotope differences precludes the studied rocks to be considered ~~co-~~
542 ~~magmatic~~comagmatic with those erupted in 1951 and 1995 (see section 4.4), samples
543 from these three eruptions plot along the same trends in most variation diagrams,
544 suggesting that they share a common magma evolution history (e.g. Fig. 8 A and C).
545 However, Fig. 8B emphasizes, despite similar trends, the lower Nb/U and Dy/Dy*

**Formatted:** Font color: Text 1
**Formatted:** Font color: Text 1

ratios of the 2014 rocks relatively to the rocks of similar degree of evolution generated during the two previous eruptions. ~~Despite these differences, even for these ratios, they exhibit the same trends with magma evolution.~~

~~The Nb/U of~~Indeed, the less evolved 2014 ~~lavas ranges between 48 and 65, with tephrites being~~rocks are characterized by lower Nb/U ratios ~~of (~~60 ± 3~~ (1σ). The~~) than the basanitic/tephritic lavas from the 1995 and 1951 ~~lavas have Nb/U ratios ranging from 70 to 100~~eruptions (95 ± 4 ~~for basanites/tephrites). Considering such significant differences between lavas with~~ ; Hildner et al., 2011; 2012). Given the similar ~~degrees~~degree of evolution, ~~primary/primitive magmas of the 2014 lavas had to~~these differences cannot be explained by fractional crystallization. The 2014 Nb/U ratios fits the typical OIB value (EM lavas excluded) of 52 ± 15 obtained by Hofmann (2003). ~~distinct from those erupted in~~ As shown by this author, either the EM-type mantle components or the continental crust have significantly lower Nb/U ratios. Consequently the higher contribution of an enriched end-member (EM type) for the 1995 and 1951(see ~~5.2~~above) lavas cannot be invoked as a cause for ~~a discussion).~~ their higher Nb/U ratios.

Nb/U ratios significantly higher than the typical OIB lavas have also been reported for some Canary lavas by Lundstrom et al. (2003). These authors defended that this can be the reflex of mixing between ascending plume-derived magmas and lithospheric melts with a significant contribution from amphibole present in low-solidus mantle domains. These domains would have been generated by metasomatic (s.l.) processes during previous stages of islands building. We suggest that a similar process may have been responsible for the significantly higher Nb/U and Dy/Dy* ratios of the 1995 and 1951 lavas. Since their vents, and probably also the ascending magma paths, were almost coincident with those of 2014, we speculate that such low-solidus lithospheric domains were already exhausted and did not contribute significantly for the composition of the subsequent 2014 eruption products.

Formatted: Font color: Text 1

As observed for the precedent 1995 eruption (Munhá et al., 1997; Silva et al., 1997; Hildner et al., 2011), the initial products erupted in 2014 were more evolved (phono-tephrites; $SiO_2$ up to 47.99 wt.%) than those emitted subsequently (tephrites, s.l.), for which $SiO_2$ contents as low as 43.03 wt.% were obtained. Considering the composition of the erupted magmas, assuming a complete degassing during eruption (suggested by very low loss on ignition), and using the algorithm of Giordano et al. (2008), the viscosity of the phonotephrites would have been some 10 times higher than that of the less evolved tephrites. This partially explains the evolution of lava flow morphology during the course of the eruption, which exhibited *a'a* characteristics during the initial eruptive stages, whilst *pāhoehoe* type lavas became more frequent during the subsequent effusion of the less viscous tephritic lava flows.

Formatted: Pattern: Clear (White)

Formatted: Font: Not Bold, Font color: Text 1, Pattern: Clear (White)

**5.~~1.1~~2 Thermobarometric evidence for magma reservoirs into the mantle**

~~Phenocrysts and cognate megacrysts are considered to grow slowly as a consequence of low magmatic cooling rates. This indicates stagnant or quasi-stagnant conditions at some stage during the process of magma transfer from the mantle source(s) to the surface, such as those characterizing magma stalling/stagnation at mantle/crustal chambers.~~ Geothermobarometric estimates based on ~~such type of crystals can thus~~ phenocrysts and cognate megacrysts have been considered to be important to constrain the magmatic plumbing system of a volcano~~.~~, given they can be used to calculate the depths of magma stalling/stagnation at mantle/crustal chambers. Indeed, silicates are characterized by very ~~slow~~low intra-crystalline diffusion rates, thus tending to preserve the composition acquired at the moment of crystallization.

We used the clinopyroxene-liquid thermobarometer of Putirka et al. (2003) for which lower uncertainties are foreseen than those reported for methods only using the clinopyroxene composition (Putirka, 2008~~).~~; see also Geiger et al., 2016 for a review on clinopyroxene thermobarometry). The method is based on jadeite–

diopside/hedenbergite exchange equilibria in hydrous conditions, which are shown to have existed at Fogo by the presence of amphibole (see also ~~below~~above for an estimate of water content in magma). As we used phenocryst cores and whole rock compositions as proxies of the crystal-liquid pairs, the P-T results obtained will be regarded as the conditions prevailing during early stages of clinopyroxene phenocrysts crystallization~~.~~, assuming that no magma mixing occurred after pyroxene crystallization.

In order to use mineral/liquid thermobarometers it is mandatory to test if the crystal/melt pairs used testify equilibrium conditions. On a first approach a visual screening was made to identify textural evidence for disequilibrium, those showing irregular or reabsorbed shapes were avoided. Furthermore, only core analyses of un-zoned or normally zoned phenocrysts where used. No mineral correction was made to the whole-rock composition due to the lack of evidence for significant accumulation (≤ 10 % of phenocryst ~~phase~~phases).

Considering the concerns regarding the efficacy of the Fe-Mg exchange in deciphering situations of pyroxene-melt equilibrium (e.g. Mollo et al., 2013), we used instead the comparison between predicted and measured components in clinopyroxene (diopside-hedenbergite; enstatite-ferrosilite; Ca-Tschermak's) as proposed by Putirka (1999). Following the recommendations of Putirka et al. (2003), only clinopyroxenes whose compositions are within the ± 2σ level of the predicted ones were used in the thermobarometric calculations. The standard errors of estimation (SEE) of the Putirka et al. (2003) method are 1.7 kbar and 33 ºC, while analytical uncertainties, calculated using the relative standard deviation of whole rock and microprobe analyses of reference materials are significantly lower than the uncertainties of the method.

The temperatures obtained for pyroxene crystallization range from 1045 to 1063 ºC for the phonotephrites and 1102 to 1143 ºC for the tephrites. ~~Concerning pressure estimates,~~Pyroxene phenocrysts crystallized from phonotephritic magmas at pressures

in the ~~phonotephrites are characterized by a~~ range between 560 and 778 MPa, whereas the tephrites yield variations between 690 and 890 MPa (Fig. 9).

~~The calculated pressures can be converted to depth estimates considering a height of 5800 m for the Fogo island edifice (≈ 3000 m below present sea level), an average density of 2400 kg.m$^{-3}$ (Dash et al., 1976) for the island edifice, a crustal density of 2800 kg.m$^{-3}$ inferred from seismic receiver functions (Lodge and Helffrich, 2006), a mantle density of about 3200 kg.m$^{-3}$ at the Fogo region (Pim et al., 2008), and a Moho depth at 12 km below sea level (Pim et al., 2008). Taking into account these values and the referred uncertainties, the crystallization depth of clinopyroxene phenocrysts ranges approximately from 14.8 to 36.4 km below Fogo's summit, or 12 to 33.6 km below sea level.~~

For amphiboles we used the single-phase thermobarometric and chemometric equations proposed by Ridolfi and Renzulli (2012), based on multivariate least-squares regression analyses of a large database of amphibole compositions in alkaline magma systems. For this method the authors claim low uncertainties: P ± 11.5%, T ± 23.5ºC~~, ΔNNO ± 0.37 log units and $H_2O$melt ± 0.78 wt%.~~. The application of the thermobarometer shows that the values obtained for kaersutites occurring in phonotephrites and tephrites are similar within error (1032 to 1050ºC and 568 to 620 MPa; see Fig. ~~9), which, considering the method uncertainties, would correspond to depths ranging from ~16 to 21.8 km below sea level. The calculated melt water content during kaersutite crystallization is very similar for both lithotypes, ranging from 3.81 to 4.14 wt%. Oxygen fugacity estimates show a range of 0.92 to 2.3 log units above NNO. The obtained $fO_2$ values are comparable to those reported for some andesitic lavas in convergent tectonic settings (e.g. Chiaradia et al., 2011), but also for other intraplate ocean islands (e.g.~~ 9). ~~Madeira; Mata and Munhá, 2004). These relatively high $fO_2$ values may have resulted from the H2O rich composition of magmas (see above), which allowed the crystallization of amphibole. Indeed, the liberation of free oxygen and the consequent increase of magma~~

~~fO2 are thought to be a consequence of amphibole crystallization (Frost and Lindsley, 1991; Chiaradia et al., 2011).~~

Formatted: Font color: Red

The kaersutite occurring in the 2014 Fogo lavas show ubiquitous signs for disequilibrium, presenting evidence for partial (reaction rims) to total (pseudomorphosis) substitution by polycrystalline aggregates of rhönite and clinopyroxene. We interpret the occurrence of rhönite and of the associated clinopyroxene as a consequence of the kaersutite destabilization resulting from magma degassing upon ascent, given the decrease of $H_2O$ solubility in magmas as pressure drops (e.g. De Angelis et al., 2015). The destabilization of amphibole most probably occurs at pressures below 100-150 MPa (e.g., Rutherford, 2008) with reaction rims developing, for hornblende compositions, at pressures from circa 100 MPa down to 40 MPa (Browne and Gardener, 2006).

Amphibole reaction rims are often used to estimate magma ascent rate since their thickness, size and the shape of the replacing mineral phases are all dependent on it (Chiaradia et al., 2011; Browne and Gardner, 2006). Since the reaction rims observed in kaersutite crystals from the 2014 lavas are thick (> 500 microns) and complete pseudomorphosis of mm-sized crystals (up to 4mm) is common, it is valid to assume on a qualitative basis and based on Browne and Gardener's (2006) experimental data that the time of exposure of kaersutite to low $PH_2O$ before quenching at the surface was relatively long ~~(several months).~~ (> 1 month). Thus, the occurrence of rhönite and the degree of kaersutite replacement by rhönite suggest a late and short stagnation/stalling at crustal levels (i.e. at pressures below 100 MPa; < 4.3 km below the island summit or < 1.5 km below sea level) after a longer storage at deeper magma chambers.

~~The pressure constraints emerging from this study, based on phenocrysts occurring in relatively evolved magmas (Ni < 42 ppm), indicate that magma evolution processes involving clinopyroxene and amphibole fractionation occurred approximately at depths of 14.8 to 36.4 km below the island's summit, or ≈12 to ≈ 33.6 km below sea level.~~

~~Considering a sub-Fogo Moho depth of 12 km below sea level (Pim et al., 2008), these data indicates that magmas stagnated and evolved at mantle depths. On the other hand, this depths range suggests that Fogo is underlain by a complex plumbing system characterized by several magma chambers at distinct depths where clinopyroxene and kaersutite crystallized.~~

~~Additionally, the occurrence of rhönite and the degree of kaersutite replacement by rhönite suggest a later (shorter and less significant) stagnation/stalling at crustal levels (i.e. at pressures below 100 MPa; < 4.3 km below the island summit or < 1.5 km below sea level). Even considering the uncertainties associated to the barometric data, it can be concluded that the magma chambers where the major magma fractionation events occurred were located in the mantle.~~

~~The scenario here proposed for the ascent of the 2014 Fogo magmas is in agreement with seismic data.~~In order to convert the calculated pressures to depths several assumptions has to be done, the depth of Moho being the one with more impact in the obtained results.

Vinnik et al. (2012), proposed that at the Cape Verde archipelago the crust would be significantly thicker than the normal oceanic crust, extending down to 20-30 km depth. This was not supported by a later study (Wilson et al., 2013), which placed the Moho at significantly shallower depths, in agreement with the models of Lodge and Helffrich (2006), Pim et al. (2008) and Wilson et al. (2010). In this study we adopt 13.5 km as the depth of Moho beneath the Fogo Island (see Wilson et al., 2010; 2013).

Considering a height of 5800 m for the Fogo island edifice (≈ 3000 m below present sea level), an average density of 2400 kg.m$^{-3}$ (Dash et al., 1976) for the island edifice, a crustal density of 2800 kg.m$^{-3}$ inferred from seismic receiver functions (Lodge and Helffrich, 2006), a mantle density of about 3200 kg.m$^{-3}$ at the Fogo region (Pim et al., 2008), a Moho depth at 13.5 km below sea level (Wilson et al., 2010; 2013) and taking into account the uncertainties of the barometric methods (see above) the crystallization

depth of clinopyroxene phenocrysts ranges approximately (± 5.5 km) from 17.8 to 28.4 km below Fogo's summit, or 15.0 to 25.6 km below sea level. For amphiboles the same presupposes allow considering their crystallization at depths between 18.2 and 19.9 km (± 3 km) below Fogo's summit, or 15.4 to 20.1km below sea level. Considering the most common estimates for the crustal thickness at the Cape Verde region (≈ 12 to 13.5 km; Lodge and Helffrich, 2006; Pim et al., 2008; Wilson et al., 2010; 2013) the obtained results suggest that the major fractionation events occurred in magma chambers located into the mantle.

~~Indeed, a seismic event on October 4, 2014 (i.e. 50 days before the eruption) with a hypocentre 17 km below sea level (19.8 km below the Fogo summit), was interpreted by Instituto Nacional de Meteorologia e Geofísica (INMG, Cabo Verde) as resulting from the rupture of the roof of a mantle reservoir allowing magma transfer to shallower levels. Also, geodetic modelling of Sentinel-TOPS interferometry by Gonzalez et al. (2015) revealed the lack of deformation at the island-scale during and pre-eruption times, further suggesting the deep location of the main magma reservoirs.~~

Geobarometric studies of the previous two eruptions also revealed pre-eruptive magma storage at shallow mantle depths, followed by a short-period of magma stalling at crustal levels (Munhá et al., 1997; Hildner et al., 2011, 2012). The depths of clinopyroxene equilibration obtained in this study for the 2014 eruption (890 to 560 MPa; see above), although partially overlapping those presented for the historical eruptions by Hildner et al. (2011, 2012) (680 to 460 MPa), extends to higher pressures. However it must be noted that the pressure estimates by those authors refer to the final crystallization level, while our data represents –the first crystallization stages of clinopyroxene phenocrysts.

The causes for the development of magma reservoirs within the mantle are still not understood. Changes in buoyancy have been considered as an explanation for magma stagnation during ascent (e.g. Ryan, 1994). However, Jagoutz (2014) emphasized that,

~~at continental arcs, melts~~ascending magmas can stagnate even when they are less dense than the surrounding rocks~~ and that its emplacement is not controlled by the existence of a neutral buoyancy level~~. A similar point of view was defended by Menand (2008) who considered that buoyancy is unlikely to be a major control in the emplacement of sills, which can be viewed as precursors of magma reservoirs (Gudmundsson, 2012). Moreover, as shown by Putirka (2017), hydrated magmas with MgO contents similar to those erupted in the 2014 Fogo eruption are less dense than the mantle, or even than the lower crustal rocks, indicating that buoyancy cannot be the explanation for the stagnation of Fogo magmas in the mantle. As proposed by Menand (2008), the presence of ~~rheology~~rheological anisotropies could be the primary factor determining the depth of magma stalling or stagnation. This can lead to the inference that the thickness of the elastic lithosphere exerts a major control on the depth of magma reservoirs. However, for the Cape Verde Archipelago the elastic thickness is estimated at 30 km (Pim et al., 2008) and our barometric data suggest magma emplacement at shallower depths, invalidating, in this case, such a proposal. Regional flexural stresses produced by the volcanic edifice loading are also thought to strongly influence the plumbing systems by generating a vertical contrast between tensile and compressive stress zones, capable of influencing the depth of magma stalling (see Putirka, 1997 and references therein). We do not have data to evaluate this hypothesis.

Whatever the cause for the development of mantle magma reservoirs, they seem to be common on ocean islands during periods of low magma supply rates (e.g. Longpré et al., 2008; Stroncik et al., 2009; Klügel et al., 2015) as was the case during the latest (this study) and the previous eruptions of Fogo volcano (Munhá et al., 1997; Hildner et al., 2011; 2012).

~~**5.2 Mantle source**~~

~~In agreement with the location of Fogo Island, all its lavas and, particularly, the products erupted in 2014, are chemically akin to those characterizing the Southern Islands of the Cape Verde Archipelago. This is true for all the isotope systems used, as shown above (Fig. 6 and 7). Previous studies (see below), explained the chemical variability of Fogo's lavas by mixing in different proportions of two recycled end-members with characteristics similar to those of the HIMU (ancient recycled ocean crust) and EM1 mantle components. These end-members would have been diluted by the presence of depleted upper mantle entrained by the upward moving plume (Gerlach et al., 1988)~~ The scenario here proposed for the ascent of the 2014 Fogo magmas and of its plumbing system receives support from independent data.~~lower mantle material (Doucelance et al., 2003; Escrig et al., 2005), as also proposed by Mourão et al. (2012a) for the neighbouring Brava Island.~~

~~The 2014 erupted lavas do not show extreme isotope compositions when compared the other Southern Cape Verde Islands, or even with other Fogo rocks (Fig. 6 and 7). This makes it difficult to determine the end-members contributing to its source, also hindering a strong contribution for the discussion of the end-members of the mantle underlying Cape Verde. Nonetheless, some remarks have to be done:~~

~~Although the low $^{206}Pb/^{204}Pb$ ratios (up to 19.001) are clearly below those presented by lavas originated from sources dominated by HIMU (recycled ocean crust) (e.g.~~ Indeed, a seismic event on October 4, 2014 (i.e. 50 days before the eruption) with a hypocentre 17 km below sea level (19.8 km below the Fogo summit), was interpreted by Instituto Nacional de Meteorologia e Geofísica (INMG, Cabo Verde) as resulting from the rupture of the roof of a mantle reservoir allowing magma transfer to shallower levels. Also, geodetic modelling of Sentinel-TOPS interferometry by Gonzalez et al. (2015) revealed the lack of deformation at the island-scale during and pre-eruption times, further suggesting the deep location of the main magma reservoirs.

- Kawabata et al., 2011), the HIMU fingerprint is shown by trace element patterns (Fig. 5) displaying enrichment in Nb (and Ta) relative to the LREE and the LILE (e.g. Niu et al., 2012).
- All the analysed rocks are characterized by positive Δ8/4 and Δ7/4 and plot below the mixing lines between a HIMU type end-member and DMM or lower mantle compositions on the $^{206}Pb/^{204}Pb$ vs. $^{143}Nd/^{144}Nd$ diagram (Fig. 10), strongly suggesting the contribution of an enriched end member to the 2014 Fogo mantle source(s).
- The products erupted in 2014 mark a change on the evolutionary trend reported by previous authors for Fogo eruptions (Gerlach et al., 1988; Escrig et al., 2005) which was characterized by an increasing contribution of the enriched component. Indeed, the 2014 lavas have less radiogenic Sr, but more radiogenic Nd signatures when compared with those from the 1951 and 1995 eruptions.

For Fogo Island, Escrig et al., (2005), based on radiogenic Os signatures (up to 0.1369), proposed the incorporation of lower continental crust materials present in Fogo lithosphere during the ascent and differentiation of plume-derived magmas. We note that, for the studied 2014 rocks there is no positive correlation between $^{87}Sr/^{86}Sr$ ratios and $SiO_2$ contents (not shown), which is at odds with what would be expectable from processes of simultaneous assimilation and fractional crystallization (e.g. EC-AFC from Bohrson and Spera, 2001) involving a typical basic/ultrabasic alkaline magma and lower continental crust materials. This could eventually be explained admitting that magmas continued to evolve after the end of the assimilation process, as proposed by Escrig et al. (2005) to explain, for the previous eruptions, the lack of correlation between $^{187}Os/^{186}Os$ ratios and differentiation indices. However, in such a model the correlation between $SiO_2$ and $^{87}Sr/^{86}Sr$ would only be lost for the most evolved rocks, which is clearly not the case. Taking these into account we consider more plausible that

the mixing of the enriched continental lithosphere (s.l.) with plume material occurred in the mantle before melting.

As shown before (see 5.1) the less evolved 2014 rocks are characterized by Nb/U ratios of 60 ± 3, while for basanitic/tephritic lavas from the 1995 and 1951 eruptions a mean value of 95 ± 4 has been assigned (Hildner et al., 2011; 2012). These differences cannot be explained by fractional crystallization (see 5.1). The 2014 Nb/U ratios fits the typical OIB value (EM lavas excluded) of 52 ± 15 obtained by Hofmann (2003). We demonstrated above that the contribution of a local enriched end member is less significant for the 2014 lavas than for those of the two previous eruptions. However, as shown by Hofmann (2003), either the EM-type mantle components or the continental crust have low Nb/U ratios. Consequently the higher contribution of an enriched end-member for the 1995 and 1951 lavas cannot be invoked as a cause for their higher Nb/U ratios.

Nb/U ratios significantly higher than the typical OIB lavas have also been reported for some Canarian lavas by Lundstrom et al. (2003). These authors defended that this can be the reflex of mixing between ascending plume-derived magmas and lithospheric melts with a significant contribution of amphibole present in low-solidus mantle domains. These domains would have been generated by metasomatic (s.l.) processes during previous stages of islands building. We defend that a similar process may have been responsible for the higher Nb/U and Dy/Dy* ratios of the 1995 and 1951 lavas. Since their vents, and probably also the ascending magma paths, were almost coincident with those of 2014 we speculate that such low-solidus lithospheric domains were already exhausted and did not contribute significantly for the composition of the subsequent 2014 eruption products.

**5.3 Evidence for small-scale mantle heterogeneity and short-term compositional evolution of Fogo volcano.**

As mentioned above, the Cape Verde Archipelago is known by its remarkable geochemical intra-island heterogeneity~~. With few exceptions, Cape Verde alkaline rocks form two groups with distinct elemental and isotopic signatures, according to their geographical location (Northern vs. Southern Islands;~~ (e.g. Gerlach et al., 1988; Doucelance et al., 2003). ~~Intra~~Significant intra-island ~~heterogeneities~~time-dependent geochemical variations are also common as shown for most Cape Verde Islands ~~and particularly for the neighbouring islands of Santiago~~ (e.g. Barker et al., ~~–~~2010~~) and Brava (~~; Mourão et al., 2012 a~~) where significant time-dependent geochemical variations were described.).~~ Intra-island ~~spatial~~ heterogeneities have also been described for presumably coeval rocks~~. This~~, such is the case of ~~lavas from~~ the Recent Volcanics of São Vicente Island ~~whose major element compositions suggest magma extraction at variable depths, and also present significantly different incompatible trace element ratios~~ (Trindade et al., 2003~~). This is~~), and also of the ~~case of~~ Fogo Island where, as shown by Escrig et al. (2005), lavas erupted since 1785 present measurable variability on isotope signatures. ~~The 2014-15 and the 1995 eruptive fissures are separated by less than 200 m, and less than 2000 m from the 1951 vents, thus offering the opportunity to further constrain mantle heterogeneity beneath Cape Verde and particularly in Fogo Island.~~

~~It is well known that ratios involving elements characterized by highly incompatible behaviour (D << 1) tend~~In opposition to ~~reflect mantle source values when the extent of partial melting is higher than about 5%. However, the behaviour of such elements can be significantly different during melting of peridotite or pyroxenite. This is true, for example, for~~ incompatible trace ~~–~~element ratios ~~involving Ba or for the La/Nb ratio~~, which ~~tend to be lower or equal to the pyroxenite source ratios~~ can be fractionated during partial melting and ~~higher or equal to the peridotite source ratios (Stracke and Bourdon, 2009). In addition we have shown that the studied rocks are significantly evolved (Ni < 42 ppm) and that amphibole, one of the crystallized phases, is capable of~~

~~fractionating elemental ratios involving Nb. In contrast, as~~crystal fractionation processes, radiogenic isotope ratios are not changed during ~~melting~~such events~~ they.~~ They are ~~considered~~thus a ~~more~~ reliable indicator of source heterogeneity, even though the isotope variability of lavas ~~tend~~tends to be smaller than that of the mantle source due to eventual mixing/homogenization processes (e.g. Stracke and Bourdon, 2009).

The 2014 volcanic products have clearly more unradiogenic Pb and Sr ($^{206}Pb/^{204}Pb$ down to 18.972; $^{87}Sr/^{86}Sr$ down to 0.703613) but more radiogenic Nd ($^{143}Nd/^{144}Nd$ up to 0.512789) signatures than the previous two eruptions ($^{206}Pb/^{204}Pb$ up to 19.273; $^{87}Sr/^{86}Sr$ up to 0.70379; $^{143}Nd/^{144}Nd$ down to 0.51272; see also Figs 6 and 7). ~~Such differences, observed in volcanic products erupted during a time span of just 63 years from vents so closely located (200 to < 2000 m)~~Considering that the 2014 lavas erupted from vents localized less than 200 and 2000 m of those from the two previous eruptions (1951 and 1995) and that these 3 eruptions occurred within a time lapse of only 63 years, such differences emphasize the presence of small-scale heterogeneities in the mantle sources feeding the volcanism of Fogo Island and the absence of significant magma mingling/homogenization before eruption.

The ability of magmas erupted from a volcano to show the source heterogeneity depends on the degree of partial melting, on the size of magma chambers and on the time of residence in such reservoirs. The higher the degree of partial melting, the higher is the capability of the extracted magmas to average the composition of a heterogeneous source. As a consequence low degree partial melts reflect better the compositional variability of the source~~. This was shown, for example, by~~ (e.g. Stracke and Bourdon, 2009; Martins et al~~. (~~., 2010~~) for the neighbouring Santiago Island, who evidenced an increasing variability of the $^{143}Nd/^{144}$ Nd ratios with decreasing degrees of partial melting.~~

). It is ~~considered~~accepted that the lithosphere exerts a major control in the final depth and extent of sub-lithospheric mantle melting ~~and, consequently, also on the extent and~~

~~mean pressure of melting (e.g.~~ (e.g. Watson and Mckenzie, 1991; Humphrey and Niu, 2009; Niu et al., 2011), even though the thickness of mature (> 70Ma) oceanic lithosphere does not surpass ≈90 km (Niu et al., 2011). The Cape Verde islands stand on a 120-140 My old oceanic crust characterized by significantly high values of admittance (geoid to depth ratio) (Monnerau and Cazennave, 1990). ~~This~~These suggests that lithosphere may extend to depths below the spinel-garnet transition~~, considered to occur at depths corresponding to ~~ (≈3 GPa ~~(e.g.,~~; Klemme and O'Neil, 2000~~). Consequently, the depth of melting would have been totally or partially confined to the mantle garnet zone.~~) in agreement with previous studies for Cape Verde islands (e.g. Gerlach et al., 1998; Barker et al., 2010; Mourão et al., 2012a). Even taking into account that the less evolved 2014 magmas (tephrites) are not characterized by primary or primitive compositions, this percept is endorsed by (Tb/Yb)n ratios higher than 2.3, which is significantly above the threshold value of 1.8 proposed by Wang et al. (2002) as a proxy for spinel-garnet facies transition. Indeed it would be necessary to consider a (Tb/Yb)n increase higher than 27% during magma evolution – which is not expectable from the commonly accepted D values (~~see for example https://earthref.org/KDD/~~)e.g. Adam and Green, 2006) – to place the mean melting depths outside the garnet zone. ~~This and~~ Moreover, 2014 magmas show a Tb/Yb decrease from tephrites for the ~~highly $SiO_2$ – undersaturated character of the Fogo lavas (2014: normative *ne* up to 23.04 %) point out to low degree of partial melting events with the consequent deficient averaging of the isotopic variability of the source.~~more evolved phonotephrites.

The thickness of the lithosphere exerts a first-order control on the extent of partial melting (e.g. Humphreys and Niu, 2009). For the present case, a lithosphere some 90 km thick (see above) would have constrained the melting to small extent. Despite the exact extent of melting is difficult to assess given the significantly evolved character of lavas (MgO < 6.4 wt%) and the uncertainty derived from the lack of knowledge about the relative proportion of peridotite and eclogite in the mantle source, the highly $SiO_2$ -

undersaturated character of the Fogo lavas (2014: normative *ne* up to 23.04 %) and the high TiO2 contents clearly suggest low percentages of partial melting, with the consequent deficient averaging of the isotopic variability of the source. The above referred lack of correlation between elemental and isotope ratios (see 4.3) also points to low degrees of melting during which a significant elemental fractionation occurs erasing any correlation between incompatible element ratios and isotope ratios (see Stracke and Bourdon, 2009).

After extraction, the degree of melt homogenization will depend on the occurrence of a plumbing system with large magmatic chamber(s), and of long magma residence times within the system, allowing mixing of different batches of melt. Data gathered from several islands suggest that for voluminous magma chambers to form, high magma supply rates are needed; conversely, during evolutionary stages characterized by low magma supply rates a plethora of small and ephemeral magma reservoirs tend to form, many of them within the mantle (see Klügel et al., 2000; 2005; Stroncik et al., 2009 and references therein), and this is also the case for the recent magmatism of Fogo. The evidence for small and ephemeral magma reservoirs beneath Fogo was already proposed for the previous eruptions (Munhá et al., 1997; Hildner et al., 2012). This may be also the case for the 2014 eruption as suggested by the compositional change during the latest two eruptions (from phonotephrites to basanites/tephrites) and, despite the associated methodological errors, by distinct depths of magma chambers where clinopyroxene and kaersutite crystalized, both evidences precluding a large homogenizing reservoir.

~~Thus, the isotopic heterogeneity depicted by the lavas erupted during the three last eruptions at Fogo Island (1951, 1995 and 2014) can be considered as the result of source heterogeneities and the presence of a thick lithosphere that, by restraining the extent of partial melting to low degrees – and consequently limiting magma supply to low rates – inhibited both significant averaging of source composition and the~~

~~subsequent mixing/homogenization during ascent to the surface. It must be emphasized that, to some degree, melt aggregation and magma mixing must have occurred (see for example the reverse zoning in some clinopyroxenes), and thus the isotopic heterogeneity of the erupted materials is considered to be smaller than that of the mantle source.~~

~~Another consequence of the low degrees of partial melting in Cape Verde is the referred lack of correlation between elemental and isotope ratios (see 4.3). Indeed, during such melting events an elemental fractionation occurs erasing any correlation between incompatible element ratios and isotope ratios characterizing the mantle source (see Stracke and Bourdon, 2009).~~

Formatted: Font: Bold

## 6. Concluding remarks

- Magmas erupted from November 23 to December 7, 2014 at Fogo Island (Cape Verde Archipelago) are alkaline, exhibit significantly evolved compositions (Ni < 42 ppm) and are classified as tephrites and phonotephrites. The compositional range is slightly smaller than that reported for the 1995 eruption, but larger than the displayed by the 1951 eruption, for which no phonotephrites were erupted.
- Similarly to 1995 (Munhá et al., 1997; Silva et al., 1997; Hildner et al., 2011), the eruption of phonotephritic lavas preceded the effusion of the tephritic ones ~~pointing to~~suggesting the existence of a compositional/density zoning inside the pre-eruptive magma chamber or of several magma reservoirs, in agreement with barometric data.
- Geobarometric estimates using clinopyroxene and kaersutite compositions indicate that fractional crystallization mainly occurred in magma chambers located in the mantle ~~(≈ 12~~(down to ~~34~~25.6 ± 5.5 km below the sea level), followed by a short residence time (< 60 days) at crustal levels.

- Erupted magmas are characterized by positive εNd, εHf, Δ8/4 and Δ7/4. Their compositions reflect a mantle source where ancient recycled ocean crust and an enriched component (EM1-type) are present. The 2014 lavas have less radiogenic Sr, but more radiogenic Nd compositions, ~~when compared with~~than those from the 1951 and 1995 eruptions, marking a change on the evolutionary trend reported by previous authors for Fogo (Gerlach et al., 1988; Escrig et al., 2005) which was characterized by an increasing contribution of the ~~enriched~~EM1-type component.
- Although the 2014 eruption vents are almost spatially coincident with those of 1995 and less than 2 km away from the 1951 vents, their lavas are isotopically different from those generated in the previous two eruptions. These differences in magmas erupted on a very limited area and short interval (63 years) reflect the heterogeneity of the mantle source and the lack of averaging/mingling during partial melting and ascent through the plumbing system. For these, the lid effect of the old (120-140 Ma) and thick lithosphere is considered of utmost importance.
- The lower Nb/U ratios of the 2014 rocks as compared with previous eruptions is considered to reflect the lack of significant mixing of ascending plume magmas with lithospheric melts, as opposed to what has been hypothesized for 1995 and 1951 magmas.
- ~~It is inferred that the lid effect of an old (120-140 Ma) and thick lithosphere, imposing low melting degrees, limited the averaging of source compositions. In turn, low melting degrees induced low magma ascent rates, a condition not favourable to the generation of voluminous magma chambers where isotopically distinct magma batches issued from heterogeneous sources could pond and mix~~

Formatted: Font: Verdana, 10 pt

Formatted: Bulleted + Level: 1 + Aligned at: 0.63 cm + Indent at: 1.27 cm

Formatted: Font: Verdana, 10 pt

Formatted: Font: Verdana, 10 pt

Formatted: Font: Verdana, 10 pt

~~with each other, producing homogeneous compositions over significant periods of time.~~

**Acknowledgements**

We dedicate this paper to the memory of Luís Celestino Silva (1936-2017), a pioneer in the geology of Cape Verde: his knowledge, enthusiasm and kindness marked most of the authors of this work.

This research received financial support from FCT (Fundação para a Ciência e Tecnologia) through projects REGENA (PTDC /GEO-FIQ/3648/2012) and FIRE (PTDC/GEO-GEO/1123/2014), as well as through project UID/GEO/50019/2013 to Instituto Dom Luiz (IDL). R. Ramalho was funded by a FP7-PEOPLE-2011-IOF Marie Curie International Outgoing Fellowship, which is acknowledged. The authors are grateful to Pedro Rodrigues for skilled assistance during electron microprobe analyses. Field work of J. Mata was partially funded by Bernardo Mata. Kayla Iacovino is acknowledged for the permission to use her Excel spreadsheet to calculate magma viscosity (see http://www.kaylaiacovino.com/tools-for-petrologists/). Cristina de Ignacio, an anonymous reviewer and the Editor (Nelson Eby) are acknowledged for their constructive comments, corrections and suggestions, which significantly contributed for the quality of this paper.

**References**

Adam, J., Green, T. 2006. Trace element partitioning between mica and amphibole-bearing garnet lherzolite and hydrous basanitic melt: 1. Experimental results and the investigation of controls on partitioning behavior. Contributions to Mineralogy and Petrology 152, 1-17.

~~Aignertorres, M., Blundy, J., Ulmer, P., Pettke, T. 2007. Laser Ablation ICPMS study of trace element partitioning between plagioclase and basaltic melts: an experimental approach. Contributions to Mineralogy and Petrology 153, 647-667.~~

Bagnardi, M., Gonzàlez, P.J., Hooper, A. 2016. High-resolution digital elevation model from tri-stereo Pleiades-1 satellite imagery for lava flow volume estimates at Fogo Volcano: Tri-stereo Pleiades DEM of Fogo Volcano. Geophys. Res. Lett.,43, doi:10.1002/2016GL06945

Barker, A.K., Holm, P.M., Peate, D.W., Baker, J.A. 2009. Geochemical stratigraphy of submarine lavas (3–5 Ma) from the Flamengos Valley, Santiago, southern Cape Verde islands. Journal of Petrology 50, 169-193.

Barker, A.K., Holm, P.M., Peate, D.W., Baker, J.A. 2010. A 5 million year record of compositional variations in mantle sources to magmatism on Santiago, southern Cape Verde archipelago. Contributions to Mineralogy and Petrology 160, 133-154.

Barker, A.K., Troll, V.R., Ellam, R.M., Hansteen, T.H., Harris, C., Stillman, C.J., Andersson, A. 2012. Magmatic evolution of the Cadamosto Seamount, Cape Verde: beyond the spatial extent of EM1. Contributions to Mineralogy and Petrology 163, 949 -965.

~~Beattie, P. 1994. Systematics and energetics of trace element partitioning between olivine and silicate melts: Implications for the nature of mineral/melt partitioning. Chemical Geology 117, 57-71.~~

Beier, C., Haase, K. M., Abouchami, W., Krienitz, M.-S., Hauff, F. 2008. Magma genesis by rifting of oceanic lithosphere above anomalous mantle: Terceira Rift, Azores. Geochemistry, Geophysics, Geosystems 9, Q12013.

~~Bohrson, Wendy A., Spera, Frank J. 2001. Energy-Constrained Open-System Magmatic Processes II: Application of Energy-Constrained Assimilation-Fractional Crystallization (EC-AFC) Model to Magmatic Systems. Journal of Petrology 42, 1019-1041.~~

~~Bottazzi, P., M. Tiepolo, R. Vannucci, A. Zanetti, S. Foley, R. Brumm, Oberti, R. 1999. Distinct site preference for heavy and light REE and the prediction of $^{Amph/L}D_{REE}$. Contributions to Mineralogy and Petrology 137, 36-45.~~

Browne, B.L., Gardner, J.E. 2006. The influence of magma ascent path on the texture, mineralogy, and formation of hornblende reaction rims. Earth and Planetary Science Letters 246, 161-176.

Brum da Silveira, A., Madeira, J., Munhá, J., Mata, J.; Martins, S., Mourão, C., Tassinari, C. 2006. The summit depression of Fogo Island (Cape Verde): caldera and/or flank collapse? Abstracts and Programme of the George P. L. Walker symposium on Advances in Volcanology, Reykolt, Islândia, 23.

Caldeira, R., Guimarães, F., Mata, J. Silva, P., Moreira, M., Ferreira, P. 2015. Mineral Chemistry of Ultramafic Nodules from Lavas of the Fogo Island 2014 Eruption (Cape Verde). Preliminary results. Livro de Resumos do X Congresso Ibérico de Geoquímica/XVIII Semana de Geoquímica, 51-53, LNEG, Lisboa.

Cappello, A., G. Ganci, S. Calvari, N. M. Pérez, P. A. Hernández, S. V. Silva, J. Cabral, and C. Del Negro. 2016. Lava flow hazard modeling during the 2014–2015 Fogo eruption, Cape Verde, Journal of Geophysical Research, Solid Earth 121, 1-14.

Chauvel, C., Blichert-Toft, J. 2001. A hafnium isotope and trace element perspective on melting of the depleted mantle. Earth Planetary Science Letters 190, 137–151.

Chauvel, C., Lewin, E., Carpentier, M., Arndt, N., Marini, J.-C. 2008. Role of recycled oceanic basalt and sediment in generating the Hf–Nd mantle array. Nature Geoscience 1, 64–67.

Chauvel, C., Bureau, S., Poggi, C. 2011. Comprehensive chemical and isotopic analyses of basalt and sediment reference materials. Geostandards and Geoanalytical Research 35, 125–143.

**Formatted:** Font color: Custom Color(RGB(34,34,34)), English (United States), Kern at 18 pt

**Formatted:** Level 1, Pattern: Clear (White)

Chiaradia, M., Müntener, O., Beate, B. 2011. Enriched basaltic andesites from mid-crustal fractional crystallization, recharge, and assimilation (Pilavo Volcano, Western Cordillera of Ecuador). Journal of Petrology 52, 1107-1141.

Christensen, B., Holm, P., Jambon, A., Wilson, J. 2001. Helium, argon and lead isotopic composition of volcanics from Santo Antão and Fogo, Cape Verde Islands. Chemical Geology 178, 127–142.

Cooper, K.M. 2017. What does a magma reservoir look like? The "crystal's eye" view. Elements 13, 23-28.

Courtney, R., White, R. 1986. Anomalous heat flow and geoid across the Cape Verde Rise: Evidence for dynamic support from a thermal plume in the mantle. Geophysical Journal of the Royal Astronomical Society 87, 815-868.

Cashman, K.V., Sparks, R.S.J., Blundy, J.D. 2017. Vertically extensive and unstable magmatic systems: A unified view of igneous processes. Science 355, eaag3055, 9 pages.

Dash, B.P., Ball, M.M., King, G.A., Butler, I.W., Rona, P.A. 1976. Geophysical investigation of the Cape Verde archipelago. Journal of Geophysical Research 81, 5249-5259.

Davidson, J., Turner, S., Plank, T. 2013. Dy/Dy*: Variations Arising from Mantle Sources and Petrogenetic Processes. Journal of Petrology 54, 525-537.

Day, S., Heleno da Silva, S., Fonseca, J. 1999. A past giant lateral collapse and present day instability of Fogo, Cape Verde Islands. Journal of Volcanology and Geothermal Research 94, 191-218.

De Angelis, S.H., Larsen, J., Coombs, Dunn, A., Hayden, L. 2015. Amphibole reaction rims as a record of pre-eruptive magmatic heating: An experimental approach. Earth and Planetary Science Letters 426, 235–245

Doucelance, R., Escrig, S., Moreira, M., Gariépy, C., Kurz, M.D. 2003. Pb-Sr-He isotope and trace element geochemistry of the Cape Verde Archipelago. Geochimica et. Cosmochimica Acta 67, 3717-3733.

Eisele, S., Reißig, S., Freundt, A., Kutterolf, S., Nürnberg, D., Wang, K.L, Kwasnitschka, T. 2015. Pleistocene to Holocene offshore tephrostratigraphy of highly explosive eruptions from the southwestern Cape Verde Archipelago. Marine Geology 369, 233-250.

Escrig, S., Doucelance, R., Moreira, M., Allègre, C.J. 2005. Os isotope systematics in Fogo Island: evidence for lower continental crust fragments under the Cape Verde Southern islands. Chemical Geology 219, 93-113.

Faria, B., Fonseca, J. F. B. D. 2014. Investigating volcanic hazard in Cape Verde Islands through geophysical monitoring: network description and first results. Natural Hazards and Earth System Sciences 14, 485–499.

Foeken, J.P.T., Day, S., Stuart, F.M. 2009. Cosmogenic $^{3}$He exposure dating of the Quaternary basalts from Fogo, Cape Verdes: Implications for rift zone and magmatic reorganisation. Quaternary Geochronology 4, 37-49.

Forte, A.M., Quere, S., Moucha, R., Simmons, N.A., Grand, S.P., Mitrovica, J.X., Rowley, D.B. 2010. Joint seismic-geodynamic-mineral physical modelling of African geodynamics: a reconciliation of deep-mantle convection with surface geophysical constraints. Earth Planetary Science Letters 295, 329–341.

Formatted: Portuguese (Portugal)

Formatted: Portuguese (Portugal)

French, S.W., Romanowicz, B. 2015. Broad plumes rooted at the base of the earth's mantle beneath major hotspots. Nature 525, 95-99.

~~Frost, B.R., Lindsley, D.H. 1991. Occurrence of iron-titanium oxides in igneous rocks. In: Lindsley, D.H. (ed.) Oxide Minerals. Mineralogical Society of America, Reviews in Mineralogy 25, 433-468.~~

Galer, S.J.G., Abouchami, W. 1998. Pratical application of lead triple spiking for correction of instrumental mass discrimination. Mineralogical Magazine 62 A, 491-492.

Geiger, H., Barker, A., Troll, V. 2016. Locating the depth of magma supply for volcanic eruptions, insights from Mt. Cameroon. Scientific Reports 6, 33629.

Gerlach, D., Cliff, R., Davies, G., Norry, M., Hodgson, N. 1988. Magma sources of the Cape Verde archipelago: Isotopic and trace element constraints. Geochimica et Cosmochimica Acta 52, 2979-2992.

Gibson, S.A., Geist, D.G., Day, J.A., Dale, C.W. 2012. Short wavelength heterogeneity in the Galápagos plume: Evidence from compositionally diverse basalts on Isla Santiago. Geochemistry, Geophysics, Geosystems 13, doi: 10.1029/2012GC004244.

Giordano, D., Russell, J. K., Dingwell, D. B. 2008. Viscosity of magmatic liquids: A model. Earth and Planetary Science Letters, 217, 123-134.

González, P. J., M. Bagnardi, A. J. Hooper, Y. Larsen, P. Marinkovic, S. V. Samsonov, Wright, T. J. 2015. The 2014–2015 eruption of Fogo volcano: Geodetic modeling of Sentinel-1 TOPS interferometry. Geophysical Research Letters 42, 9239–9246.

Gudmundsson, A., 2012. Magma chambers: Formation, local stresses, excess pressures, and compartments: Journal of Volcanology and Geothermal Research 237–238, 19–41.

Hart, S.R. 1984. A large-scale isotope anomaly in the Southern Hemisphere mantle. Nature 309, 753-757.

Hildner, H., Klügle, A., Hauff, F. 2011. Magma storage and ascent during the 1995 eruption of Fogo, Cape Verde Archipelago. Contributions to Mineralogy and Petrology 162, 751–772.

Hildner, H., Klügle, A., Hansteen, T.2012. Barometry of lavas from 1951 eruption of Fogo, Cape Verde Islands: Implications for historic and prehistoric magma plumbing system. Journal of Volcanology and Geothermal Research 217-218, 73-90.

Hoernle, K., Tilton, G., Le Bas, M.J., Duggen, S., Garbe-Schönberg, D. 2002. Geochemistry of oceanic carbonatites compared with continental carbonatites: mantle recycling of oceanic crustal carbonate. Contribution to Mineralogy and Petrology 142, 520-542.

Hofmann, A.W. 2003. Sampling mantle heterogeneity trough oceanic basalts: isotopes and trace elements, in: Carlson, R. (Ed.), Treatise on geochemistry, vol. 2 - The mantle and core. Elsevier-Pergamon, Oxford, pp. 61-101.

Holm, P.M., Wilson, J.R., Christensen, B.P., Hansen, L., Hansen S.L., Hein, K.M., Mortensen, A.K., Pedersen, R., Plesner, S., Runge, M.K. 2006. Sampling the Cape Verde mantle plume: evolution of the melt compositions on Santo Antão, Cape Verde Islands. Journal of Petrology 47, 145-189.

Holm, P.M., Grandvuinet, T., Friis, J., Wilson, J.R., Barker, A.K., Plesner, S. 2008. An $^{40}$Ar-$^{39}$Ar study of the Cape Verde hot spot: Temporal evolution in a semistationary plate environment. Journal of Geophysical Research 113, B08201.

Humphreys, E., Niu, Y. 2009. On the composition of ocean island basalts (OIB): the effects of lithospheric thickness variation and mantle metasomatism. Lithos 112, 118-136.

Iwamori, H., Nakamura, H. 2015. Isotopic heterogeneity of oceanic, arc and continental basalts and its implications for mantle dynamics. Gondwana Research 27, 1131-1152.

Jagoutz O. 2014. Arc crustal differentiation mechanisms. Earth Planetary Science Letters 396, 67–77.

Jørgensen, J.Ø., Holm, P.M. 2002. Temporal variation and carbonatite contamination in primitive ocean island volcanics from S. Vicente, Cape Verde Islands. Chemical Geology 192, 249-267.

Kawabata, H., Hanyu, T., Chang, Q., Kimura, J., Nichols, A.R.L., Tatsumi, Y. 2011. The Petrology and Geochemistry of St. Helena Alkali Basalts: Evaluation of the Oceanic Crust-recycling Model for HIMU OIB. Journal of Petrology 52, 791-838.

Klemme, S., O'Neill, H., 2000. The near solidus transition from garnet lherzolite to spinel lherzolite. Contributions to Mineralogy and Petrology 138, 237-248.

Klügel, A., Hoernle, K.A., Schmincke, H-U, White, J.D.L. 2000. The chemically zoned 1949 eruption on La Palma (Canary Islands): Petrologic evolution and magma supply dynamics of a rift-zone eruption. Journal of Geophysical Research 105, 5997-6016.

Klügel, A., Hansteen, T.H., Galipp, K. 2005. Magma storage and underplating beneath Cumbre Vieja volcano, La Palma (Canary Islands). Earth and Planetary Science Letters 236, 211-226.

Klügel, A., Longpré, M-A., Cañada, L. C., Stix, J. 2015. Deep intrusions, lateral magma transport and related uplift at ocean island volcanoes. Earth and Planetary Science Letters 431, 140-149.

Kogarko, L.N., Asavin, A.M. 2007. Regional Features of Primary Alkaline Magmas of the Atlantic Ocean. Geochemistry International 45, 841-856.

Le Bas, M. 1989. Nephelinitic and basanitic rocks. Journal of Petrology 30, 1299-1312.

~~Le Bas, T.P., Masson, D.G., Holtom, R.T., Grevemeyer, I. 2007. Slope failures of the flanks of the southern Cape Verde Islands. Submarine Mass Movements and Their Consequences, 337-345. V. Lykousis, D. Sakellariou and J. Locat (eds.), Springer.~~

Le Maitre, R.W., 2002. Igneous rocks. A classification and glossary of terms. Recommendations of the International Union of Geological Sciences Subcommission on the systematics of igneous rocks. Cambridge University Press, Cambridge. 236pp.

Liu, X., Zhao, D. 2014. Seismic evidence for a mantle plume beneath the Cape Verde hotspot. International Geology Review 56, 1213-1225.

Lodge, A., Helffrich, G. 2006. Depleted swell root beneath the Cape Verde Islands. Geology 34, 449-452.

Longpré, M., Troll, V.R., Hansteen, T.H. 2008. Upper mantle magma storage and transport under a Canarian shield-volcano, Teno, Tenerife (Spain). Journal of Geophysical Research 113, doi: 10.1029/2007JB005422.

Lundstrom, C.C., Hoernle, K., Gill, J. 2003. U-series disequilibria in volcanic rocks from the Canary Islands: Plume versus lithospheric melting: Geochimica et Cosmochimica Acta 67, 4153–4177.

**Formatted:** List Paragraph

MacDonlad, G.A. 1968. Composition and origin of Hawaiian lavas. Geological Society of America Memoir 116, 477-452.

Madeira, J., Munhá, J., Tassinari, C., Mata, J., Brum, A., Martins, S. 2005. K/Ar ages of carbonatites from the Island of Fogo (Cape Verde). VIII Congresso Ibérico de Geoquímica e XIV Semana de Geoquímica (Portugal).

Madeira, J., Brum da Silveira, A., Mata, J., Mourão, C., Martins, S. 2008. The role of mass movements on the geomorphologic evolution of ocean islands: examples from Fogo and Brava in the Cape Verde archipelago. Comunicações Geológicas 95, 99-112.

Madeira, J., Mata, J., Mourão, C., Brum da Silveira, A., Martins, S., Ramalho, R., Hoffmann, D.L. 2010. Volcano-stratigraphic and structural evolution of Brava Island (Cape Verde) based on $^{40}Ar/^{39}Ar$, U–Th and field constraints. Journal of Volcanology and Geothermal Research 196, 219-235.

Madureira, P., Mata, J., Mattielli, N., Queiroz, G., Silva, P. 2011. Mantle source heterogeneity, magma generation and magmatic evolution at Terceira Island (Azores archipelago): Constraints from elemental and isotopic (Sr, Nd, Hf, and Pb) data. Lithos 126, 402-418.

Martins, S., Mata, J., Munhá, J., Mendes, M.H., Maerschalk, C., Caldeira, R., Mattielli, N. 2010. Chemical and mineralogical evidence of the occurrence of mantle metasomatism by carbonate-rich melts in an oceanic environment (Santiago Island, Cape Verde). Mineralogy and Petrology 99, 43-65.

Masson, D.G., Le Bas, T.P., Grevemeyer, I., Weinrebe, W., 2008. Flank collapse and large-scale landsliding in the Cape Verde Islands, off West Africa. Geochemistry, Geophysics, Geosystems 9 (7).

Mata, J., Munhá, J. 2004. Madeira Island alkaline lava spinels: petrogenetic implications. Mineralogy and Petrology 81, 85-111.

Mata, J., Moreira, M., Doucelance, R., Ader, M., Silva, L.C. 2010. Noble gas and carbon isotopic signatures of Cape Verde oceanic carbonatites: Implications for carbon provenance. Earth Planetary Science Letters 291, 70-83.

McKenzie, D., O'Nions, R.K. 1991. Partial melt distributions from inversion of rare earth element concentrations. Journal of Petrology 32, 1021-1091.

Menand, T. 2008. The mechanics and dynamics of sills in elastic layered media and their implications for the growth of laccoliths. Earth Planetary Science Letters 267, 93–99.

Millet, M.A., Doucelance, R., Schiano, P., David, K., Bosq, C. 2008. Mantle plume heterogeneity versus shallow-level interactions: A case study, the São Nicolau Island, Cape Verde archipelago. Journal of Volcanology and Geothermal Research 176, 265-276.

Mollo, S., Putirka, K., Misiti, V., Soligo, M., Scarlato, P. 2013. A new test for equilibrium based on clinopyroxene-melt pairs: Clues on the solidification temperatures of Etnean alkaline melts at post-eruptive conditions. Chemical Geology 352, 92-100.

Monnereau, M., Cazenave, A. 1990. Depth and geoid anomalies over oceanic hotspot swells: A global survey. Journal of Geophysical Research (Solid Earth) 95, 15-429.

Montelli, R., Nolet, G., Dahlen, F.A., Masters, G. 2006. A catalogue of deep mantle plumes: new results from finite-frequency tomography. Geochemistry, Geophysics, Geosystems 7, doi:10.1029/2006GC001248.

Mourão, C., Mata, J., Doucelance, R., Madeira, J., Millet, M-A., Moreira, M. 2012a. Geochemical temporal evolution of Brava Island magmatism: constraints on the variability of Cape Verde mantle sources and on the carbonatite-silicate magma link. Chemical Geology 334, 44-61.

Mourão, C., Moreira, M., Mata, J., Raquin, A., Madeira, J. 2012b. Primary and secondary processes constraining the noble gas isotopic signatures of carbonatites and silicate rocks from Brava Island: evidence for a lower mantle origin of the Cape Verde plume. Contributions to Mineralogy and Petrology 163, 995-1009.

Munhá, J.M., Mendes, M.H., Palácios, T., Silva, L.C., Torres, P.C., 1997. Petrologia e geoquímica da erupção de 1995 e de outras lavas históricas da ilha do Fogo, Cabo Verde. In: Réffega A et al. (eds). A Erupção Vulcânica de 1995 na Ilha do Fogo, Cabo Verde. IICT, Lisboa, 171-186.

Niu, Y., Wilson, M., Humphreys, E.R., O'Hara, M.J. 2011. The Origin of Intra-plate Ocean Island Basalts (OIB): the Lid Effect and its Geodynamic Implications. Journal of Petrology 52, 1443-1468.

Niu, Y.L., Wilson, M., Humphreys, E.R., O'Hara, M.J. 2012. A trace element perspective on the source of ocean island basalts (OIB) and fate of subducted ocean crust (SOC) and mantle lithosphere (SML). Episodes 35, 310-327.

Nobre Silva, I., Weis, D., Scoates, J. 2013. Isotopic systematics of the early Mauna Kea shield phase and insight into the deep mantle beneath the Pacific Ocean. Geochemistry, Geophysics, Geosystems 11, Q 09011. doi:10.1029/2010gc003176.

Palme, H., O'Neill, H.S.C. 2003. Cosmochemical estimates of mantle compositions. In: Carlson, R. (Ed.). The mantle and core. Treatise on Geochemistry 2, 1-38.

Paris, R., Giachetti, T., Chevalier, J., Guillou, H., Frank, N. 2011. Tsunami deposits in Santiago Island (Cape Verde archipelago) as possible evidence of a massive flank failure of Fogo volcano. Sedimentary Geology 239, 129-145.

~~Paster, T.P., Schauwecker, D.S.Haskin, L.A. 1974. The behavior of some trace elements during solidification of the Skaergaard layered series. Geochimica et Cosmochimica Acta 38, 1549-1577.~~

Pim, J., Peirce, C., Watts, A.B., Grevemeyer, I., Krabbenhoeft, A. 2008. Crustal structure and the origin of the Cape Verde Rise. Earth Planetary Science Letters 272, 422-428.

Pollitz, F. 1991. Two-stage model of African absolute motion during the last 30 million years. Tectonophysics 194, 91-106.

Putirka, K. 1997. Magma transport at Hawaii: Inferences based on igneous thermobarometry. Geology 25, 69–72.

Putirka, K. 1999. Clinopyroxene + liquid equilibria to 100 kbar and 2450 K. Contributions to Mineralogy and Petrology 135, 151-163.

Putirka, K.D. 2008. Thermometers and barometers for volcanic systems. Reviews in Mineralogy and Geochemistry 69, 61-120.

Putirka, K.D. 2017. Down the crater: where magmas are stored and why they erupt. Elements 13, 11-16.

Putirka, K., Mikaelian, H., Ryerson, F., Shaw, H., 2003. New clinopyroxene-liquid thermobarometers for mafic, evolved, and volatile-bearing lava compositions, with applications to lavas from Tibet and the Snake River Plain, Idaho. American Mineralogist 88, 1542-1554.

Ramalho, R. 2011. Building the Cape Verde Islands. Springer Theses, 207 pp.

Ramalho, R., Helffrich, G., Cosca, M., Vance, D., Hoffmann, D., Schmidt, D.N. 2010. Episodic swell growth inferred from variable uplift of the Cape Verde hotspot islands. Nature Geoscience 3, 774-777.

Ramalho, R., Winckler, G., Madeira, J., Helffrich, G., Hipólito, A., Quartau, R., Adena, K., Schaefer, J. 2015 Hazard potential of volcanic flank collapses raised by new megatsunami evidence. Science Advances 1, doi: 10.1126/sciadv.1500456.

Ribeiro, O. 1954. A ilha do Fogo e as suas erupções. Junta de Investigações do Ultramar, Memórias, Série Geográfica I, Lisboa.

Richter, N., Favalli, M., Dalfsen, E.Z., Fornaciai, A., Fernandes, R.M.S., Rodriguez, N.P., Levy, J., Victória, S.S., Walter, Th.R. 2016. Lava flow hazard at Fogo Volcano, Cape Verde, before and after the 2014-2015 eruption. Natural Hazards and Earth Systems 16, 1925-1951.

Ridolfi, F, Renzulli, A. 2012. Calcic amphiboles in calc-alkaline and alkaline magmas: thermobarometric and chemometric empirical equations valid up to 1130 ºC and 2.2 GPa. Contributions to Mineralogy and Petrology 163, 877–895.

Rutherford, M.J. 2008. Magma ascent rates. In: Putirka, K.D. and Tepley, F.J., III (eds) Minerals, Inclusions and Volcanic Processes. Mineralogical Society of America and Geochemical Society Reviews, in Mineralogy and Geochemistry 69, 241-271

Ryan, M. 1994. Neutral-buoyancy controlled magma transport and storage in mid-ocean ridge magma reservoirs and their sheeted-dike complex: A summary of basic relationships. In: Magmatic Systems. Eds: M. P. Ryan, Chap. 6, Academic, San Diego, Caliornia.

Saki, M., Thomas, C., Nippress, S.E.J., Lessing, S. 2015. Topography of upper mantle seismic discontinuities beneath the North Atlantic: the Azores, Canary and Cape Verde plumes. Earth and Planetary Science Letters 409, 193-202.

Satoh, H., Yamaguchi, Y., Makino, K. 2004. Ti-substitution mechanism in plutonic oxy-kaersutite from the Larvik alkaline complex, Oslo rift, Norway. Mineralogical Magazine, Vol. 68, 687–697.

Silva, L.C., Mendes, M.H., Torres, P.C., Palácios, T., Munhá, J.1997. Petrografia das Formações Vulcânicas da Erupção de 1995 na Ilha do Fogo, Cabo Verde. In: Réffega, A. et al. (eds.). A Erupção Vulcânica de 1995, na Ilha do Fogo, Cabo Verde. IICT, Lisboa, 164-170.

Staudigel, H., Park, K.H., Pringle, M., Rubenstone, J.L., Smith, W.H.F., Zindler, A., 1991. The longevity of the South-Pacific isotopic and thermal anomaly. Earth and Planetary Science Letters 102, 24–44.

Stracke, A., Hofmann, A.W., Hart, S.R. 2005. FOZO, HIMU, and the rest of the mantle zoo. Geochemistry, Geophysics, Geosystems 6, Q05007, doi:10.1029/2004GC000824.

Stracke, A., Bourdon, B. 2009. The importance of melt extraction for tracing mantle heterogeneity. Geochimica et Cosmochimica Acta 73, 218-238.

Stroncik, N.A, Klügel A., Hansteen, T. H. 2009. The magmatic plumbing system beneath El Hierro (Canary Islands): Constraints from phenocrysts and naturally quenched basaltic glasses in submarine rocks. Contributions to Mineralogy and Petrology 157, 593-607.

Formatted: Portuguese (Portugal)

Formatted: English (United States)

Torres, P.C., Madeira, J., Silva, L.C., Brum da Silveira, A., Serralheiro, A., Mota Gomes, A. 1998. Carta Geológica das Erupções Históricas da Ilha do Fogo (Cabo Verde): revisão e actualização. Comunicações do Instituto Geológico e Mineiro 84, A193-196.

Torres, P., Silva, L.C., Munhá, J., Caldeira, R., Mata, J., Tassinari, C. 2010. Petrology and Geochemistry of lavas from Sal Island: Implications for the variability of the Cape Verde magmatism. Comunicações Geológicas 97, 35-62.

Trindade, M.J., Mata, J., Munhá, J. 2003. Petrogenesis of the Quaternary magmatism from the S. Vicente Island (Cape Verde). Comunicações do Instituto Geológico e Mineiro 90, 169-188.

Vervoort, J., Patchett, P., Blichert-Toft, J., Albarède, F. 1999. Relationships between Lu-Hf and Sm-Nd isotopic systems in the global sedimentary system. Earth and Planetary Science Letters 168, 79-99.

Vinnik, L., Silveira, G., Kiselev, S., Farra, V., Weber, M., Stutzmann, E. 2012. Cape Verde hotspot from the upper crust to the top of the lower mantle. Earth Planetary Science Letters 319-320, 259-268.

Wang, K., Plank, T., Walker J.D., Smith, E.I. 2002. A mantle melting profile across the Basin and Range, SW USA. Journal of Geophysical Research 107, ECV 5, 1-21.

Watson, S., McKenzie, D. 1991. Melt generation by plumes: A study of Hawaiian volcanism. Journal of Petrology 32, 501-537.

Weis, D., Kieffer, B., Maerschalk, C., Barling, J., de Jong, J., Williams, G., Hanano, D., Pretorius, W., Mattielli, N., Scoates, J., Goolaerts, A., Friedman, R., Mahoney, J. 2006. High-precision isotopic characterization of USGS reference materials by TIMS and MC-ICP-MS. Geochemistry, Geophysics, Geosystems 7, doi:10.1029/2006GC001283.

White, W.M. 2015. Isotopes, DUPAL, LLSVPs, and Anekantavada. Chemical Geology 419, 10-28.

Williams, C., Hill, I., Young, R., White, R.S. 1990. Fracture zones across the Cape Verde Rise, NE Atlantic. Journal of the Geological Society of London 147, 851-857.

Wilson, D., Peirce, C., Watts, A., Grevemeyer, I., Krabbenhoeft, A. 2013. Uplift at lithospheric swells-I: Seismic and gravity constraints on the crust and uppermost mantle structure of the Cape Verde mid-plate swell. Geophysical Journal International 182, 531-550.

Wilson, D., Peirce, C., Watts, A., Grevemeyer, I. 2013. Uplift at lithospheric swells-II: is the Cape Verde mid-plate swell supported by a lithosphere of varying mechanical strength? Geophysical Journal International 193, 798-819.

Zindler, A., Hart, S.R. 1986. Chemical geodynamics. Annual Reviews of Earth Planetary Sciences 14, 493-571.

**Formatted:** Portuguese (Portugal)

**Formatted:** English (United States)

**Formatted:** Portuguese (Portugal)

**Formatted:** Font: Verdana, 10 pt, Font color: Auto

**Formatted:** Line spacing: Multiple 1.15 li

**Captions**

**Fig. 1** – Geological map of the identified historical eruptions in Fogo (modified from Torres et al., 1998) superimposed on the digital terrain model of the island. The upper inset shows the location of the Island of Fogo in the archipelago of Cape Verde. The lower insets correspond to the legend of the geological map and to a structural sketch showing the geometry and location of the eruptive fissures of the last three eruptions (1951, 1995 and 2014/15), the Bordeira wall (continuous line represents the top; dashed line represents the base), and the crater rim of Pico do Fogo.

**Fig 2** – Photos of the 2014/15 Fogo eruption: A- general view looking East of Pico do Fogo with the active vents at the base of the cone, the flat region of Chã das Caldeiras covered with the 1995 and 2014 lava flows and the south-eastern tip of the Bordeira wall; the eruptive column rises 3 km above the vents and is dispersed by south-eastward

wind at an altitude of approximately 5 km (photo taken on November 29, 2014, at 15:44 UTC); B- the alignment of active vents, viewed from the south, during a low activity phase; the new cone is growing against the southeast flank of the 1995 cone (to the left); the lava flow is being fed by the southernmost vent; the lava flow at the base of the cone presents a lava channel and several skylights with degassing white columns (photo taken on December 2, 2014, at 19:35 UTC); C- night aspect of the central crater projecting plastic spatter fragments from the explosion of lava bubbles during an hawaiian lava lake phase (photo taken on November 28, 2014, at 20:48 UTC); D- aspect of vulcanian activity at the northernmost vent producing ash-laden episodic eruptive columns with the wind blowing from the north; the white plume marks the position of the effusive south vent (photo taken on November 30, 2014, at 19:24 UTC); E- aspect of the surface of the active lava flow seen from the northwest presenting strong thermal emission and degassing (photo taken on November 29, 2014, at 15:48 UTC); F- the village of Portela invaded by the front of the lava flow 3.5 km away from the effusive vent (photo taken on December 2, 2014, at 14:39 UTC). For more photos see Supplementary Material S1.

**Fig. 3** - Total alkali-silica (TAS) diagram (Le Maître, 2002) for the 2014 magmatic rocks and interstitial glass occurring in the matrix of the lava samples. The thick line is a compositional divider between alkaline and subalkaline volcanic rocks (MacDonald, 1968). The compositional fields of the 1951 and 1995 are also shown for comparison (data from Doucelance et al., 2003; Escrig et al., 2005; Hildner et al., 2011;). U1, U2, U3 and Ph correspond to the field designations of Le Maitre et al. ~~(2002). For complete rock systematics of the 2014 rocks see *Section* 4.3).~~(2002) (U1: Tephrite/Basanite; U2: Pnotephrite; U3: Tephriphonolite; Ph: Phonolite). See the main text (*Section* 4.3) for a details on the systematics.

**Fig. 4** – Petrographic aspects of the lava flow samples showing the presence of clinopyroxene and kaersutite phenocrysts (A and B) in a hypocrystalline matrix with plagioclase, clinopyroxene and Fe-Ti oxides (A, B, C and D). Note the partial (A and B) or total (D) replacement of kaersutite by rhönite (opaque inosilicate of the aenigmatite group) which is marked by an arrow. Backscattered electron images showing a detailed view of the kaersutite rim replacement (E and F).

**Fig. 5** – Trace element characteristics of the 2014 eruptive products compared with those of the 1951 and 1995 eruptions (see Hildner et al., 2012 and Hildner et al., 2011, respectively). Normalizing values of Palme and O'Neil (2003).

**Fig. 6** - Pb isotopic compositions (A: $^{206}Pb/^{204}Pb$ vs. $^{207}Pb/^{204}Pb$; B: $^{206}Pb/^{204}Pb$ vs. $^{208}Pb/^{204}Pb$). Data sources: Northern Islands (Santo Antão, São Vicente and São Nicolau: Jørgensen and Holm, 2002; Holm et al., 2006; Millet et al., 2008) and Southern Islands (Fogo and Santiago: Doucelance et al., 2003; Barker et al., 2010; Martins et al., 2010). The 1951 and 1995 eruptions data are from Escrig et al., 2005. The heavy line represents the Northern Hemisphere Reference Line (NHRL) defined by Hart (1984). Also plotted are the compositions of mantle components (see main text for references).

**Fig. 7** – Sr, Nd (A) and Hf (B) isotope compositions. Data sources: the Santiago Island field was defined using data from Barker et al. (2009) and Martins et al. (2010). See caption of Fig. 6 for further references~~?~~. No Hf isotope data exist for the 1951 and 1995 eruptions.

**Fig 8 -** The role of clinopyroxene, olivine, amphibole and apatite fractionation on the liquid lines of descent for the 2014, 1995 and 1951 eruptions. In 8A and 8B fractional

crystallization was modelled using the Rayleigh equation. Partition coefficients ~~are from Aignertorres et al. (2007), Adam~~used in calculations can be find in the Supplementary Material S5-1 and ~~Green (2006), Bottazzi et al. (1999), Beattie (1994), McKenzie and O'Nions (1991) and Paster et al. (1974).~~data relative to the fractional crystallization vectors in the S5-2. Circular ticks represent consecutive increments of 5% crystallization. Crystallization vectors corresponds to F=0.7. ~~Note that despite similar liquid lines of descent the 2014 rocks are characterized by lower Nb/U ratios than their 1995 and 1951 counterparts.~~

**Formatted:** Font color: Auto

**Fig. 9** – ~~T vs. P diagram~~Temperature and pressure conditions for crystallization of clinopyroxene and amphibole from the 2014 tephritic and phonotephritic rocks ~~from the 2014 eruption~~.

**Fig.10 -** Mixing model between depleted mantle (DMM) and recycled oceanic crust (ROC; ≈ HIMU), and between ROC and EM1and the lower mantle (LM). Values for these end-members are from Doucelance et al. (2003) (lower mantle), Iwamoro (2015) (EM1, DMM) and Mourão et al. ~~(2012) (ROC).~~ (2012a) (ROC). Given that the 2014 Fogo lavas are characterized by a diluted contribution of ROC (see main text), making difficult its constraint, we considered 1.3 Ga as the age of recycling for mixing calculations, as determined by Mourão et al. (2012a) for the neighbouring Brava Island. Additional line corresponds to a mixture between recycled oceanic crust and lower mantle material in a 60:40 proportion, with EM1. Circular marks represent 10% increments. See Supplementary Material S5-3 for mixing calculations.

**Figure 1**

**Click here to download high resolution image**

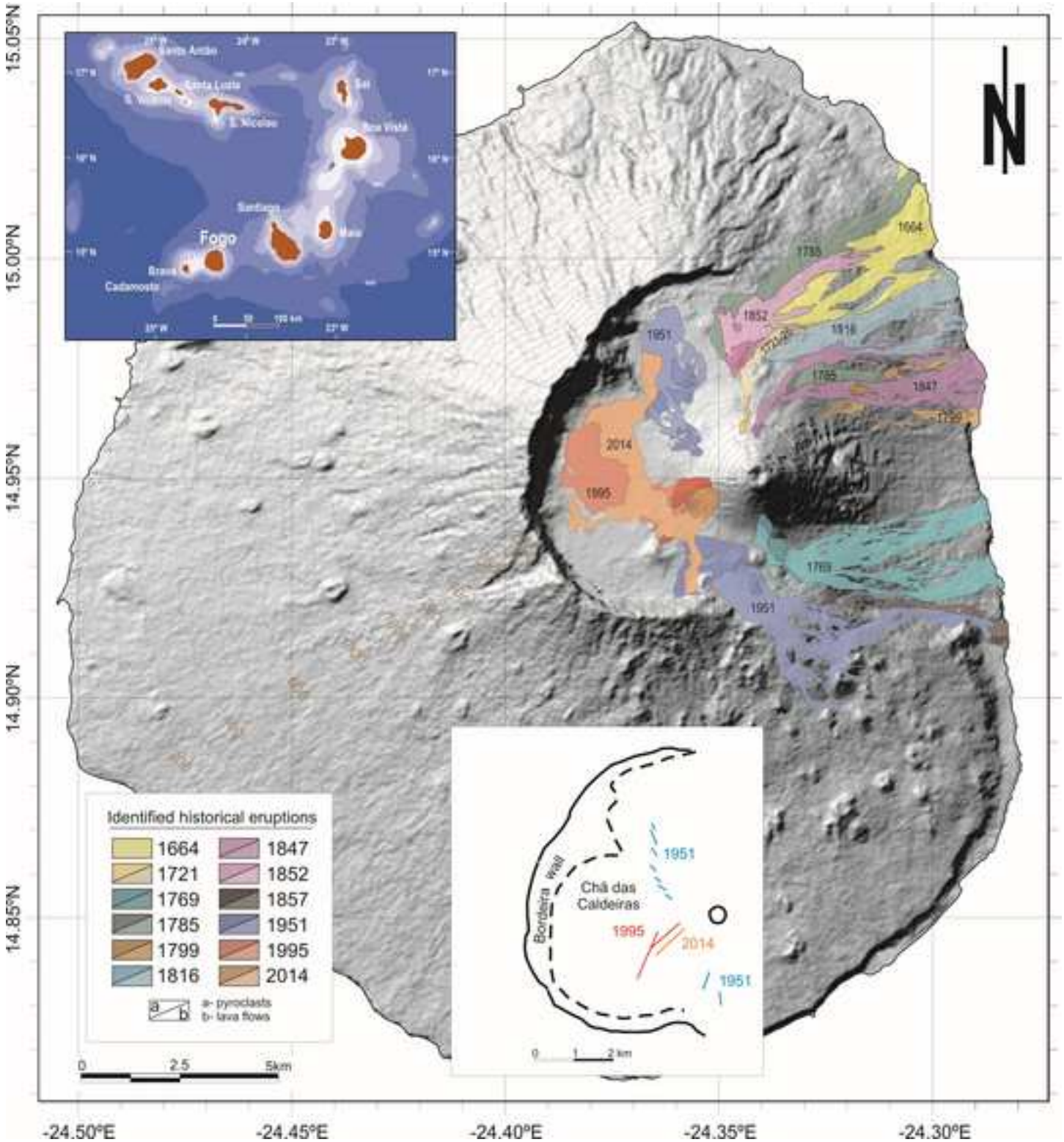

**Figure 2**

**Figure 2 B&W**

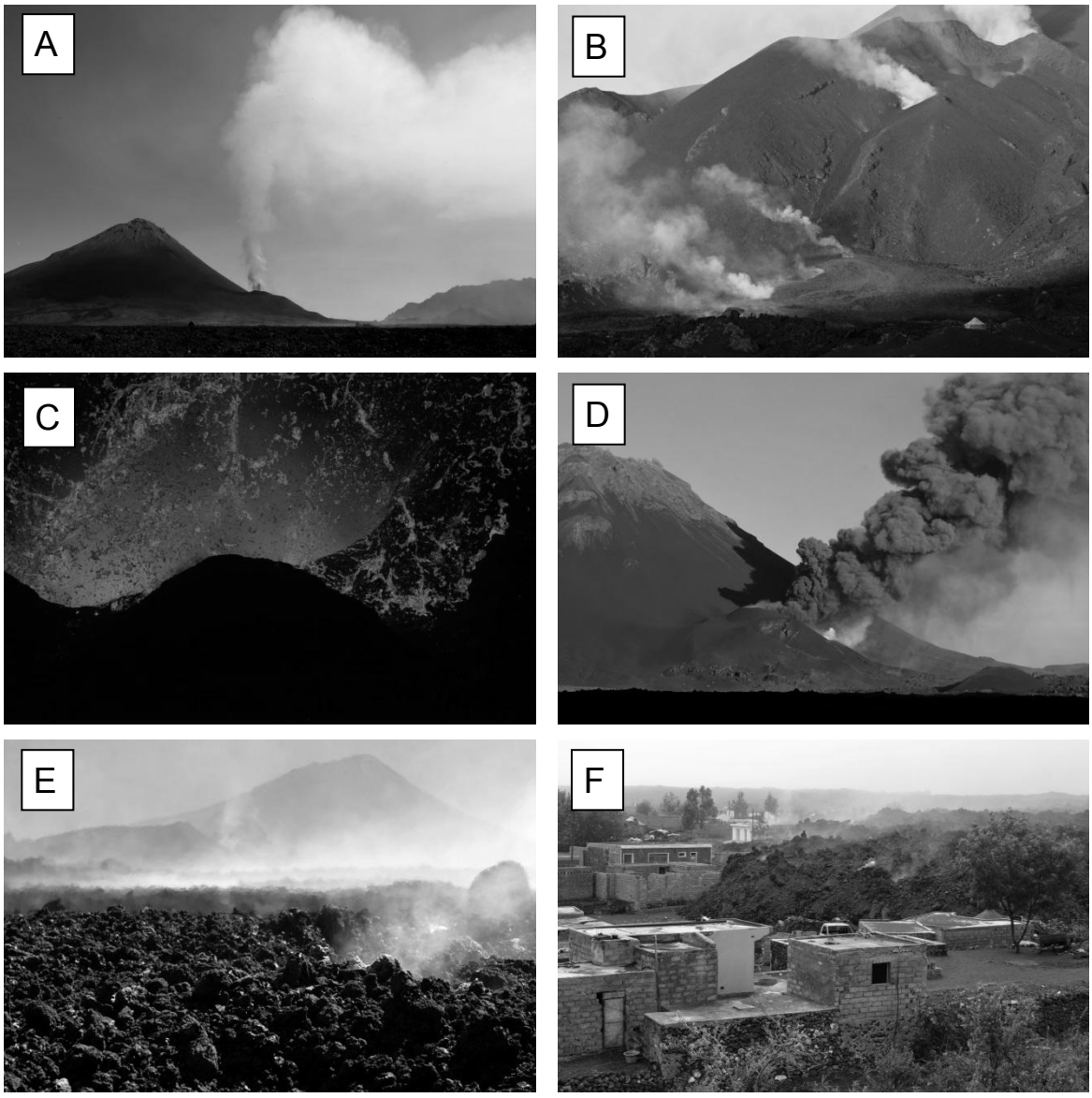

Figure 3

Click here to download high resolution image

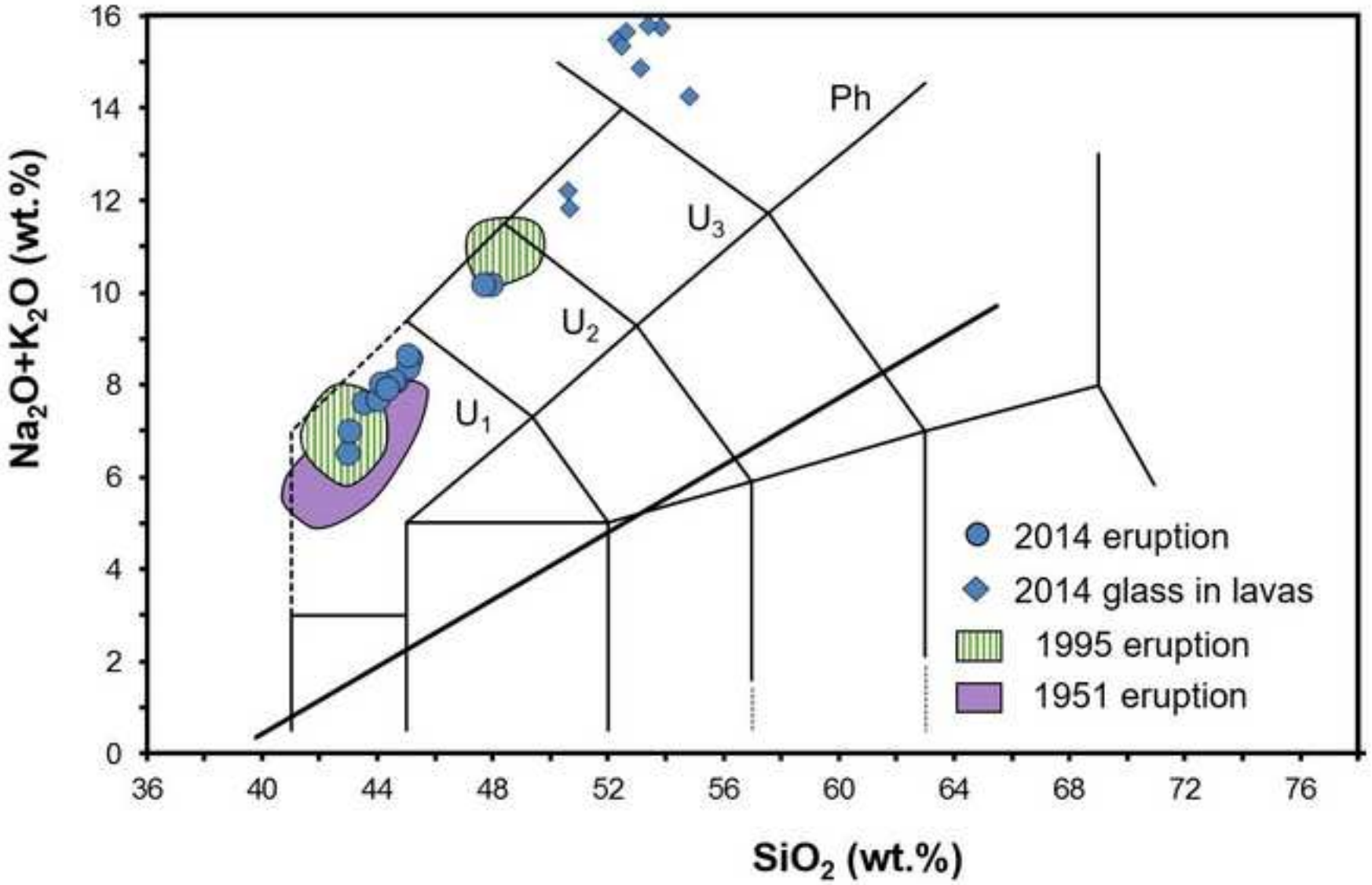

Figure 3 B&W
Click here to download high resolution image

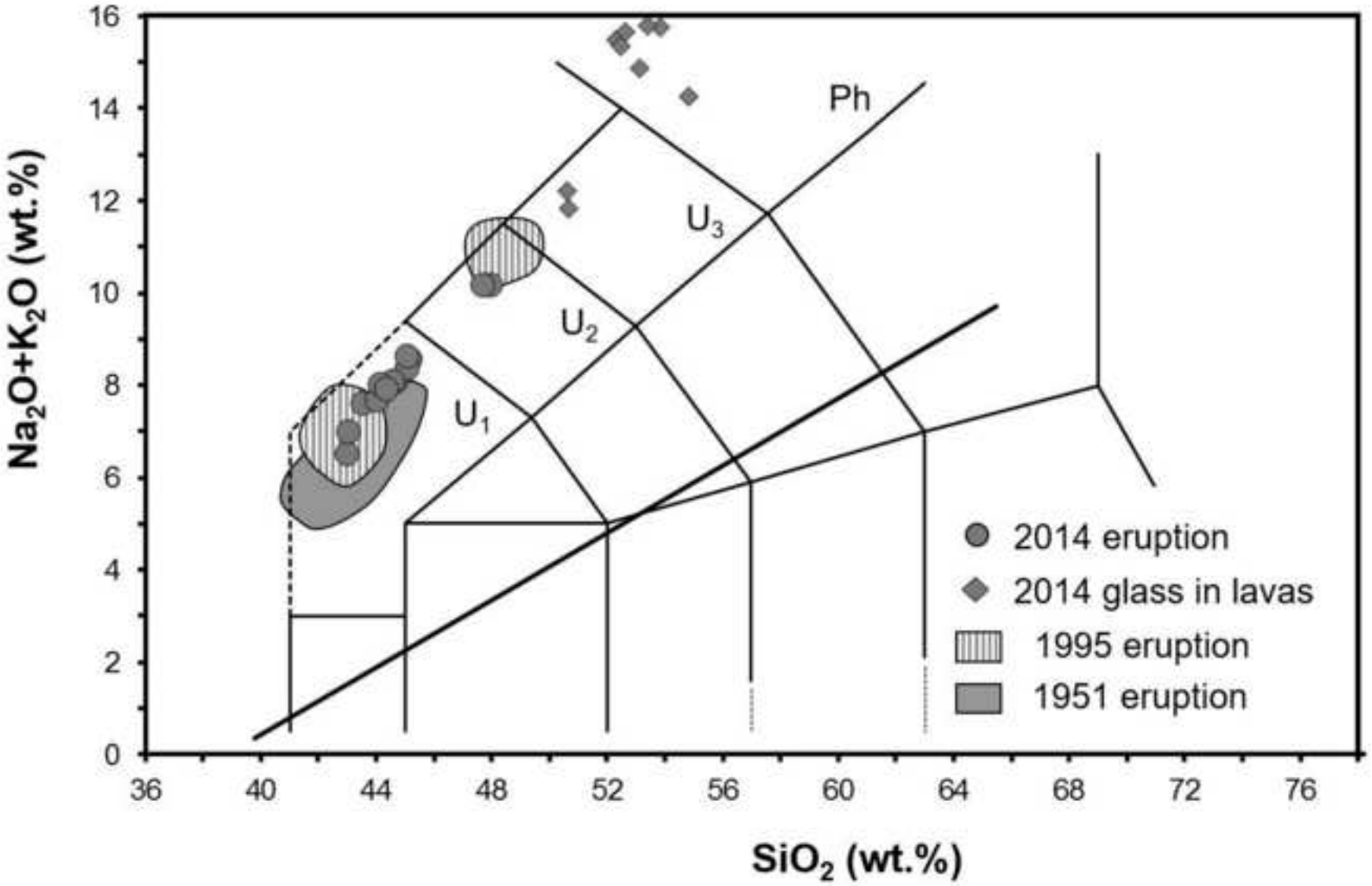

Figure 4
Click here to download high resolution image

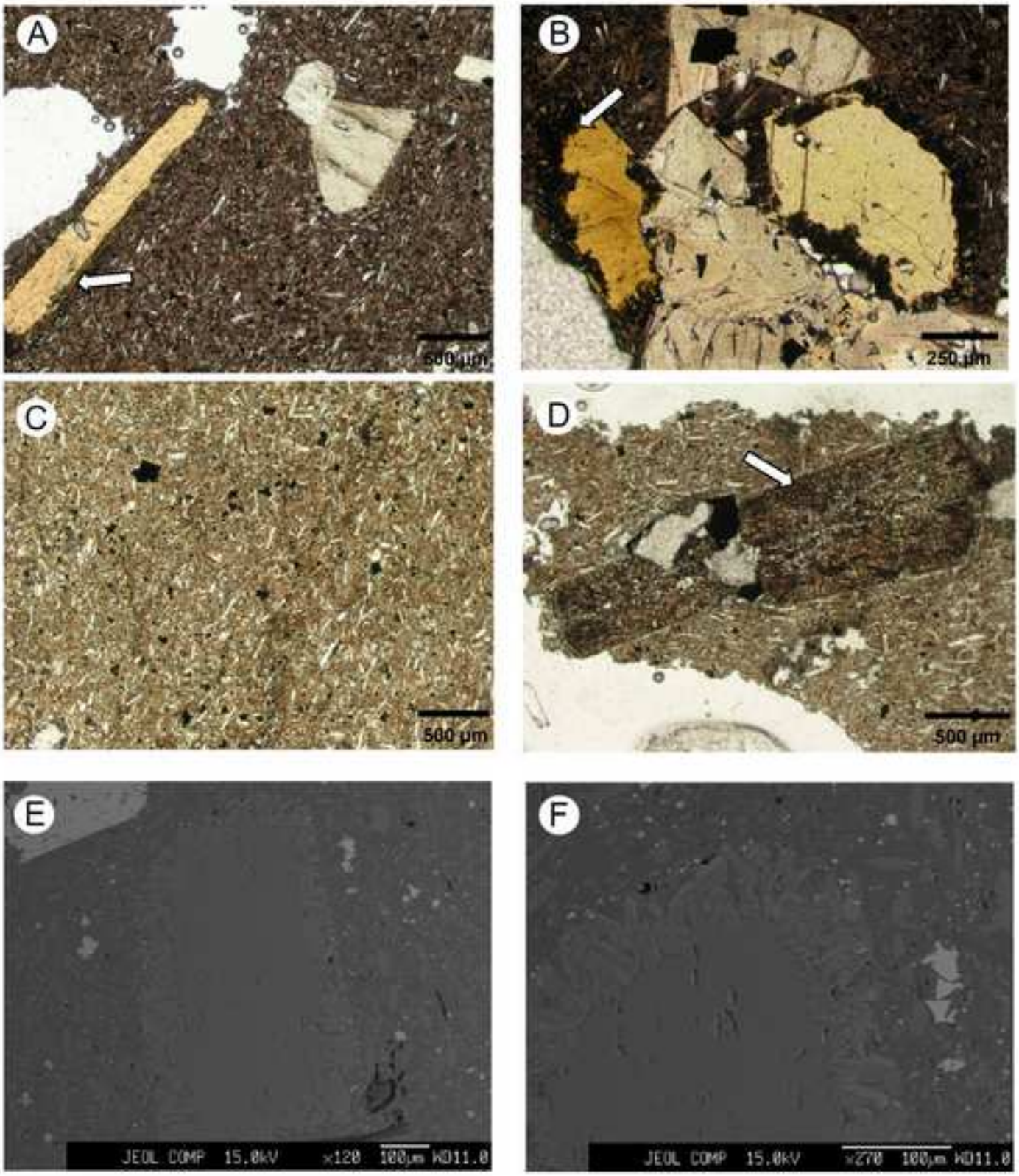

Figure 4 B&W

Click here to download high resolution image

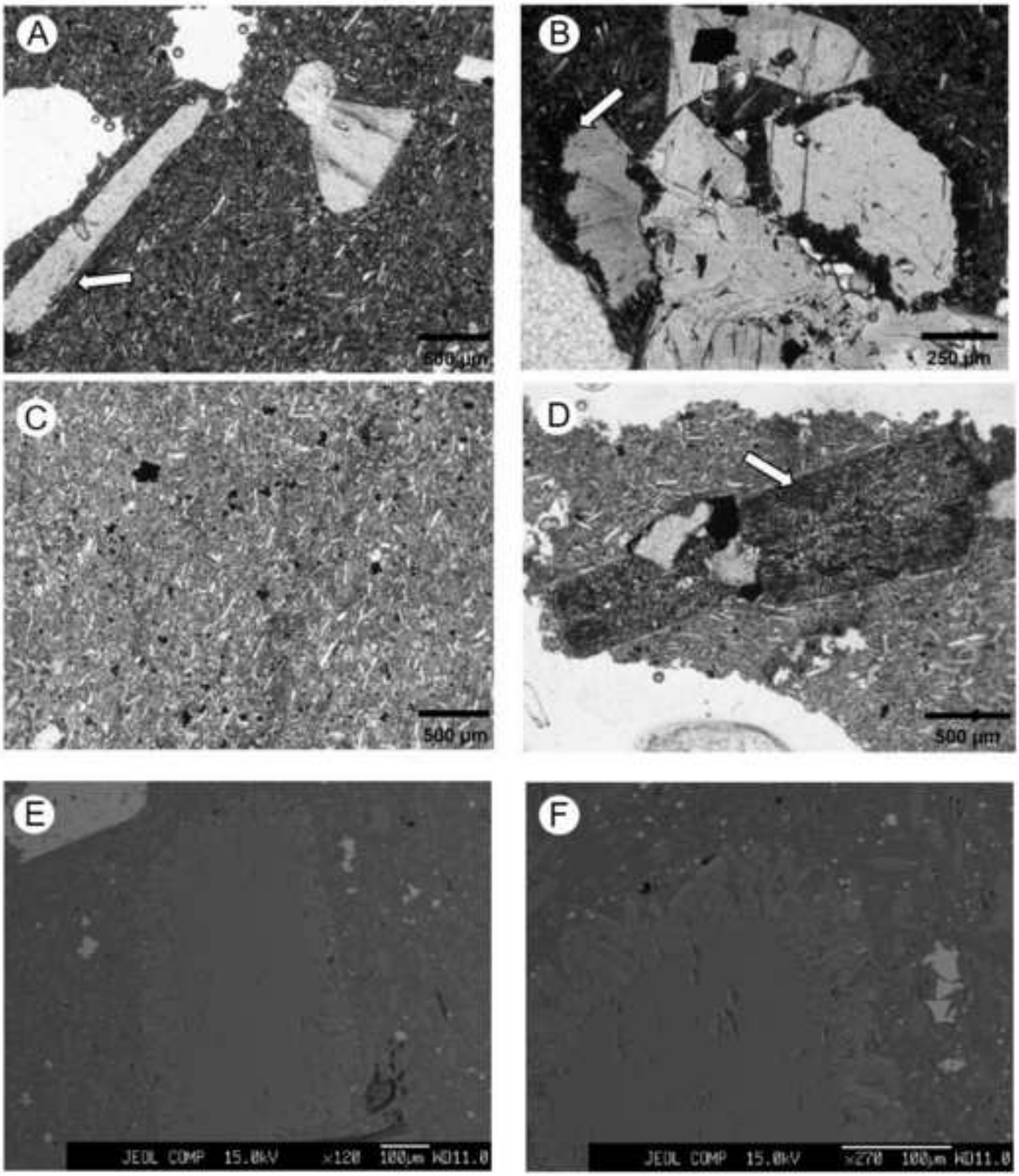

Figure 5

Click here to download high resolution image

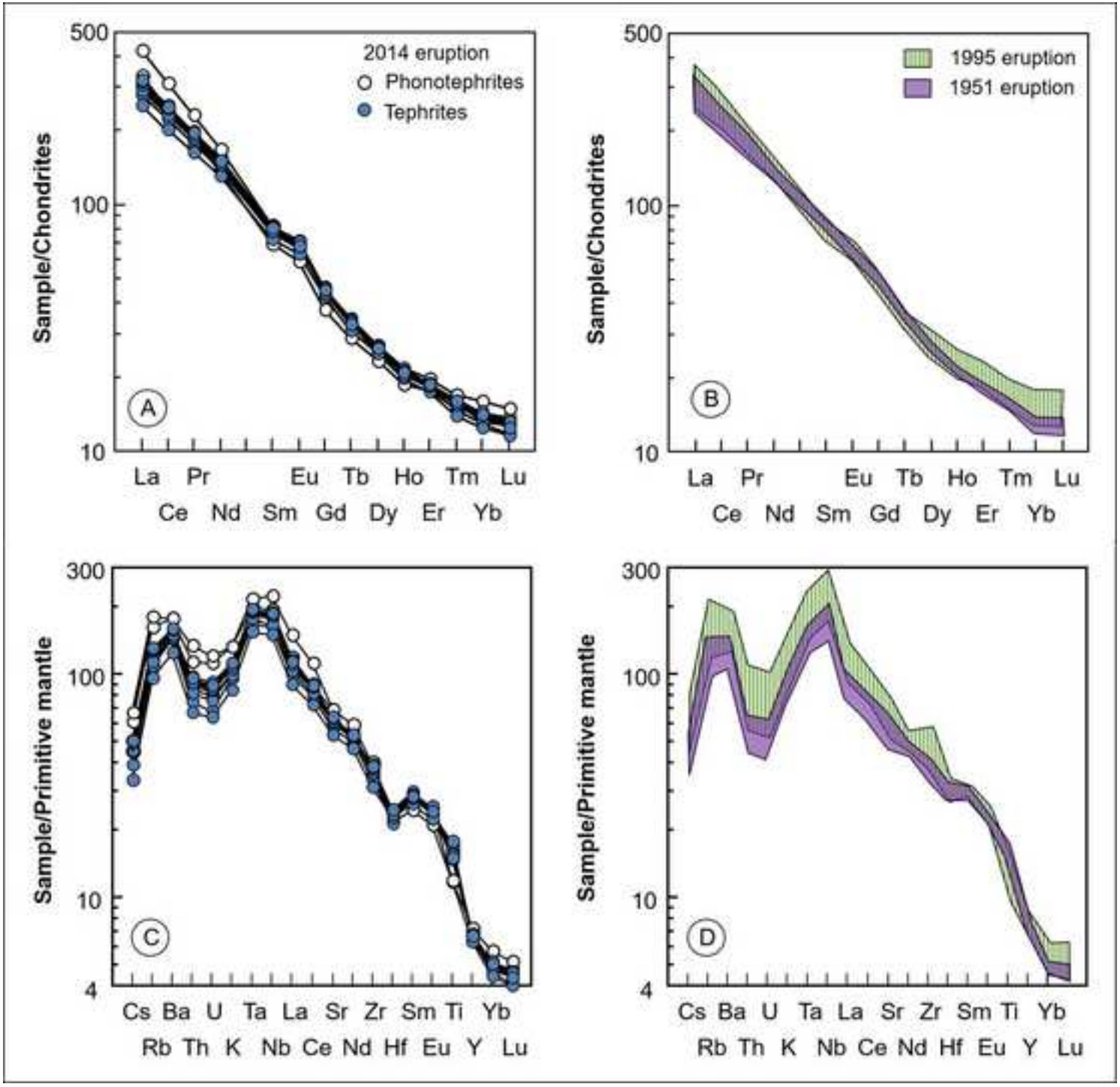

Figure 5 B&W

Click here to download high resolution image

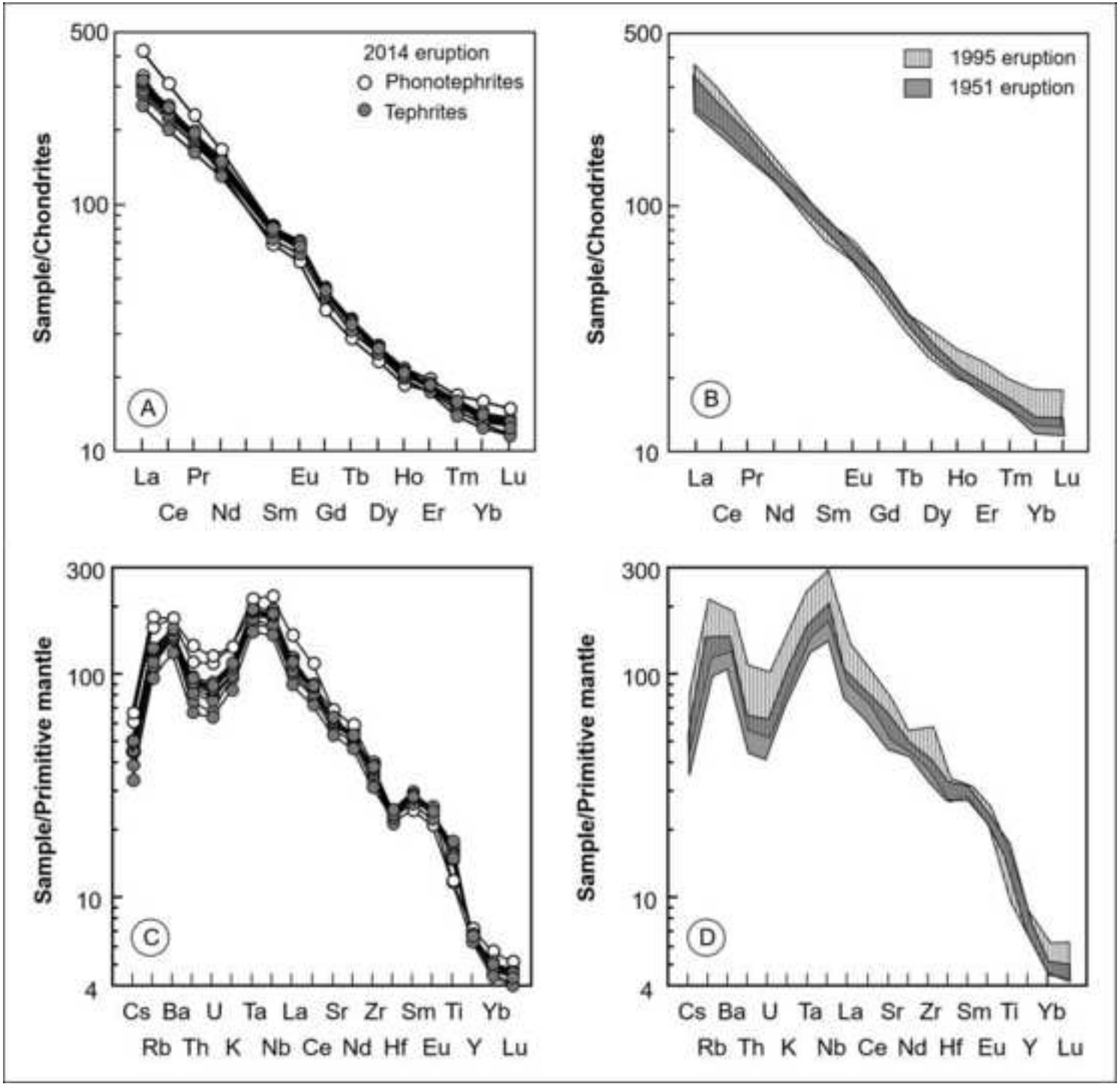

Figure 6
Click here to download high resolution image

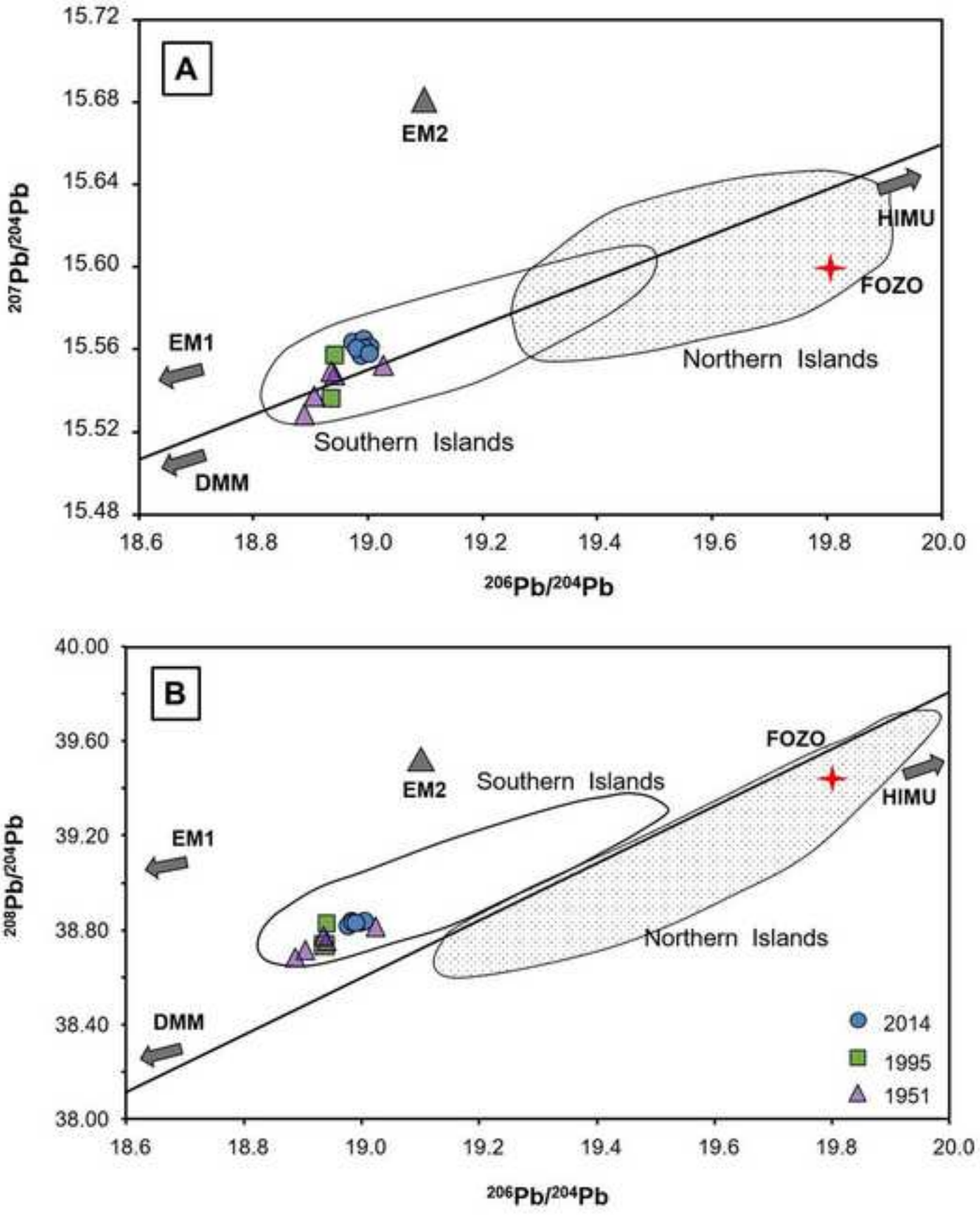

Figure 6 B&W
Click here to download high resolution image

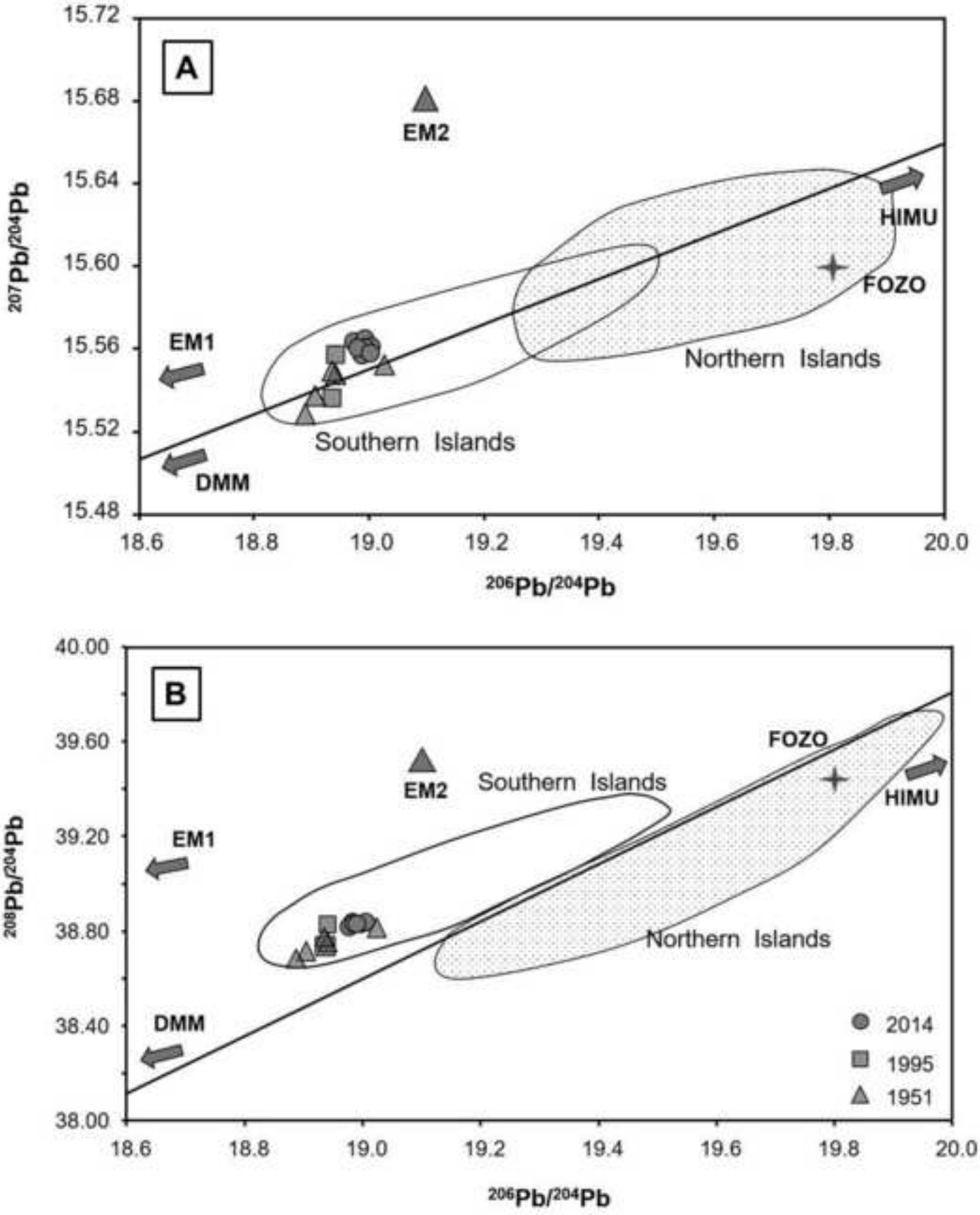

Figure 7
Click here to download high resolution image

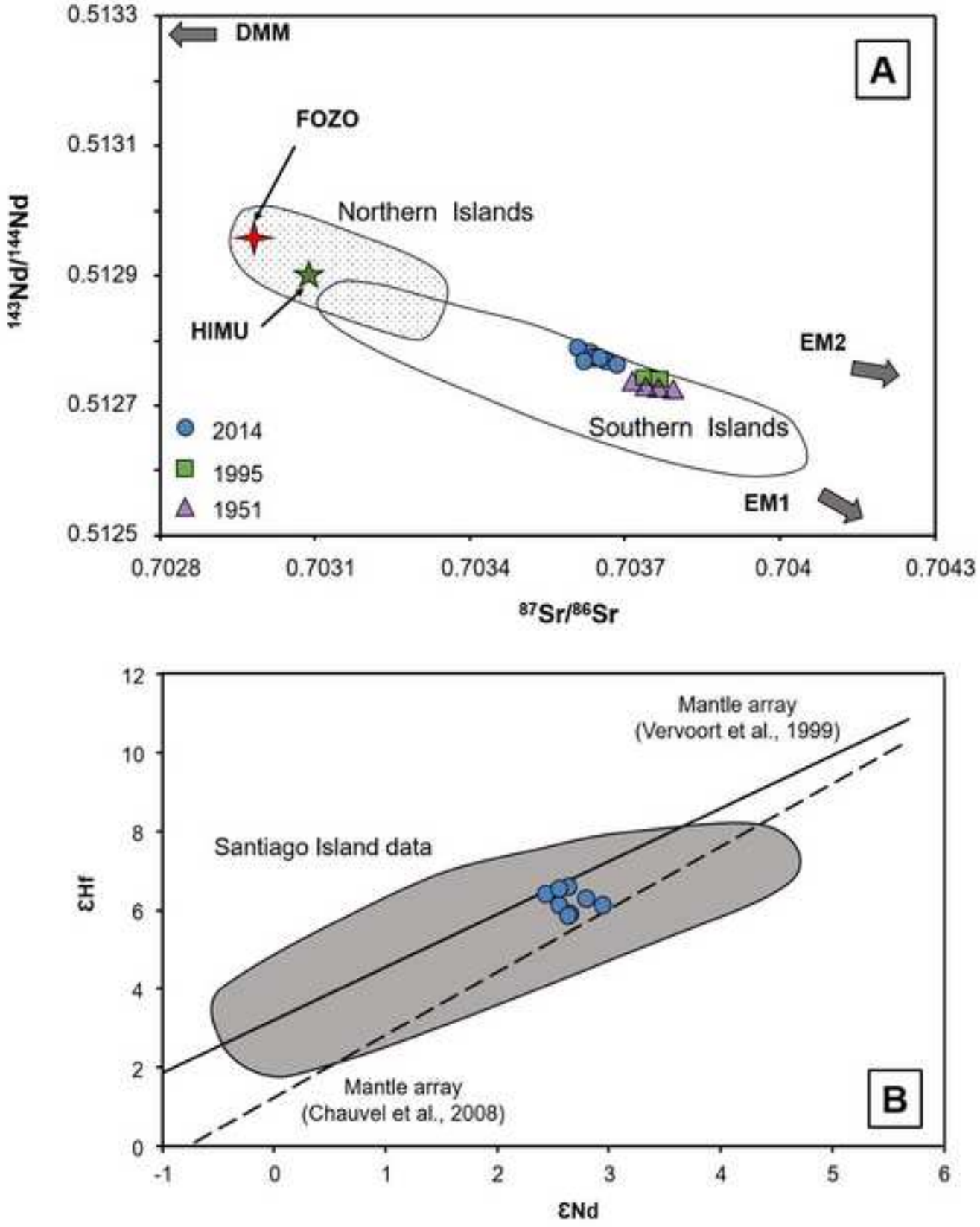

Figure 7 B&W
Click here to download high resolution image

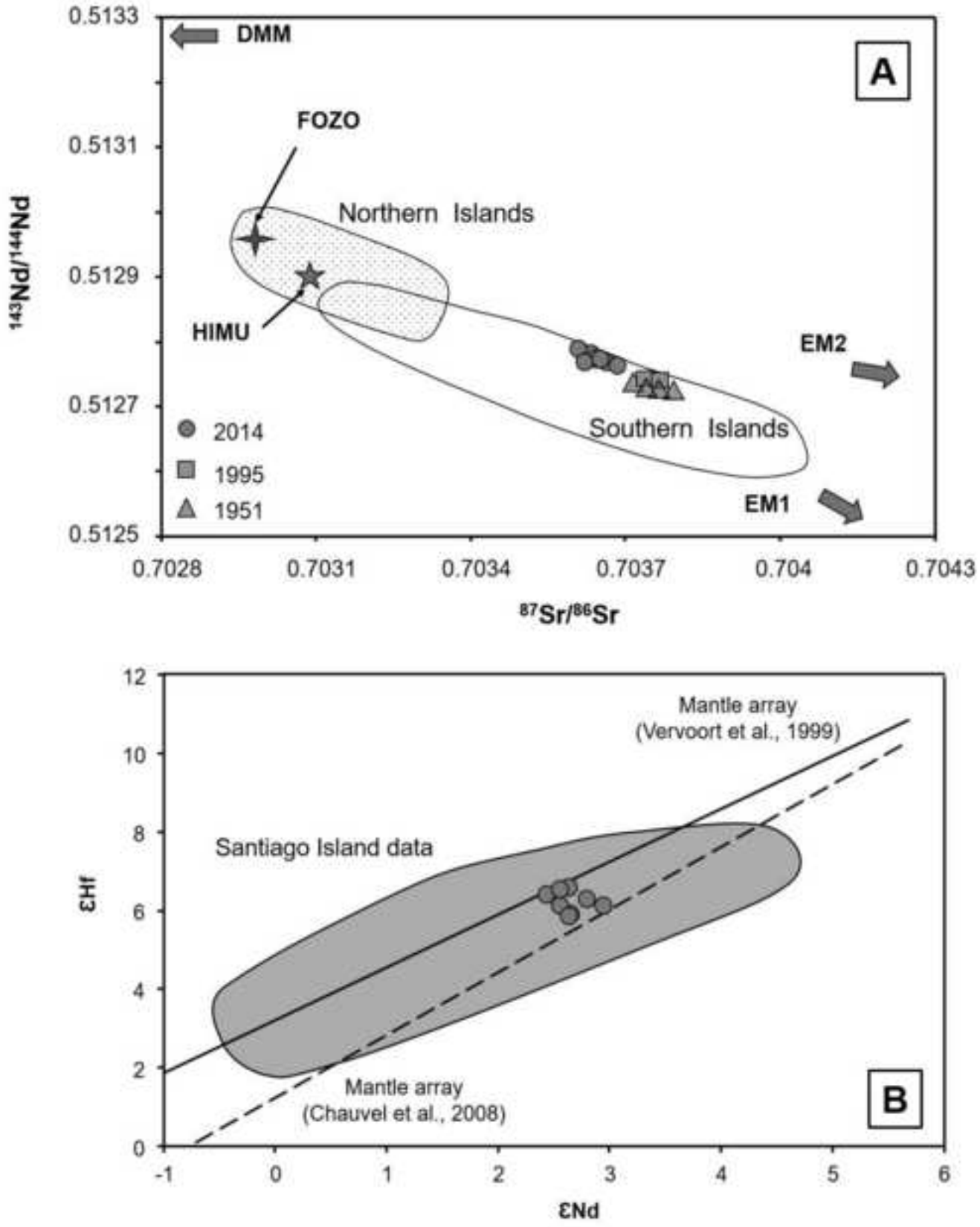

**Figure 8**

**Click here to download high resolution image**

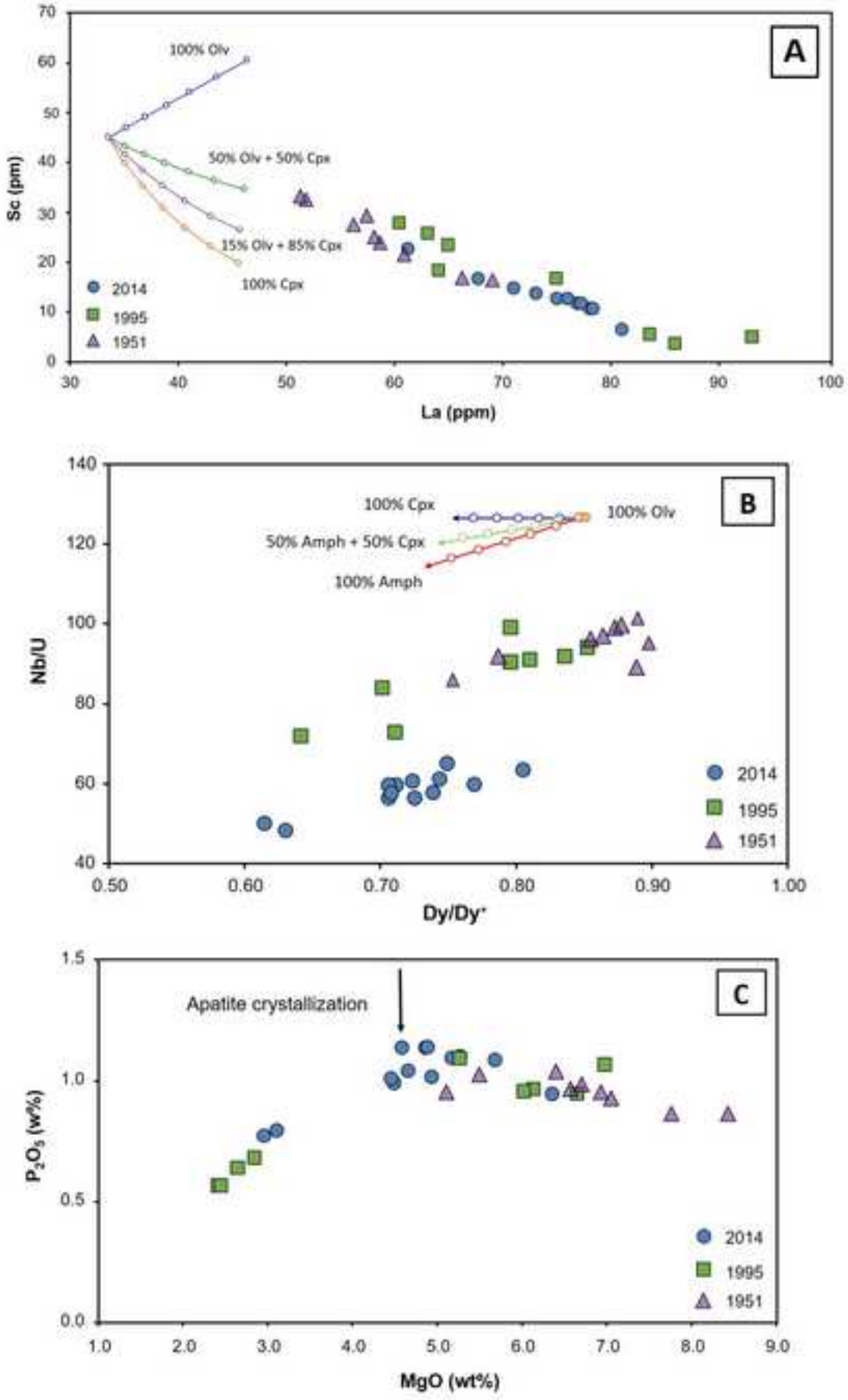

**Figure 8 B&W**

**Click here to download high resolution image**

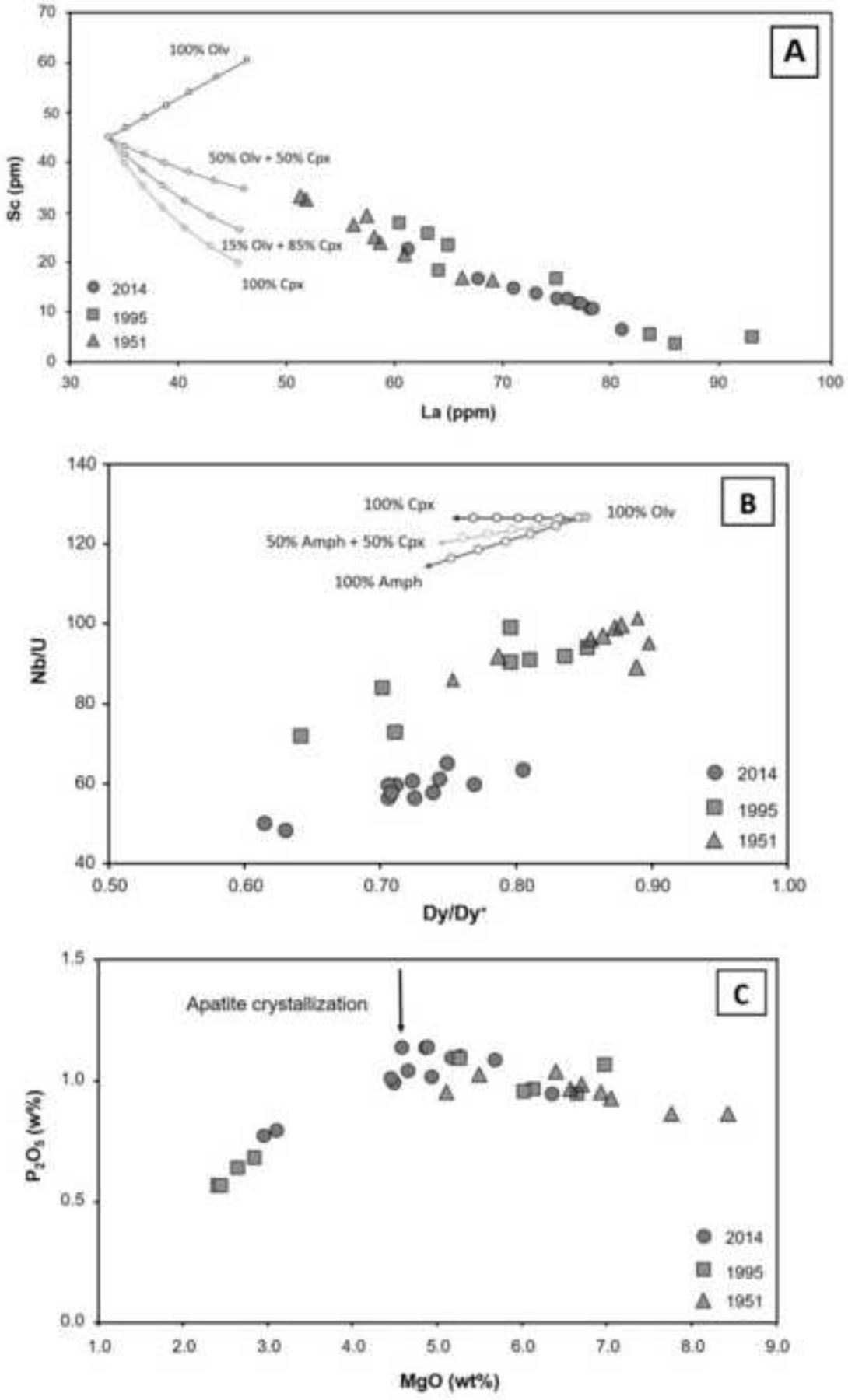

Figure 9

Click here to download high resolution image

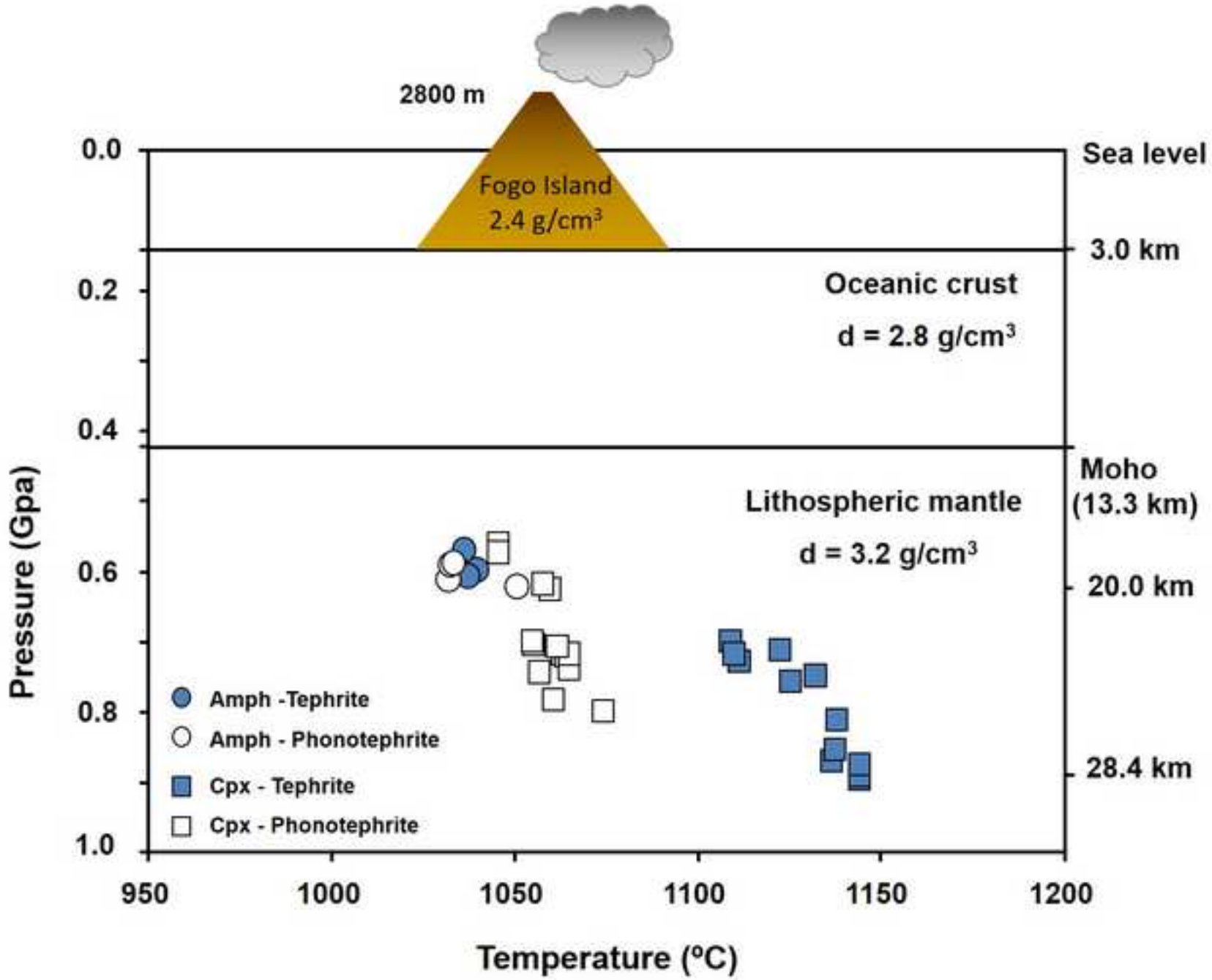

Figure 9 B&W

Click here to download high resolution image

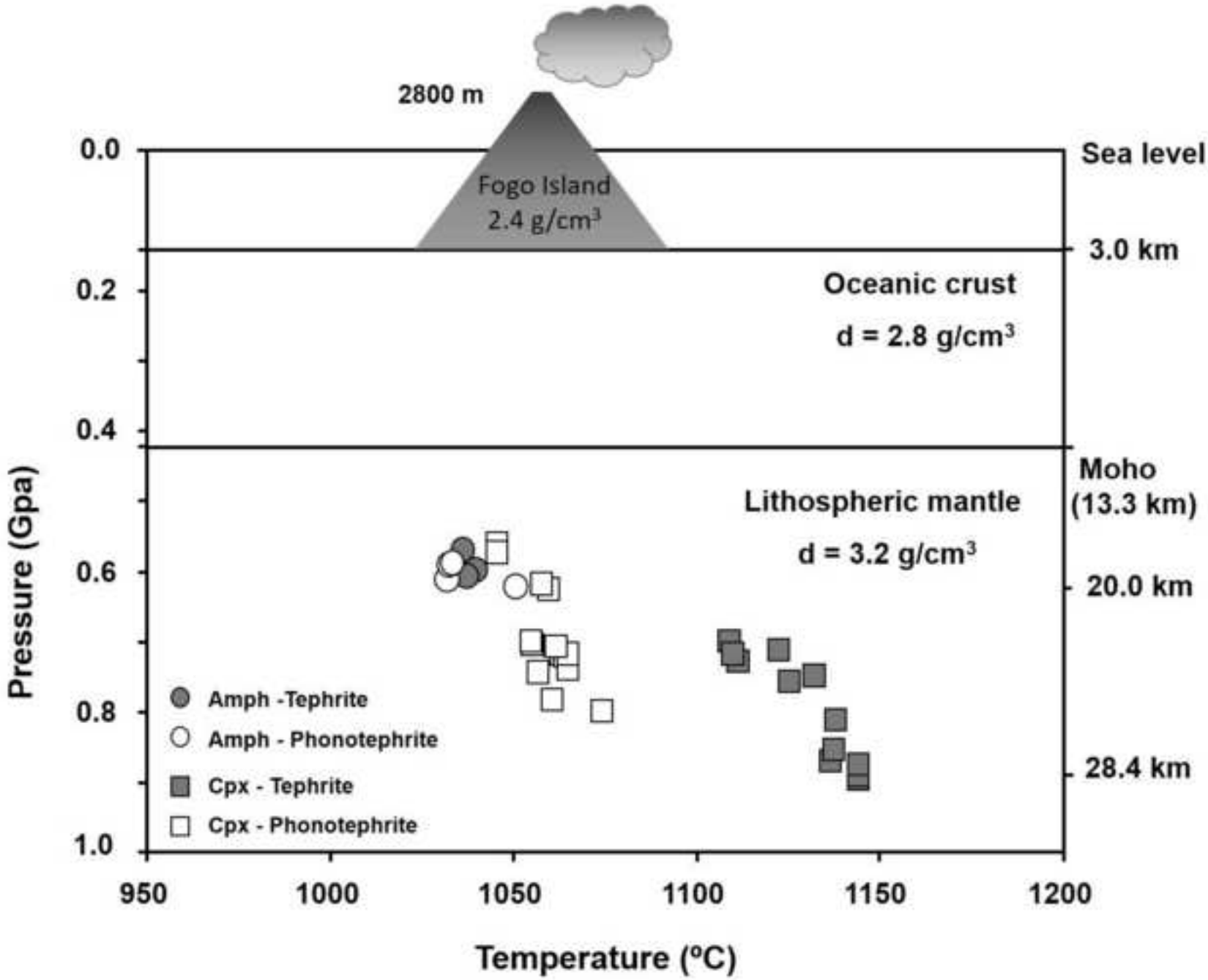

Figure 10

Click here to download high resolution image

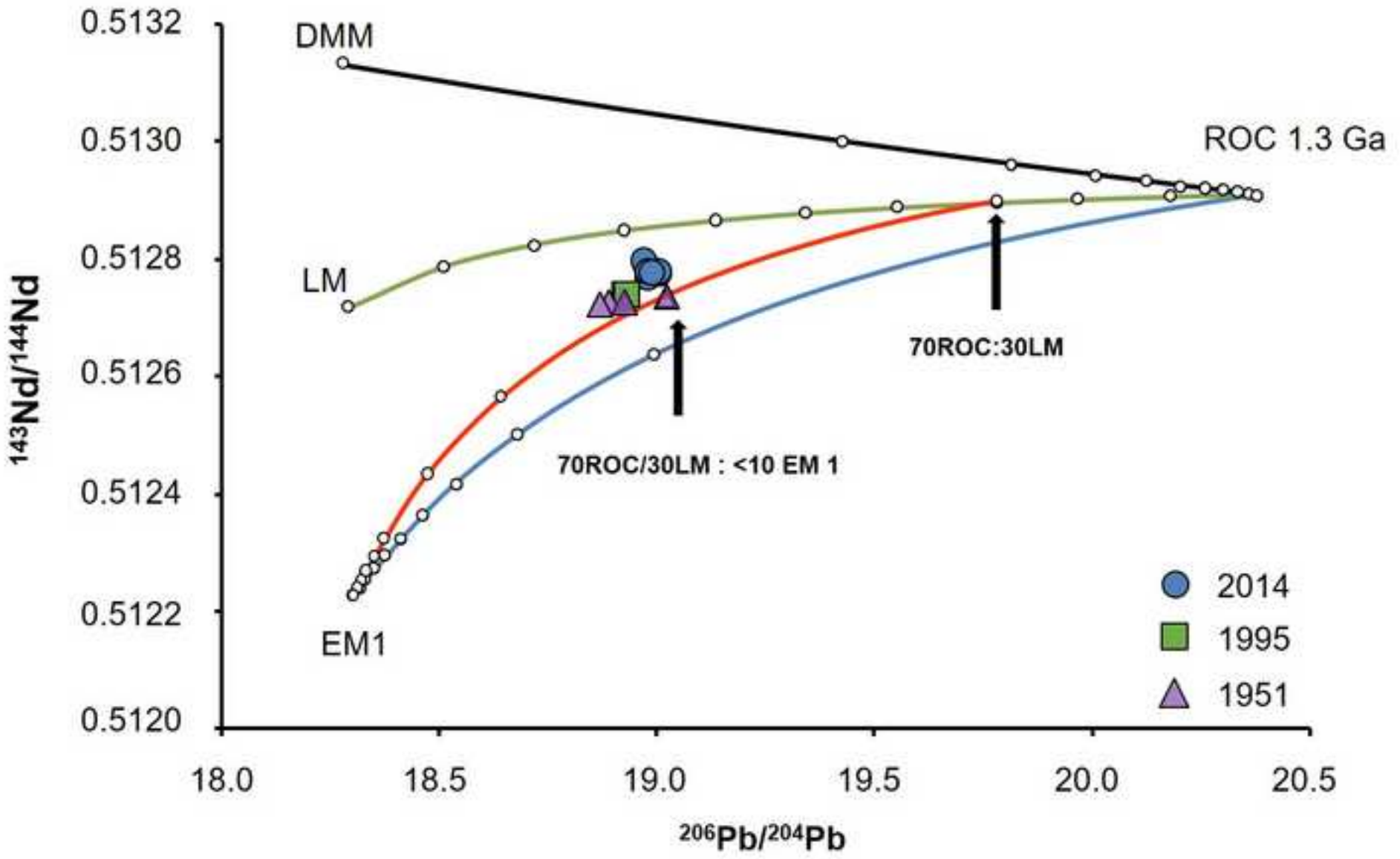

Figure 10 B&W

Click here to download high resolution image

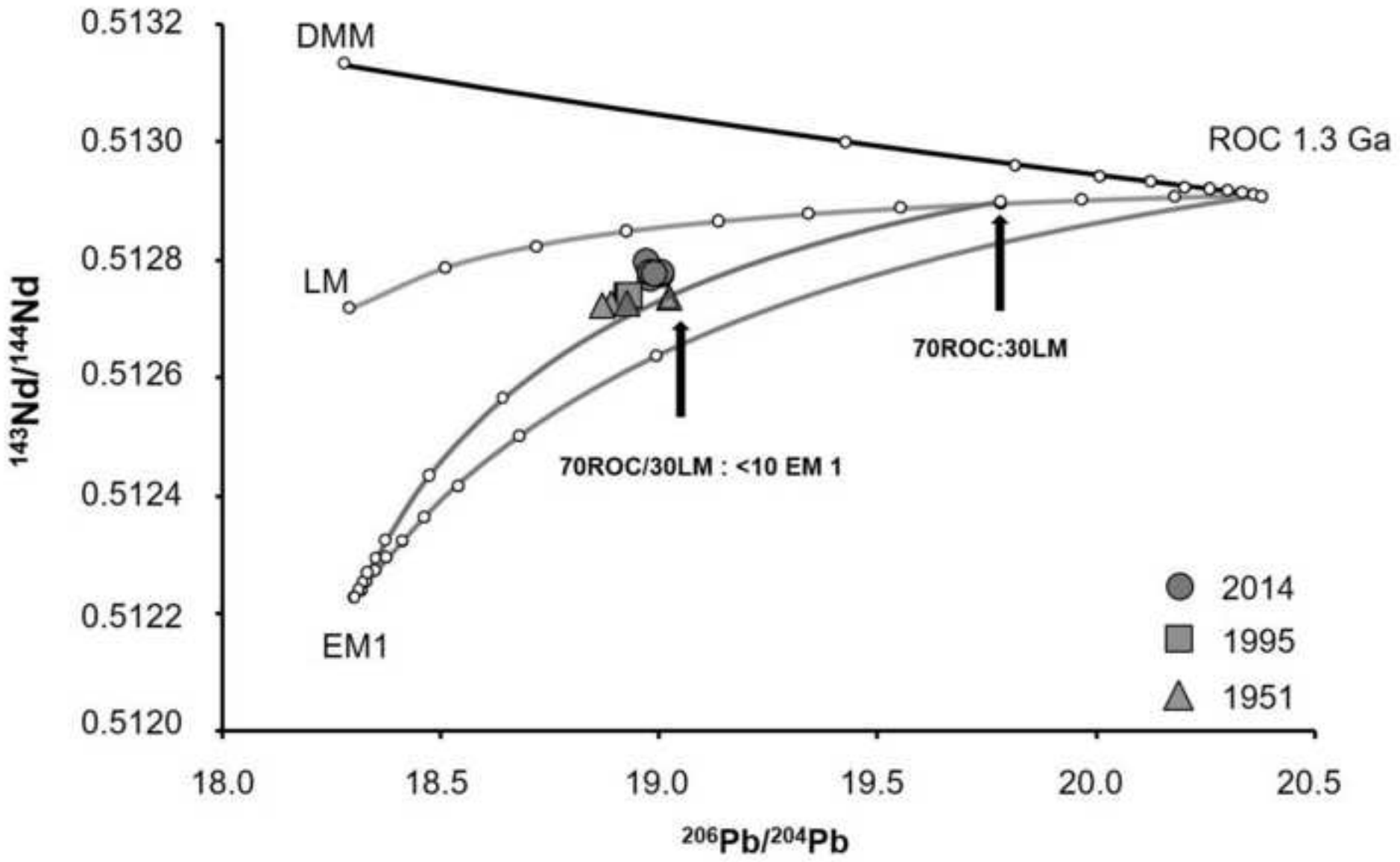

**Table I**

Click here to download Table: Table I.docx

## Table I: Whole rock chemical analyses of 2014 erupted lava flows and pyroclasts

| Sample | F14-1 | F14-2 | F14-4 | F14-5 | F14-6 | F14-7 | F14-8 | F14-9 | F14-10 | F14-11 | F14-12 | F14-13 | F14-14 |
|---|---|---|---|---|---|---|---|---|---|---|---|---|---|
| | Lava | Lava | Lava | Lava | Lava | Lava | Lava | Lava | Lava | Pyroc. | Pyroc. | Pyroc. | Pyroc. |
| Lithotype | Pht | Pht | Tep | Tep | Tep | Tep | Tep | Tep | Tep | Tep | Tep | Tep | Tep |
| $SiO_2$ (wt%) | 47.99 | 47.74 | 45.19 | 43.54 | 43.03 | 44.70 | 45.10 | 45.07 | 44.03 | 44.62 | 44.16 | 43.10 | 44.40 |
| $TiO_2$ | 2.50 | 2.54 | 3.16 | 3.58 | 3.81 | 3.37 | 3.31 | 3.17 | 3.46 | 3.34 | 3.38 | 3.71 | 3.37 |
| $Al_2O_3$ | 19.28 | 18.53 | 17.58 | 16.80 | 15.35 | 16.86 | 16.85 | 17.58 | 16.54 | 16.84 | 16.80 | 16.28 | 16.66 |
| $Fe_2O_3$* | 2.12 | 2.26 | 2.28 | 2.53 | 2.74 | 2.40 | 2.36 | 2.32 | 2.54 | 2.47 | 2.51 | 2.66 | 2.47 |
| FeO* | 6.06 | 6.46 | 7.61 | 8.44 | 9.12 | 7.99 | 7.86 | 7.73 | 8.48 | 8.24 | 8.36 | 8.88 | 8.22 |
| MnO | 0.21 | 0.22 | 0.21 | 0.22 | 0.21 | 0.22 | 0.22 | 0.22 | 0.22 | 0.22 | 0.22 | 0.21 | 0.22 |
| MgO | 2.93 | 3.08 | 4.47 | 5.25 | 6.33 | 4.91 | 4.63 | 4.43 | 5.15 | 4.55 | 4.83 | 5.66 | 4.87 |
| CaO | 7.96 | 8.21 | 9.95 | 10.95 | 11.98 | 10.47 | 10.30 | 9.83 | 10.82 | 10.51 | 10.62 | 11.43 | 10.74 |
| $Na_2O$ | 6.00 | 6.00 | 5.06 | 4.51 | 3.84 | 4.78 | 4.95 | 5.13 | 4.55 | 4.76 | 4.69 | 4.01 | 4.64 |
| $K_2O$ | 4.17 | 4.16 | 3.48 | 3.09 | 2.64 | 3.29 | 3.39 | 3.51 | 3.12 | 3.31 | 3.30 | 2.97 | 3.26 |
| $P_2O_5$ | 0.78 | 0.80 | 1.00 | 1.11 | 0.96 | 1.02 | 1.05 | 1.02 | 1.10 | 1.14 | 1.14 | 1.10 | 1.15 |
| LOI | -0.17 | -0.18 | -0.26 | -0.42 | -0.53 | -0.4 | -0.37 | -0.30 | -0.51 | -0.09 | 0.65 | -0.04 | -0.19 |
| Mg# | 46.25 | 45.98 | 51.14 | 52.58 | 55.32 | 52.26 | 51.21 | 50.53 | 51.97 | 49.63 | 50.75 | 53.16 | 51.34 |
| S (%) | 0.012 | 0.008 | 0.007 | 0.006 | 0.009 | 0.009 | 0.008 | 0.009 | 0.008 | 0.023 | 0.012 | 0.023 | 0.022 |
| Sc (ppm) | 5 | 5 | 11 | 15 | 23 | 13 | 12 | 11 | 14 | 11 | 12 | 17 | 13 |
| V | 217 | 223 | 280 | 322 | 363 | 306 | 299 | 286 | 322 | 300 | 305 | 353 | 311 |
| Cr | 30 | <20 | 40 | 60 | 90 | 50 | 50 | 60 | 50 | 70 | 30 | 30 | 20 |
| Co | 17 | 20 | 26 | 30 | 37 | 28 | 27 | 26 | 29 | 28 | 29 | 34 | 29 |
| Ni | 6 | 20 | 17 | 22 | 42 | 21 | 19 | 17 | 31 | 15 | 16 | 28 | 17 |
| Rb | 97 | 108 | 79 | 68 | 58 | 76 | 78 | 79 | 70 | 75 | 75 | 65 | 72 |
| Sr | 1408 | 1403 | 1256 | 1213 | 1084 | 1242 | 1280 | 1295 | 1212 | 1243 | 1194 | 1140 | 1214 |
| Y | 27.40 | 31.70 | 29.40 | 29.40 | 27.60 | 29.80 | 29.80 | 29.10 | 29.90 | 30.20 | 30.20 | 28.90 | 29.90 |
| Zr | 433 | 422 | 394 | 382 | 336 | 394 | 406 | 412 | 384 | 387 | 374 | 360 | 390 |
| Nb | 117 | 133 | 112 | 98.4 | 89 | 110 | 112 | 111 | 107 | 113 | 108 | 97.4 | 110 |
| Cs | 1.10 | 1.20 | 0.90 | 0.80 | 0.60 | 0.80 | 0.90 | 0.90 | 0.80 | 0.80 | 0.80 | 0.70 | 0.80 |
| Ba | 1198 | 1204 | 1043 | 973 | 839 | 1013 | 1050 | 1076 | 1000 | 1025 | 1013 | 960 | 1024 |
| La | 81.30 | 103.00 | 78.00 | 71.10 | 61.30 | 75.10 | 77.00 | 78.10 | 73.10 | 78.40 | 77.30 | 67.80 | 76.10 |
| Ce | 157 | 199 | 157 | 147 | 129 | 155 | 156 | 158 | 152 | 160 | 159 | 141 | 155 |
| Pr | 17.80 | 22.20 | 18.50 | 17.70 | 15.70 | 18.50 | 18.40 | 18.80 | 18.10 | 18.90 | 19.10 | 17.10 | 18.70 |
| Nd | 64.20 | 78.90 | 68.90 | 68.30 | 61.40 | 69.30 | 70.60 | 70.90 | 69.20 | 72.60 | 72.50 | 66.20 | 71.80 |
| Sm | 10.60 | 12.70 | 11.80 | 12.00 | 11.20 | 12.00 | 12.40 | 12.20 | 12.30 | 12.50 | 12.50 | 11.80 | 12.40 |
| Eu | 3.39 | 4.03 | 3.90 | 3.96 | 3.62 | 3.93 | 4.08 | 3.92 | 3.93 | 4.02 | 4.11 | 3.83 | 3.99 |
| Gd | 7.59 | 9.02 | 9.41 | 9.30 | 8.61 | 9.03 | 8.95 | 9.11 | 9.19 | 9.10 | 9.27 | 9.21 | 9.31 |
| Tb | 1.07 | 1.24 | 1.23 | 1.24 | 1.16 | 1.22 | 1.26 | 1.22 | 1.26 | 1.29 | 1.29 | 1.24 | 1.28 |
| Dy | 5.91 | 6.82 | 6.60 | 6.63 | 6.35 | 6.61 | 6.69 | 6.56 | 6.61 | 6.79 | 6.78 | 6.30 | 6.61 |
| Ho | 1.05 | 1.22 | 1.19 | 1.20 | 1.11 | 1.14 | 1.19 | 1.17 | 1.21 | 1.19 | 1.23 | 1.16 | 1.19 |
| Er | 2.90 | 3.25 | 3.08 | 3.11 | 2.86 | 3.06 | 3.04 | 3.07 | 3.01 | 3.05 | 3.10 | 2.99 | 3.09 |
| Tm | 0.38 | 0.43 | 0.39 | 0.41 | 0.35 | 0.41 | 0.40 | 0.41 | 0.40 | 0.41 | 0.42 | 0.38 | 0.40 |
| Yb | 2.30 | 2.64 | 2.33 | 2.16 | 2.03 | 2.35 | 2.39 | 2.30 | 2.23 | 2.27 | 2.34 | 2.13 | 2.28 |
| Lu | 0.33 | 0.37 | 0.33 | 0.32 | 0.29 | 0.32 | 0.33 | 0.31 | 0.31 | 0.31 | 0.34 | 0.29 | 0.31 |
| Hf | 6.50 | 7.40 | 6.90 | 6.90 | 6.80 | 7.00 | 7.00 | 7.30 | 7.30 | 7.00 | 6.40 | 6.80 | 7.10 |
| Ta | 7.85 | 8.70 | 7.65 | 7.04 | 6.13 | 7.49 | 7.61 | 7.75 | 7.32 | 7.63 | 7.59 | 6.70 | 7.50 |
| Th | 9.38 | 11.20 | 8.09 | 6.83 | 5.62 | 7.58 | 7.59 | 7.95 | 7.15 | 7.54 | 7.54 | 6.24 | 7.32 |
| U | 2.41 | 2.64 | 1.98 | 1.64 | 1.40 | 1.84 | 1.87 | 1.92 | 1.74 | 1.95 | 1.91 | 1.49 | 1.81 |

(*) $Fe_2O_3/FeO$ ratio calculated from the analysed $Fe_2O_3^T$ by the method of Middlemost (1989).

**Table II**

Click here to download Table: Table II.docx

## Table II: Isotope analyses for selected samples

| | $^{87}Sr/^{86}Sr$ | $^{143}Nd/^{144}Nd$ | $^{176}Hf/^{177}Hf$ | $^{206}Pb/^{204}Pb$ | $^{207}Pb/^{204}Pb$ | $^{208}Pb/^{204}Pb$ | $\varepsilon_{Nd}$ | $\varepsilon_{Hf}$ | Δ7/4 | Δ8/4 |
|---|---|---|---|---|---|---|---|---|---|---|
| F14-1 | 0.703655 ± 15 | 0.512774 ± 7 | 0.282940 ± 5 | 18.9901 ± 08 | 15.5642 ± 7 | 38.8462 ± 19 | 2.65 | 5.93 | 1.47 | 26.01 |
| F14-2 | 0.703669 ± 12 | 0.512769 ± 7 | 0.282946 ± 5 | 18.9993 ± 09 | 15.5625 ± 8 | 38.8509 ± 23 | 2.55 | 6.15 | 1.20 | 25.38 |
| F14-5 | 0.703689 ± 10 | 0.512762 ± 8 | 0.282954 ± 4 | 18.9811 ± 10 | 15.5588 ± 9 | 38.8470 ± 24 | 2.43 | 6.42 | 1.03 | 27.19 |
| F14-6 | 0.703638 ± 09 | 0.512781 ± 7 | 0.282951 ± 5 | 18.9766 ± 10 | 15.5618 ± 9 | 38.8578 ± 21 | 2.79 | 6.33 | 1.37 | 28.80 |
| F14-7 | 0.703613 ± 09 | 0.512789 ± 8 | 0.282946 ± 5 | 18.9717 ± 10 | 15.5632 ± 9 | 38.8341 ± 23 | 2.94 | 6.15 | 1.57 | 27.03 |
| F14-10 | 0.703647 ± 10 | 0.512772 ± 7 | 0.282959 ± 5 | 18.9799 ± 07 | 15.5611 ± 7 | 38.8467 ± 15 | 2.62 | 6.62 | 1.27 | 27.30 |
| F14-11 | 0.703656 ± 10 | 0.512773 ± 7 | 0.282938 ± 4 | 19.0008 ± 10 | 15.5609 ± 8 | 38.8553 ± 22 | 2.63 | 5.88 | 1.03 | 25.63 |
| F14-14 | 0.703626 ± 09 | 0.512769 ± 6 | 0.282958 ± 5 | 18.9859 ± 09 | 15.5590 ± 7 | 38.8480 ± 18 | 2.55 | 6.57 | 0.99 | 26.70 |

**S1**

**Click here to download Background dataset for online publication only: S1-Photos.docx**

**S2**

**Click here to download Background dataset for online publication only: S2- Standards, duplicate and blank_2017.xlsx**

**S3**

**Click here to download Background dataset for online publication only: S3- Mineral Chemistry and Glass compositions_2017.xls**

**S4**

**Click here to download Background dataset for online publication only: S4- Normative Compositions.xlsx**

**S5**

**Click here to download Background dataset for online publication only: S5- Modelling.xlsx**